ผลของอุณหภูมิต่อการหาลักษณะเฉพาะของฟิล์มไฮดรอกซีอะพาไทต์ที่เตรียมโดยวิธีโซล-เจล

นายภาสิต หงษ์ทอง

วิทยานิพนธ์นี้เป็นส่วนหนึ่งของการศึกษาตามหลักสูตรปริญญาวิทยาศาสตรมหาบัณฑิต
สาขาวิชาฟิสิกส์ ภาควิชาฟิสิกส์
คณะวิทยาศาสตร์ จุฬาลงกรณ์มหาวิทยาลัย
ปีการศึกษา 2552

TEMPERATURE EFFECTS ON CHARACTERIZATIONS OF

HYDROXYAPATITE FILMS PREPARED BY SOL-GEL METHOD

Mr. Bhasit Hongthong

ศูนย์วิทยทรัพยากร

จุฬาลงกรณ์มหาวิทยาลัย

A Thesis Submitted in Partial Fulfillment of the Requirements

for the Degree of Master of Science Program in Physics

Department of Physics

Faculty of Science

Chulalongkorn University

Academic year 2009

Thesis Title   TEMPERATURE EFFECTS ON CHARACTERIZATIONS
OF HYDROXYAPATITE FILMS PREPARED BY SOL-GEL
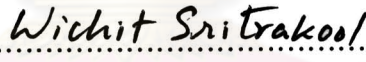METHOD

By   Mr. Bhasit Hongthong
Field of Study Physics
Thesis Advisor Assistant Professor Sukkaneste Tungasmita, Ph.D.
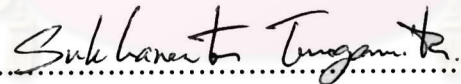Thesis Co-Advisor Assistant Professor Satreerat Kampangkeaw Hodak, Ph.D.

Accepted by the Faculty of Science, Chulalongkorn University in Partial Fulfillment of the Requirements for the Master's Degree
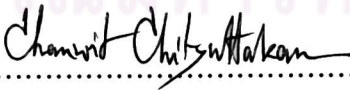
....Dean of the Faculty of Science

(Professor Supot Hannongbua, Ph.D.)

THESIS COMMITTEE

.....................................Chairman

(Associate Professor Wichit Sritrakool, Ph.D.)

.....................................Thesis Advisor

(Assistant Professor Sukkaneste Tungasmita, Ph.D.)

.....................................Thesis Co-Advisor

(Assistant Professor Satreerat Kampangkeaw Hodak, Ph.D.)

.....................................Examiner

(Chanwit Chityuttakan, Ph.D.)

.....................................External Examiner

(Associate Professor Surasing Chaiyakun, Ph.D.)

ภาสิต หงษ์ทอง : ผลของอุณหภูมิต่อการหาลักษณะเฉพาะของฟิล์มไฮดรอกซีอะพาไทต์ที่เตรียมโดยวิธีโซล-เจล. (TEMPERATURE EFFECTS ON CHARACTERIZATIONS OF HYDROXYAPATITE FILMS PREPARED BY SOL-GEL METHOD) อ.ที่ปรึกษาวิทยานิพนธ์หลัก: ผศ.ดร.สุคคเณศ ตุงคะสมิต อ.ที่ปรึกษาวิทยานิพนธ์ร่วม: ผศ.ดร.สตรีรัตน์ กำแพงแก้ว โฮดัค, 77 หน้า.

ในวิทยานิพนธ์ ไฮดรอกซีอะพาไทต์ (HAp) ถูกสังเคราะห์ในรูปของผงและฟิล์มโดยเทคนิคโซล-เจล วิธี spin coating ถูกใช้ในการเคลือบชั้น HAp บนวัสดุรองรับซิลิกอน และ สเตนเลส สตีล 316L ฟิล์ม HAp ถูกเผาที่อุณหภูมิ 300, 500, 700 , 900 และ 1,100°C ผลการทดลองแสดงว่าโครงสร้างได้พัฒนาจนมีความเป็นผลึกมากขึ้น เมื่ออุณหภูมิเพิ่มสูงขึ้น เฟสของ HAp สลายตัวเป็น เฟส β-TCP ที่ 1,100°C ภาพจากกล้องจุลทรรศน์อิเล็กตรอนแสดงว่า ขนาดของผลึกเพิ่มขึ้นเมื่ออุณหภูมิเพิ่มขึ้นถึง 1,100°C และโครงสร้างจุลภาคของ HAp มีโครงสร้างที่พรุน ค่าเฉลี่ยของค่าความแข็งและโมดูลัสยืดหยุ่นของฟิล์ม HAp มีค่าประมาณ 1.2 และ 35 GPa ตามลำดับ โดยไม่มีนัยสำคัญกับอุณหภูมิในการเผา ไฮดรอกซีอะพาไทต์ที่ถูกแทนที่โดยสตรอนเทียม(SrHAp) ถูกสร้างขึ้นโดยวิธี โซล-เจลเพื่อเพิ่มสมบัติพิเศษ การเพิ่มขึ้นของการแทนที่สทอนเทียมในแคลเซียมแสดงการขยายตัวของ โครงสร้างผลึกอธิบายได้จากการเพิ่มขึ้นแบบเส้นตรงของ ค่าคงที่โครงผลึกโครงสร้างจุลภาคของฟิล์ม SrHAp ที่เผาที่ 300 และ 500°C นั้นแสดงให้เห็นว่าส่วนใหญ่มีลักษณะเป็นแท่ง และ จากนั้นขนาดของผลึกใหญ่ขึ้นเมื่ออุณหภูมิสูงขึ้นและเป็นโครงสร้างที่เชื่อมติดกัน ฟิล์ม HAp/TiO_2 คอมโพสิท ถูกเตรียมโดยการเพิ่มอนุภาค TiO_2 ลงไปใน HAp โซล 20 เปอร์เซ็นต์โดยปริมาตร จากผลของ XRD พบว่า เฟสของ TiO_2 คือ อะนาเทส ที่อุณหภูมิต่ำกว่า 500°C และมีการเปลี่ยนเฟสเป็น รูไทล์ ที่อุณหภูมิสูงกว่า สามารถสังเกตเห็นได้ว่าอนุภาค TiO_2 มีขนาดระดับนาโนและเชื่อมกับโครงสร้างของ HAp HAp ถูกเสริมแรงโดยอนุภาค TiO_2 ซึ่งสังเกตได้จากค่าความแข็งและโมดูลัสยืดหยุ่นที่มีค่าเพิ่มขึ้น

ภาควิชา.............ฟิสิกส์.............. ลายมือชื่อนิสิต.......ภาสิต หงษ์ทอง..............

สาขาวิชา...........ฟิสิกส์.............. ลายมือชื่ออ.ที่ปรึกษาวิทยานิพนธ์หลัก...............

ปีการศึกษา.........2552................ ลายมือชื่ออ.ที่ปรึกษาวิทยานิพนธ์ร่วม.....Satreerat Hodak.....

4972434523: MAJOR PHYSICS

KEYWORDS: HYDROXYAPATITE / SOL-GEL / SrHAp / TiO_2

BHASIT   HONGTHONG: TEMPERATURE   EFFECTS   ON CHARACTERIZATIONS OF HYDROXYAPATITE FILMS PREPARED BY SOL-GEL METHOD.   THESIS ADVISOR: ASST. PROF. SUKKANESTE TUNGASMITA, PH.D., THESIS CO-ADVISOR: ASST. PROF. SATREERAT KAMPANGKEAW HODAK, PH.D., 77 pp.

In the thesis, hydroxyapatite (HAp) was synthesized in the form of powder and thin film by the sol-gel technique. The spin coating method has been used for the deposition of HAp layer on silicon and stainless steel 316L substrates. The HAp films were annealed at 300, 500, 700, 900 and 1,100°C. The results showed the structure development toward more crystalline with an increasing of the temperature. The HAp phase decomposed to β-TCP phase at 1,100 °C. The SEM micrographs showed that the crystal size increased with an increasing of annealing temperature to 1,100 °C and the microstructure of HAp contained a porous structure. The average values of hardness and elastic modulus of HAp films are about 1.2 and 35 GPa, respectively, no significant effects to the annealing temperatures. Strontium-substituted hydroxyapatite (SrHAp) was fabricated to improve a special property. Increasing Sr substitution for Ca exhibited the expansion of the crystal structure, explained by a linear increasing in lattice parameters. The microstructure of SrHAp film annealed at 300 and 500°C exhibited almost rod shape, and then grain size expanded at high annealing temperature with a development of cross-linking structure. The HAp/TiO_2 composite films were also prepared by adding 20% volume of TiO_2 particle to HAp sol. From XRD results, phase of TiO_2 was anatase at temperature below 500°C and transformed to rutile phase at above. The TiO_2 particles can be seen in nano-size linking with HAp structure. HAp was reinforced by TiO_2 inclusions resulting an increasing in hardness and elastic modulus.

Department: ....Physics.......   Student's Signature...Bhasit Hongthong........

Field of Study: ...Physics.......   Advisor's Signature...Sukkaneste Tungasmita...

Academic Year: .2009...........   Co-Advisor's Signature...Satreerat Hodak...

Acknowledgements

First of all, I am pleased and grateful for Associate Professor Dr. Prapaipan Chantikul that she is my inspiration and her work is excellent background knowledge in my work.

I would like to express my sincere gratitude to Assistant Professor Dr. Sukkaneste Tungasmita and Assistant Professor Dr. Satreerat Kampangkeaw Hodak for guidance, valuable suggestions, useful discussions and encouragement throughout my study.

I would like to thank Associate Professor Dr. Wichit Sritrakool, Dr.Chanwit Chityuttakan, and Associate Professor Dr. Surasing Chaiyakun for serving as chairman and committee, respectively. Their comments on this thesis are also greatly appreciated.

I would like to thank Advanced Materials Physics Research Group (AMPRG) especially Assistant Professor Dr. Sakuntam Sanorpim for looking after in the Lab. Sincere thanks are extended to Dr. Piyabut Burikham for chairing experience outside the Lab. Moreover, I would like to thank Mr. Thanakorn Tepamat and Mr. Manop Tiraratanasomphod for their helpful cooperation in using SEM and XRD, respectively.

I would like to acknowledge the financial supports from the Graduate School, and Department of Physics, Faculty of Science for providing teaching and paying fund to attend conferences. Special thanks go to Development and Promotion of Science and Technology talents project (DPST) that gives me an occasion to learn physics from 2001 until 2007.

I would like to thank every friend of mine in Department of Physics, Faculty of Science, Chulalongkorn University, friends from the former school or university, friends from other laboratories or departments for useful discussion, helping, nice friendship, playing football for relaxation and joyful moment after class at everywhere.

Finally, I would like to sincerely thank to my family for love, understanding, supports and everything.

Contents

List of Tables

List of Figures

Figure   **Page**

Figure   **Page**

CHAPTER I

INTRODUCTION

1.1   Biomaterials

Biomaterials are defined as any substance, other than a drug, or combination of substances, synthetic or natural in original, which can be used for any period of time, as a whole or as a part of a system which treats, or replaces any tissue, organ or function of the body [1]. In addition, biomaterials must be compatible with the body, and there are often issues of biocompatibility. Biomaterials are also used in joint replacements, artificial ligaments and tendons, heart valves, and also in dental implants. With today medical technology, lost organs may be replaced by utilizing biomaterials.

All the materials implanted in the body can elicit responses from living tissue. There are four possible responses of living tissue to the implants [2]: (1) The surrounding tissue dies due to the toxicity of the materials when they are implanted. These toxic materials should not be used as biomaterials. (2) The living tissue is compatible with the implanted materials. However, such implanted materials are encapsulated by dense fibrous tissue, which prevents distribution of stresses and may cause loosening of the implant. Such material is referred as *the nontoxic and biological inactive biomaterials*. (3) The living tissue is not only compatible with the implanted material, but it also binds to the implant, thus forming tight natural bonding between the implant and the surrounding tissue. Such materials would be referred as *the biocompatible and surface-active biomaterials*. (4) The material is nontoxic and dissolves with the surrounding tissue. Such materials would be classified as *resorbable biomaterials*.

Nowadays, varieties of materials have been used as the implants depend on their ability to sustain high stresses. Some metals are used for heavy load-bearing orthopedic implantation. However, many problems have been encountered when metallic materials are used as implantations, such as wear, corrosion and/or negative tissue reactions. In addition, most of metallic implants are encapsulated by dense fibrous tissue that prevents distribution of stresses and may cause loosening of the implantation [3].

Since modern bioceramics are compatible with physiological environments [1,2], various ceramics have been medically used for implantations. The compatibility of bioceramics is the result of the fact that they compose of ions usually found in the physiological environment, such as calcium, potassium and sodium ions. They also show very limited toxic to body tissue. Thus bioceramics do not cause inflammatory or rejection response by the body. This advantage makes bioceramics become more attraction in many medical applications.

1.2 Hydroxyapatite as Bioactive Material

Apatite materials are a family of inorganic crystalline compounds, which are general formula $M_{10}(XO_4)_6Y_2$. M is usually a bivalent cation, such as Ca^{2+}, Sr^{2+}, Ba^{2+}, Cd^{2+}, Pb^{2+}, but monovalent and trivalent cations, such as Na^+, K^+ and Al^{3+}, can be hosted as well. XO_4 is usually PO_4^{3-}, VO_4^{3-} or AsO_4^{3-}, but the possible substitutions also include SiO_4^{4-}, CO_3^{2-} and SO_4^{2-}. Y is a monovalent anion, OH^-, F^-, Cl^-, Br^-[4]. Apatites are widely spread in nature, for example, the inorganic phase of hard tissues of vertebrates is assimilated to the synthetic hydroxyapatite.

In 1971, hydroxyapatite was proposed by Monroe et al [5]. for using as hard tissue replacement. The major interest of hydorxyapatite [HAp; chemical formula $Ca_{10}(PO_4)_6(OH)_2$], arises from the fact that HAp crystals are the main mineral constituent of vertebrate skeletal systems, comprising 60 to 70 percent of bone and 98 percent of dental enamel. HAp has now been proven to be the most biocompatible, non-bioresorbable and surface active implants [6]. HAp is one of few materials that are classed as bioactive, meaning that it will support bone

ingrowth and osseointegration when used in orthopaedic, dental and maxillofacial applications. Bone and dental implants that made of HAp are naturally bonded tightly to bone or teeth without having to use mechanical interlocking or biological cements. Due to these advantages of HAp over other biomaterials, it is a challengeable material to be developed for using in orthopedic and dental surgeries, such as hip joints, jaw augmentation and tooth root replacement.

Unfortunately, brittleness of the material limits the ultimate usefulness of HAp. The fracture toughness (K_c) of HAp does not exceed the value of about 1.0 MPam$^{1/2}$ where K_c of human bone has the value of 2-12 MPam$^{1/2}$[7,8]. For this mechanical property reasons, HAp ceramics can not be used as heavy-loaded implants. Therefore, various attempts have been made to improve the mechanical properties of HAp. For example, various reinforcements, including whiskers[9], fibers[10], particles[11], have been dispersed into the HAp matrix. These HAp composites possess higher mechanical properties, but may lead to decrease of biocompatibility. Coatings of HAp are often applied to metallic implants (most commonly titanium/titanium alloys and stainless steels) to alter the surface properties. The coating methods, such as plasma spray, pulsed-laser deposition, electrodeposition, sol-gel processing, have been commonly used to produce thin film form of the material.

1.2.1 Hydroxyapatite structure

The crystal structure of HAp was previously reported to belong to the space group P6$_3$/m in the hexagonal system with the lattice parameters, a = 9.432 Å and c = 6.881 Å. A simplified unit cell of HAp is shown in Fig. 1.1, in which oxygen atoms form the tetrahedron of PO$_4$. Calcium ions occupy two different sites; the column Ca (CaI) at z = 0, 1/2 and the screw axis Ca (CaII) at z = 1/4 and 3/4 [12].

1.3 Strontium-Substituted Hydroxyapatite

According to the previous topic, a bivalent cation, such as Sr^{2+}, Ba^{2+}, Zn^{2+}, Pb^{2+}, can be replaced Ca^{2+} in hydroxyapatite [4,13,14]. Among these cations, strontium has attracted a remarkable interest because of its chemical and physical properties similarly to calcium. In particular, strontium ions (Sr^{2+}) have been examined in the field of osteoporosis treatment due to its inhibition of bone resorption and stimulation of bone formation. Strontium is also present in the mineral phase of the bone. Even 99% of the total amount of Sr in the body is localized in bone, the total amount of Sr in the skeleton is only 3.5% of the Ca molar content [15]. Strontium partially substituted hydroxyapatite is represented as $Sr_{10-x}Ca_x(PO_4)_6(OH)_2$, where $0 \leq x \leq 10$, while $Sr_{10}(PO_4)_6(OH)_2$ is called strontium hydroxyapatite (SrHAp). In addition, it has been reported that strontium can improve the mechanical properties [16]. There are many *in-vitro* and *in-vivo* studies indicated that strontium can increases bone formation and reduces bone resorption [15,17].
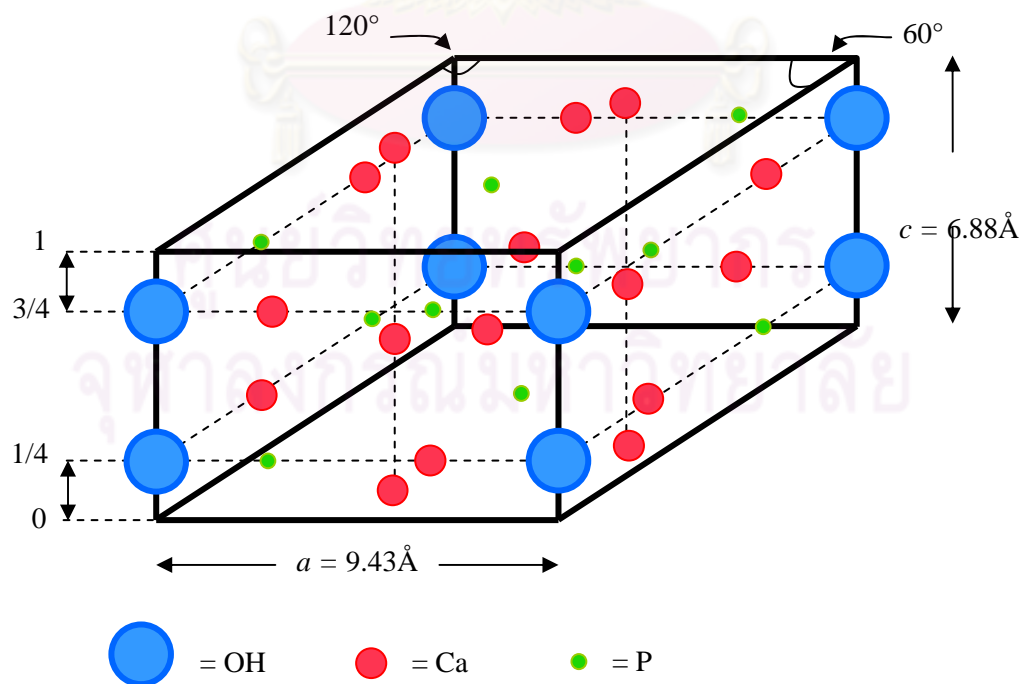
Figure 1: The unit cell of hydroxyapatite

1.4 Objectives and Scope of This Work

The scope of this work is first to synthesize HAp by using the synthesis method from the previous work [18]. The product will be used as a reference, in order to check the structure and composition of the HAp material. Then, we propose to transform HAp to be thin film form on silicon and stainless steel 316L substrates by sol-gel spin coating technique. To enhance the knowledge of the fundamental physics, the below topics are mainly focused.

I. Effects of annealing temperatures on the crystal structure, microstructure, grain size and elemental compositions. To study these phenomenons, the specimens are characterized by using x-ray diffraction (XRD), scanning electron microscopy (SEM) and energy dispersive x-ray spectroscopy (EDS).

II. To improve the properties of HAp, Ca-atoms in the HAp structure was substituted by strontium atom, called SrHAp. It has been investigated the crystal structure and microstructure after substitution by XRD, SEM and EDS. An antibacterial test was performed.

III. It is also necessary to investigate the mechanical properties, the hardness and elastic modulus of HAp film, were measured by nanoindentation method. To improve the mechanical property, HAp/TiO$_2$ composite films have been fabricated and measured the mechanical properties comparison with HAp films.

CHAPTER II
SOL-GEL PROCESSING

Sol-gel processing methods were first used historically for decorative and constructional materials. In the last century many new applications were developed some examples of scientific basis became available. Today sol-gel methods are reaching their full potential, so these were studied in the areas of chemistry, physics and materials science. The specific uses of sol-gel products are derived from the various material shapes, such as monoliths, films, fibers, and powders. Many specific applications including optics, protective and porous films, optical coatings, window insulators, dielectric and electronic coatings, high temperature semiconductors, reinforcement fibers, fillers, and catalysts, all of these can now be produced by sol-gel techniques. In this chapter, we explain the terms that concern in sol-gel, and the process of sol-gel which consist of hydrolysis, condensation, drying and sintering. The sol-gel coating methods spin coating and dip coating will be described in this chapter.

2.1 Sols, Gels and Gelation

First, the definitions of some words are defined before studying in sol-gel process. A *sol* is a stable suspension of colloidal particles within a liquid [19]. The solid particles must be small enough for the forces responsible of dispersion to be greater than those of gravity. Moreover, these particles must include a number of atoms macroscopically significant. Originally, colloidal only referred to macroscopic particles. However, this definition did not give limited and values of the size range of the particle concerned. Practically, particles in a colloidal sol must have a size between 2nm and 0.2μm. The solvent used to disperse the

colloidal particles of a sol is often either pure water or a solution composed mostly of water. Nevertheless, other solvents such as alcohol can also be used.

A *gel* is a porous 3-dimensionally interconnected solid network that expands throughout a liquid medium [19]. If the solid network is made of colloidal sol particles the gel is said to be colloidal. If the solid network is made of sub-colloidal chemical units then the gel is polymer. The nature of gels depends on the coexistence between the solid network and the liquid medium. If the liquid is mostly composed of water, then the corresponding gel is called *an aquagel (or hydrogel)*. If the liquid phase is largely composed of an alcohol then the gel is *an alcogel*. Finally, if most of the liquid is removed, then the brittle solid obtained is either called *a xerogel* or *an aerogel*, depending on the drying method.

Gelation is a process according to which a sol, or a solution, transforms to a gel. It consists of establishing links between the sol particles, or the solution molecules, so as to form a 3-dimensional solid network. A sol, or a solution, can be transformed into a colloidal gel by going through what is called a gel-point. Practically, it is at this point that the sol abruptly changes from a viscous liquid state to a solid phase called the gel. This gel-point and the properties of sols and gels near this point are now known as "theory of critical phenomena".

2.2   Sol-Gel Process

The sol-gel process is a wet-chemical technique widely used recently in the fields of materials science and ceramic engineering. The sol-gel process involves the evolution of organic or inorganic networks through the formation of a colloidal suspension (sol) and gelation of the sol to form a network in a continuous liquid phase (gel). If inorganic sols and gels can be obtained by various methods, they are often directly synthesized from chemical reactants dissolved in a liquid medium. The chemical reactant which contains the cation M present in the final inorganic sol or gel is called *the chemical precursor*. Two main groups are therefore distinguished: the metal salts and the alkoxides. The general formula of a matallic salt is M_mX_n where M is the metal, X an anionic group, and m and n stoichiometric coefficients. As for aloxides, their general

formula is M(OR)$_n$, which indicates that they are a combination of a cation M with n alcohol groups ROH [20].

In sol-gel processing, when metal salts are used, they are often dissolved in an aqueous medium. The metal salt MX dissociates into ions which disperse in the solution, and the anions negative charge X^{z-} balances the positive charge of the metal atom M^{z+}. The cation and the anion then have the same absolute formal charge z. Since water has a dipolar moment, the positive charge z+ of the cation attracts the partial negative charge, which is the oxygen atom, of H$_2$O molecules [19]. As a consequence, the cation is entrapped by a number of water molecules that shown in Fig. 2.1.

In general, the sol-gel process involves the following steps. The first step of any sol-gel process always consists in selecting the precursors of the wanted materials. Then, the hydrolysis of precursor and condensation occur respectively. Finally, drying and sintering are employed.

2.2.1 Hydrolysis

Hydrolysis is the deprotonation of a solvated metal cation. It consists in the loss of a proton by one or more of the water molecules that surrounds the metal M. Generally, for alkoxide, the hydrolysis reaction replaces alkoxide groups(OR) with hydroxyl groups(OH). When there is no acid or base catalyst presented, alkoxides react first by hydrolysis involving nucleophilic addition of a water molecule followed by proton transfer from water to the alkoxy group which then leaves as alcohol (Fig. 2.2) [20].

2.2.2 Condensation

In condensation, or polymerization, one of the ligands acts as an attacking group for linking with a second metal species and one of the existing ligand groups may act as a leaving group. Two mononuclear complexes of M, each comprising only one metal atom M, can react with one another in a polymerization reaction in order to form a polynuclear complex consisting of two metal atoms. Condensation generally occurs if at least one hydroxo ligand(OH) is

bounded to the cation M. The first step of any condensation reaction always includes the construction of an "ol" bridge, called *condensation by olation*. There is condensation by oxolation, an "ol" bridge is first established between the two metal atoms before transforming into an "oxo" bridge. Fig. 2.3 is shown the step by step of condensation [20].
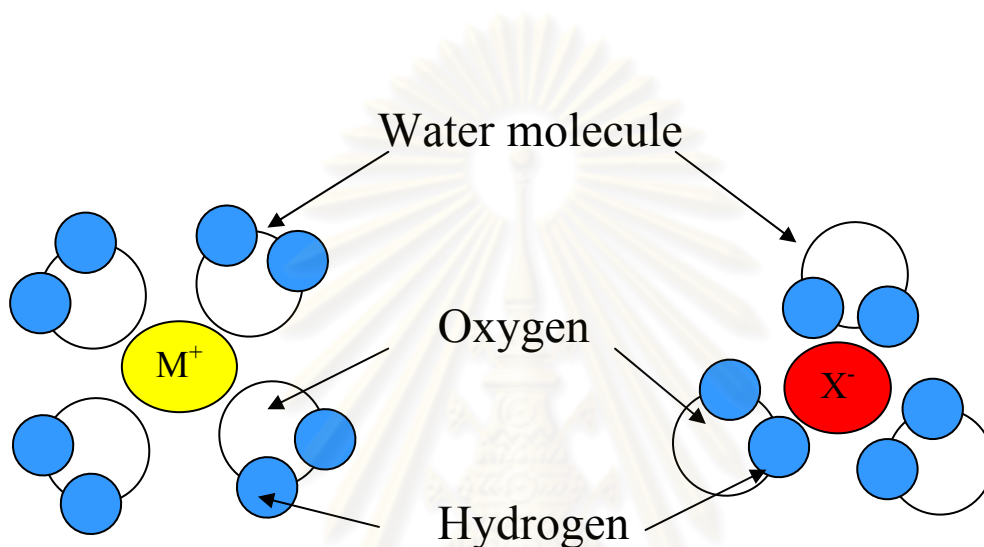
Figure 2.1: The attractions of a cation(M^+), an anion(X^-) and water molecules
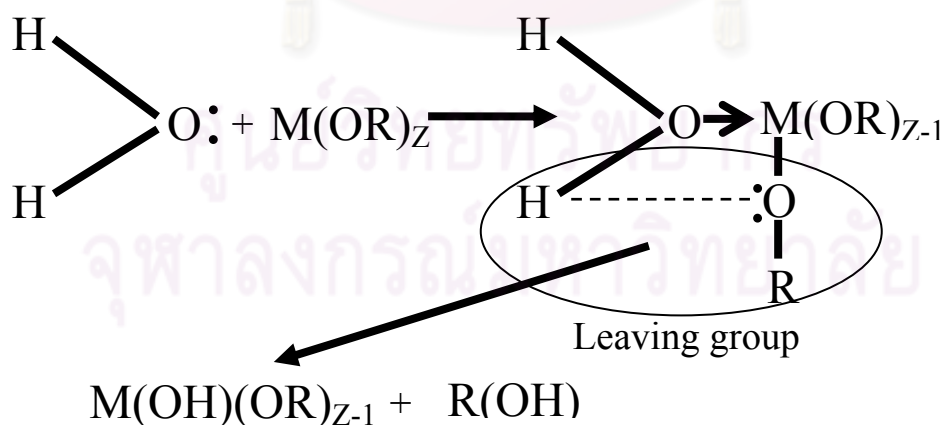
Figure 2.2: The mechanism of hydrolysis consist in a substitution in which a water molecule attacks the alkoxide

$$M\text{—}OH + M\text{—}OH \longrightarrow M\text{—}O\text{—}M\text{—}OH$$

H --- proton transfer

nucleophilic attack

"ol" bridge

$$M\text{—}O\text{—}M\text{—}OH_2 \longrightarrow M\text{—}O\text{—}M + H_2O$$

Leaving group

"oxo" bridge
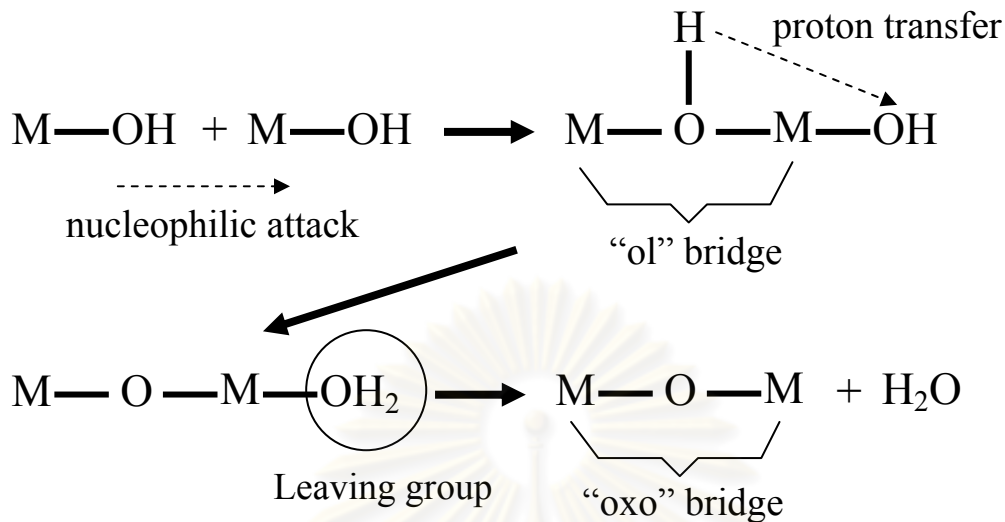
Figure 2.3: The mechanism of condensation

2.2.3 Drying

All particles in a formed moist body are surrounded by liquid medium. The particles move closer together as the water is removed and then, a volume reduction takes place. This is referred to drying process. In this step, the drying temperature should be high enough to remove the free alcohol, water, catalyst and other compound. The critical problem in drying is cracking can built up from stresses. The film consists of two phases, the solid phase and connected pores filled with liquid phase. The liquid is removed from pores during drying process. The surface tensile stress and cracks begin to propagate which result from driving forces for liquid transport. In addition, the chemical or physical interaction of liquids with pore walls is a crucial cause of the capillary forces and the stress formation [21].

2.2.4 Sintering

There is only a small degree of bonding between the particles of the material. The ceramic bonding, and the very high strength associated with it, is obtained only when sintering at high temperatures. Sintering (Firing) of materials is the method involving consolidation of particles by heating the sample part to a high temperature below the melting point, when the material of the separate particles difuse to the neighboring particles. The processes that occur during the

sintering of the materials, Fig. 2.4, are very complex. The sintering rate is dependent on purity, grain size, compaction and the sintering atmosphere. During the diffusion process the pores, taking place in the sample, diminish or even close up, resulting in densification of the part, improvement of its mechanical properties. Decreasing of the porosity that caused by the sintering process, can be determined by the level of the initial porosity of the green compact, sintering temperature and time. Through reactions that occur during sintering, a strengthening and densification of the ceramic takes place, resulting in a reduction in porosity. This process results in a volume reduction; this is called *sintering shrinkage*. The amount of shrinkage for the various materials is widely different. Similar to drying, well-defined times and suitable atmospheres are required when firing products. Thinner shapes and densely formed products behave better and can be sintered faster than large ones with greater wall thickness [21].
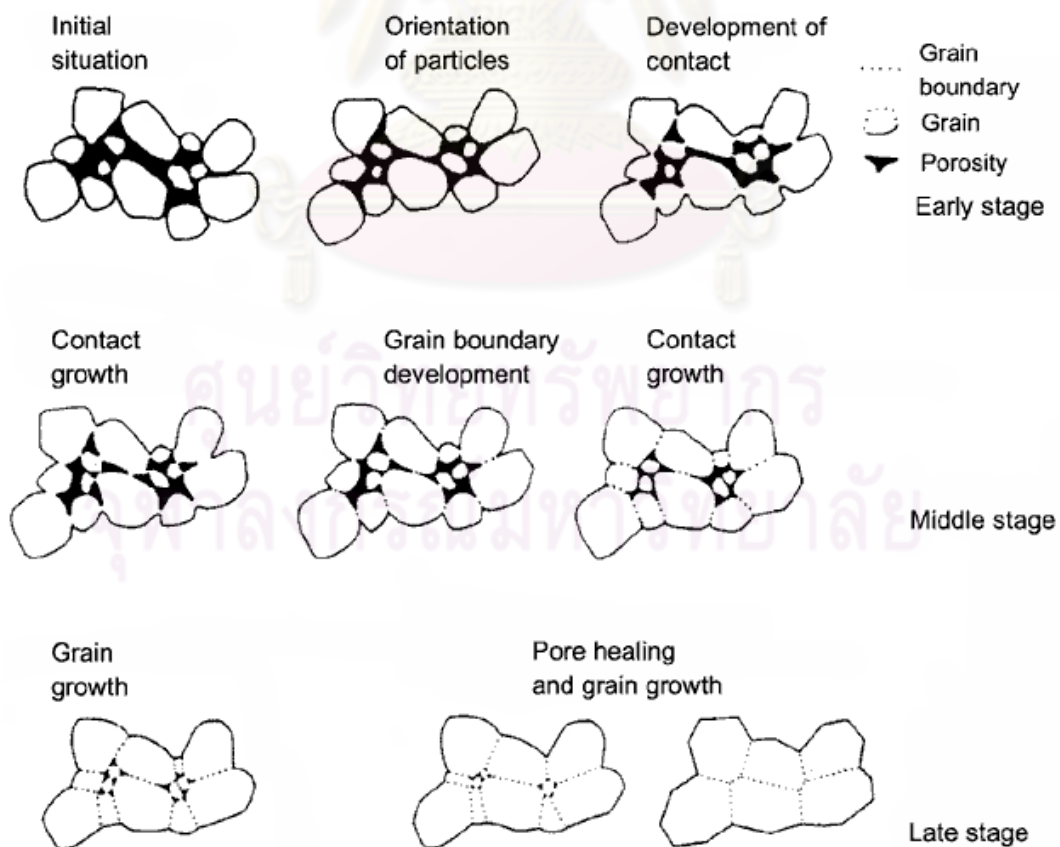
Figure 2.4: Grain growth during the sintering process [21]

2.3   Sol-Gel Coating Methods

Several methods can be used to make sol-gel coatings with the sol-gel process. Spin coating and dip coating are two basic techniques used to deposit sol-gel coating materials. Spin coating produces a one-sided coating, while dip coating yields a double-sided coating. Both techniques are used in manufacturing to make different coating and thin film. Roll coating is another coating technique and is widely used for industrial coatings, especially for flexible substrates. It can make coatings at a speed up to 200 ft a minute.[19]

2.3.1 Spin coating

Spin coating is used for many applications where relatively flat substrates or objects are coated with thin layers of material. An amount of a solution is placed on the substrate, which is then rotated at high speed in order to spread the fluid by centrifugal force. Rotation is continued while the fluid spins off the edges of the substrate, until the thickness of the film is achieved. The applied solvent is usually volatile, and simultaneously evaporates. So, the higher the angular speed of spinning, the thinner the film. The thickness of the film also depends on the concentration of the solution and the solvent. Stages of spin coating are shown following these steps and demonstrated in Fig. 2.5.[19]

- Deposition of the coating fluid onto the wafer or substrate. This can be done by using a nozzle and pouring the coating solution or by spraying it onto the surface. A substantial excess of coating solution is usually applied compared to the amount that is required.
- The substrate is accelerated up to its final, desired, rotation speed
- The substrate is spinning at a constant rate and fluid viscous forces dominate the fluid thinning behavior.
- The substrate is spinning at a constant rate and solvent evaporation dominates the coating thinning behavior

2.3.2 Dip coating

Dip coating is a process where the substrate to be coated is immersed in a liquid and then withdrawn with a well-defined withdrawal speed under controlled temperature and atmospheric conditions. The coating thickness is mainly defined by the withdrawn speed, the solid content and the viscosity of the liquid. It may be divided in five stages: immersion, start-up, deposition, evaporation and drainage. In the dip coating method the substrate is slowly dipped into and withdrawn from a tank containing the sol, with a uniform velocity, in order to obtain a uniform coating. It is a popular way of creating thin film coated materials along with the spin coating technique. The dip coating process can be, generally, separated into three stages and shown in Fig 2.6.[19]

- Immersion: the substrate is immersed in the solution of the coating material at a constant speed preferably judder free.
- Dwell time: the substrate remains fully immersed and motionless to allow for the coating material to apply itself to the substrate
- Withdrawal: the substrate is withdrawn from the tank again at a constant speed to avoid any shake.

2.4   Advantages and Limitations of Sol-Gel Processing

There are many advantages to sol-gel processing [20]

- Sol-gel processing not only allows for materials to have any oxide composition, but it also permits the production of organic-inorganic materials.
- Very pure products are obtained by purifying the precursors.
- The thermal degradation of any materials is minimized with higher purity and stoichiometry since the temperature required in the process is low.
- The growth of the colloidal particles can be controlled in order to give particles with given shape, size, and size distribution.
- The association of the solid colloidal state with a liquid medium, thus avoiding any pollution by the dispersion of dust.

However, it should be noted that there are also some limitations from the sol-gel process. Those are [20]:

- The precursors are often expensive and sensitive to moisture especially for alkoxide. The sol-gel process is time consuming, particularly where careful aging and drying are required.
- It is likely to occur the problem of dimensional change, such as densification, stress cracking or cracking on drying.

      (a)   (b)   (c)
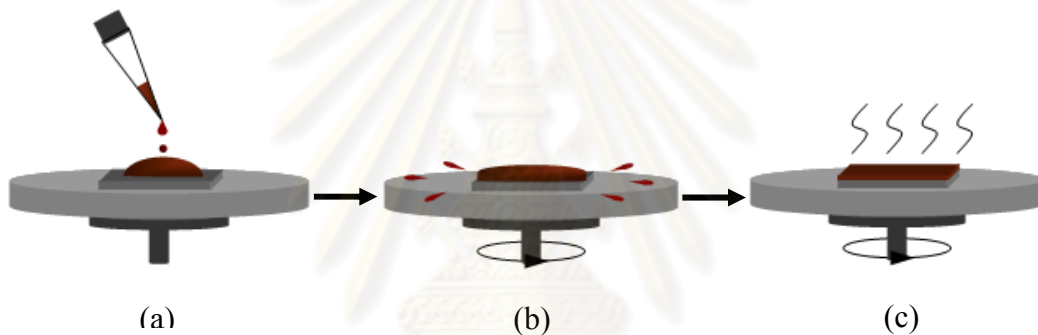
Figure 2.5: The spin coaing process begin with dropping (a), spinning (b) and evaporation(c)

    (a)   (b)   (c)   (d)
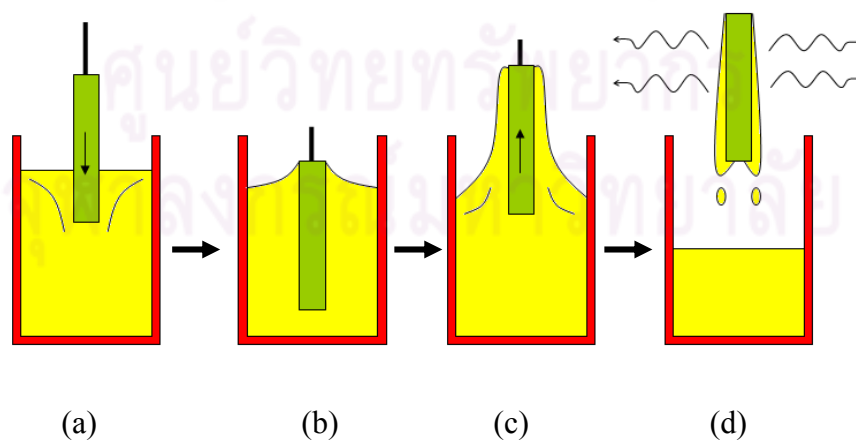
Figure 2.6: The dip coating process begins with immersion(a), dwelling(b), withdrawal(c) and evaporation(d)
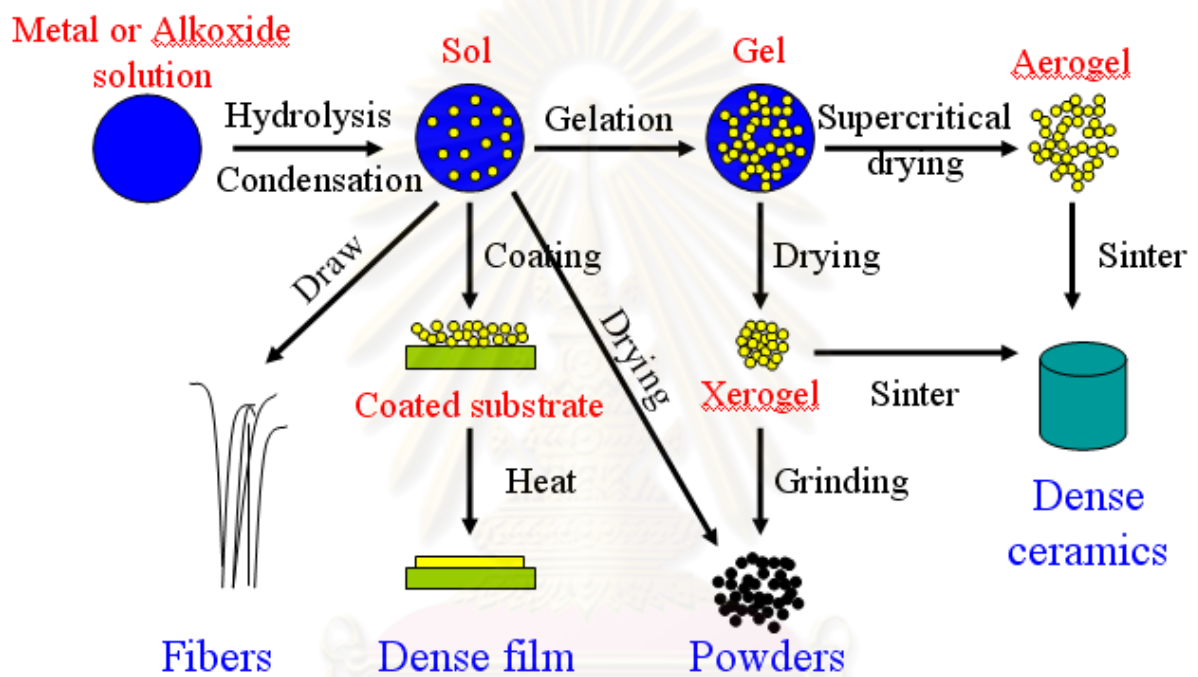
Figure 2.7: Summary of sol-gel from starting materials to final products

CHAPTER III

THEORETICAL BACKGROUND OF CHARACTERIZATION METHOD

There are several characterizations methods were used in this work, so the basic understandings of them are explained in this chapter. The essential characterizations of this chapter consist of scanning electron microscopy (SEM), energy dispersive x-ray spectroscopy (EDS), x-ray diffraction technique (XRD) and nanoindentation for mechanical properties.

3.1 Scanning Electron Microscopy (SEM)

Scanning electron microscope (SEM) is a type of electron microscope that images the sample surface or microstructure by scanning a high-energy beam of electrons throughout the surface. The first SEM image was obtained by Max Knoll, who in 1935 obtained an image of silicon steel showing electron channeling contrast. Further pioneering work on the physical principles of the SEM and beam specimen interactions was performed by Manfred von Ardenne in 1937, who produced a British patent but never made a practical instrument. The SEM was further developed by Professor Sir Charles Oatley and his postgraduate student Gary Stewart and was first marketed in 1965 by Cambridge Instrument Company [22].

3.1.1 Scanning process and image formation

There are many types of signals produced by an electron beam in SEM, e.g., secondary electrons, back-scattered electrons (BSE), characteristic x-rays, light (cathodoluminescence), specimen current and transmitted electrons (see Fig. 3.1). These types of signal all require specialized detectors that are not usually all present on a single machine. The signals result from interactions of the electron
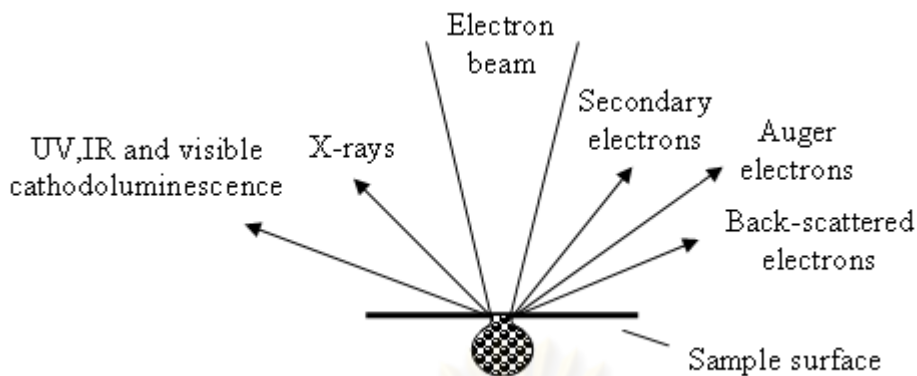
Figure 3.1: Schematic representation of the energies produced from electron beam

beam with atoms at or near the surface of the sample. As the primary electron beam interacts with the sample, the electrons lose energy by repeated random scattering and absorption within a teardrop-shaped volume inside the specimen known as the *interaction volume*. The energy exchange between the electrons and the sample results in the reflection of high-energy electrons by elastic scattering, emission of secondary electrons by inelastic scattering and the emission of electromagnetic radiation. The beam current absorbed by the specimen can also be detected and used to create images of the distribution of specimen current. Electronic amplifiers of various types are used to amplify the signals which are displayed as variations in brightness on a cathode ray tube. The raster scanning of the CRT display is synchronized with that of the beam on the specimen in the microscope, and the resulting image is therefore a distribution map of the intensity of the signal being emitted from the scanned area of the specimen. The image may be captured by photography from a high resolution cathode ray tube, but in modern machines is digitally captured by CCD and displayed on a monitor.

A basic diagram of SEM is shown in Fig. 3.2. The electron gun produces a beam of electrons that is attracted through the anode and condensed by the condenser lens and then focused as a very fine point on the specimen by the objective lens. A set of small coils of wire, called the scan coils, is located within the objective lens. The coils are energized by a varying voltage produced by the scan generator and create a magnetic field that defects the beam of electrons back and forth in a CRT or television receiver.
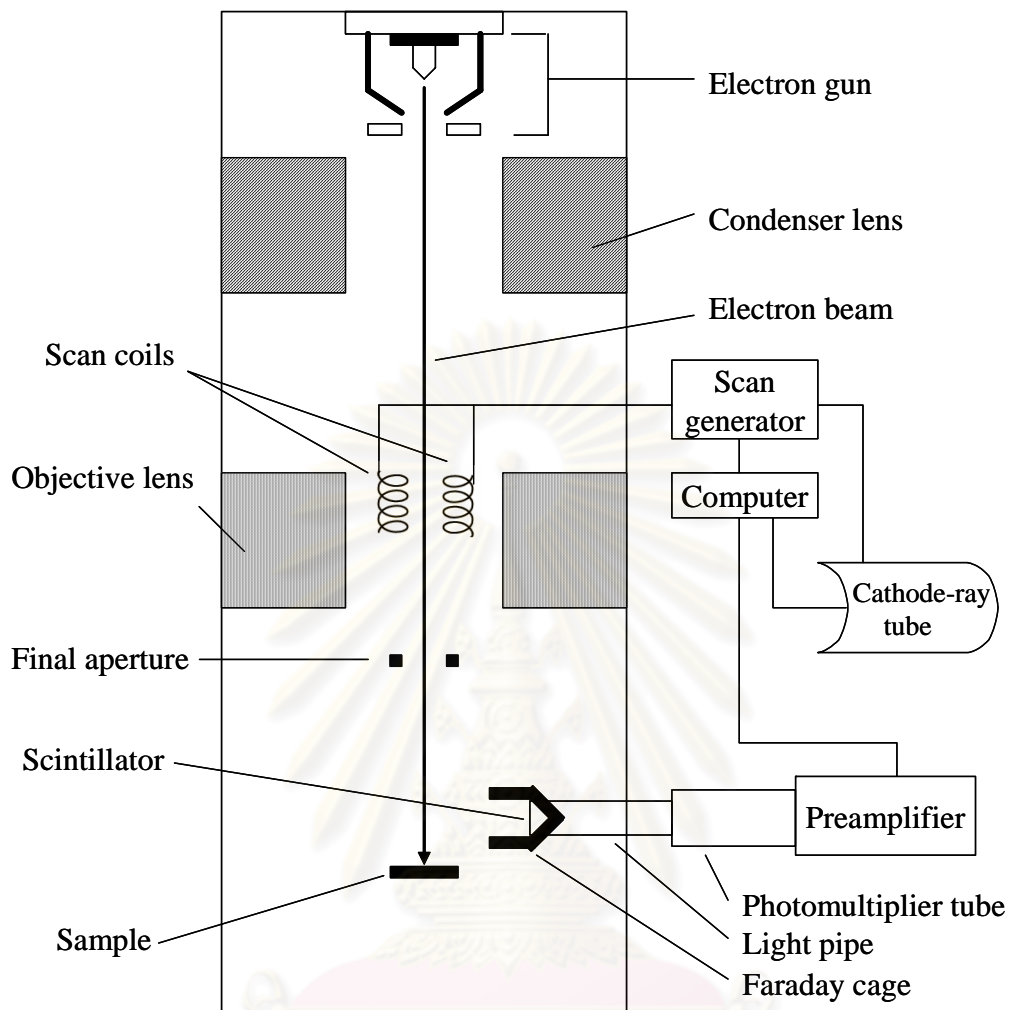
Figure 3.2: Schematic of a scanning electron microscope.

3.1.2 Interaction volume

When electron beam interacts with the atoms of the sample, each interaction causes the incident electron to change direction, and many interactions cause the lose of energy. The interaction is a scattering process in which there are no sharply defined limits to the extent of scattering (Fig. 3.3). For ease of illustration, a defined limit may be placed on the remaining incident electron energy and on the region of interaction illustrated. Such an illustration would describe the area in which the interactions are most likely to occur. The interaction volume is usually described as tea-drop or pear-shaped. In whole sample, the volume (both depth and width) of the interaction varies directly with the accelerating voltage (Fig. 3.4) and inversely with the average atomic number of the sample (Fig. 3.5).

3.1.3 Accelerating voltage

The accelerating voltage in most SEMs varies between several hundred volts up to forty thousand volts and has a tremendous effect on the images produced. In theory, a higher voltage gives better resolution because the reduction in wavelength of the beam of electrons enables a spot size of smaller diameter to be obtained. The interaction volume increases with increasing accelerating voltages (see also in Fig. 3.4) because of the greater energy of the beam of electrons. In general, hard specimens like metal may benefit from higher voltages, but most biological samples produce better images at lower voltages (low energy).

3.1.4 Working distance and aperture size affect depth of field and resolution

The beam of electrons is cone-shaped when it strikes the sample. The angle of the cone, and whether it is a wide cone or narrow cone, is determined by the diameter of the final apertures and the working distance. A final aperture with a small diameter produces a narrow cone of electrons, on the other hand, with a large diameter produces a wide cone (Fig. 3.6). Working distance is the distance between the objective lens and the sample. Most SEMs have a working distance that varies from about 10 mm. to 50 mm. A large working distance results in a narrow cone of electrons, a small one in wide cone (Fig 3.7). The angle of the cone is the most important factor in determining the depth of field at any given magnification. Depth of field is the amount of sample that is in acceptably sharp focus. The effect of the angle of the cone on depth of field is due to the fact that the focused beam of electrons normally scans not a flat sample, but a sample with a irregular surface.
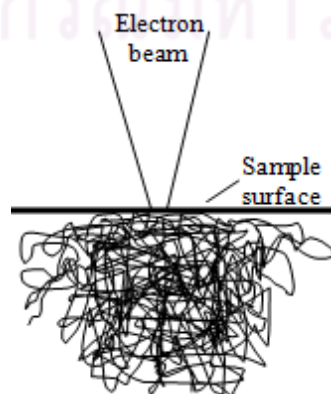
Figure 3.3: Scattering of beam electrons in the interior of a sample.
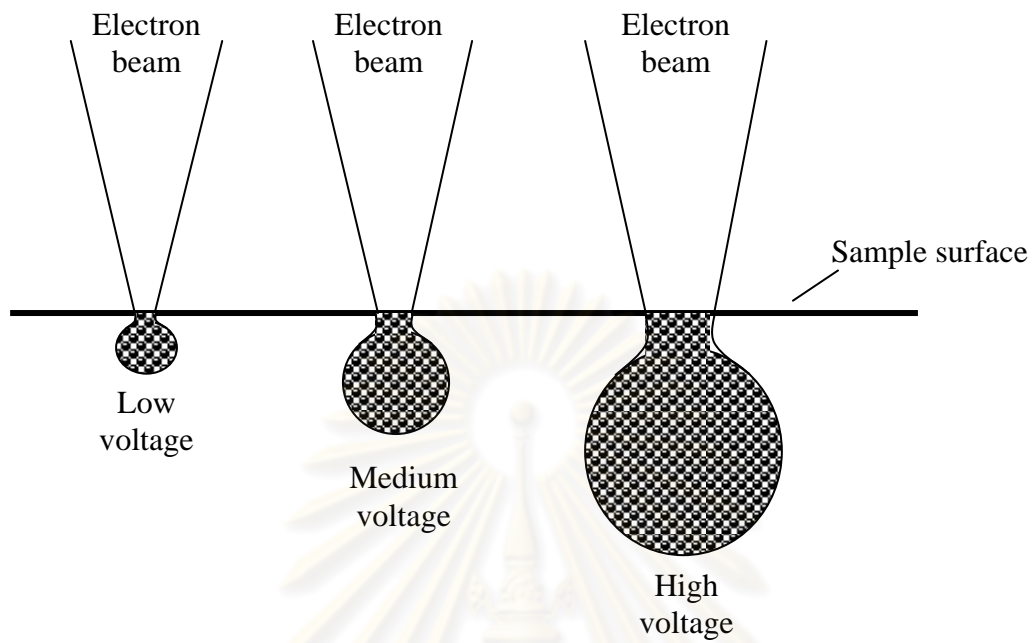
Figure 3.4: Interaction-volume variation with accelerating voltage.
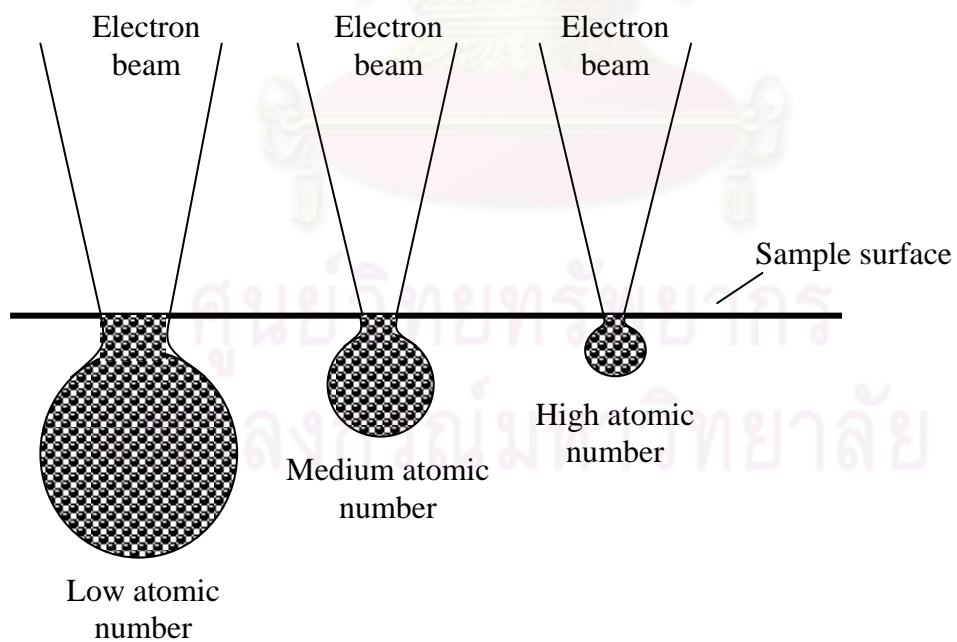
Figure 3.5: Interaction-volume variation with average atomic number of sample.
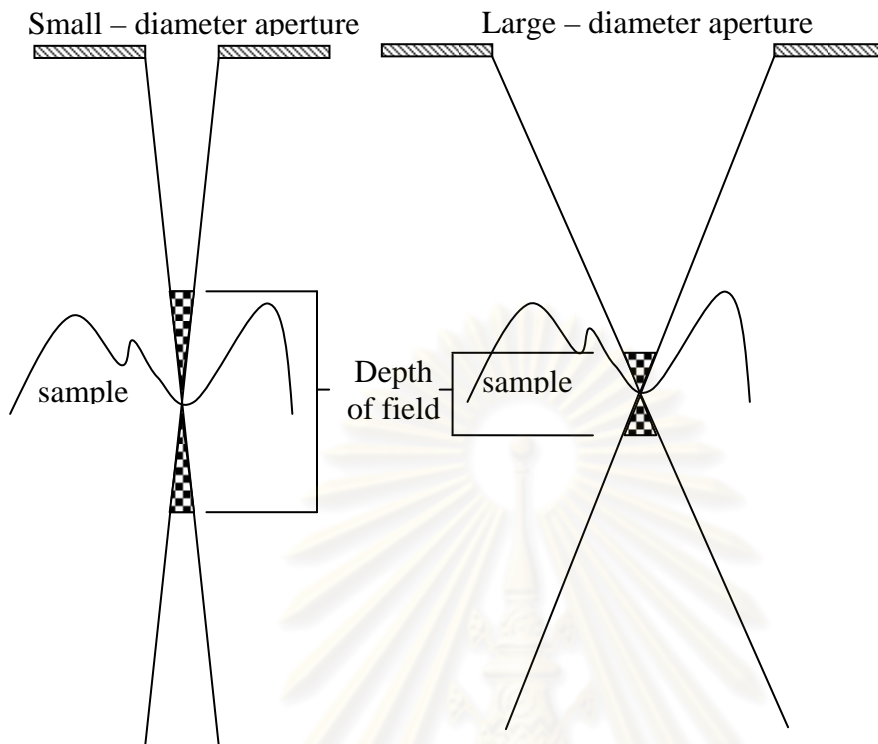
Figure 3.6: Aperture size and depth of field. The depth of field is greater with a final aperture of smaller diameter.
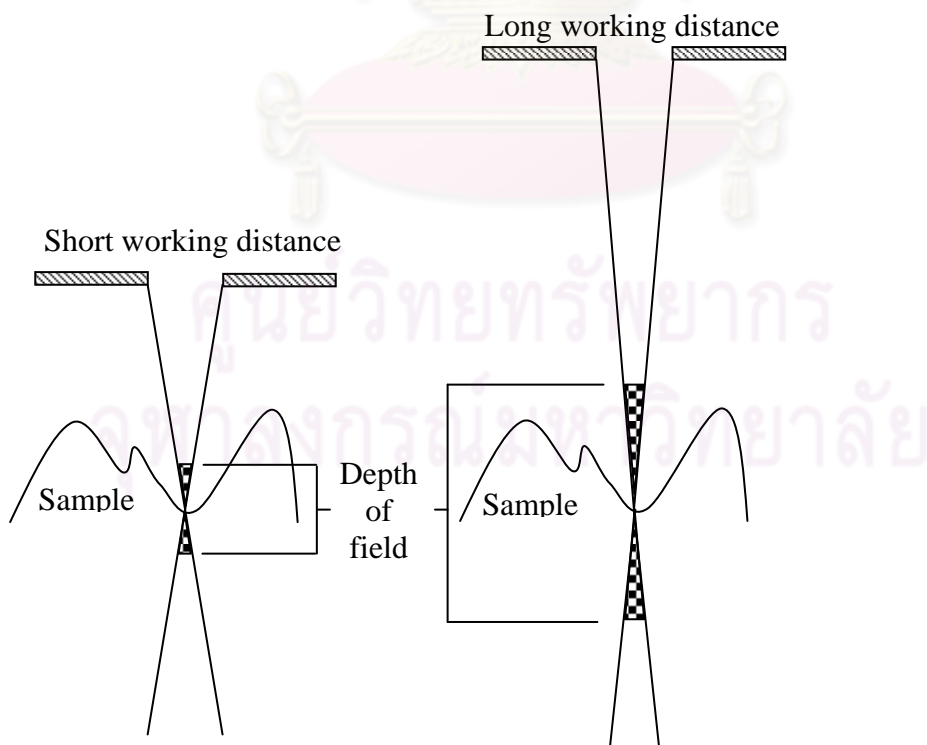
Figure 3.7: Working distance and depth of field. The depth of field is greater at long working distance.

3.2 Energy Dispersive X-ray Spectroscopy (EDS)

Due to the principle of a scanning electron microscope (SEM), the sample in this instrument is bombarded by an electron beam in order to obtain an image of the surface of the sample. At rest, an atom within the sample contains ground state (or unexcited) electrons in discrete energy levels or electron shells bound to the nucleus. The incident beam may excite electrons in an inner shell, ejecting them from the shell while creating hole where the electron was. An electron from an outer, higher-energy shell then fills the hole, and the difference in energy between the higher-energy shell and the lower energy shell may be released in the form of X-ray photons (Fig 3.8). The number and energy of the X-rays emitted from a specimen can be measured by an energy dispersive spectrometer. As the energy of the X-rays are characteristic of the difference in energy between the two shells, and of the atomic structure of the element from which they were emitted, this allows the elemental composition of the specimen to be measured [23].
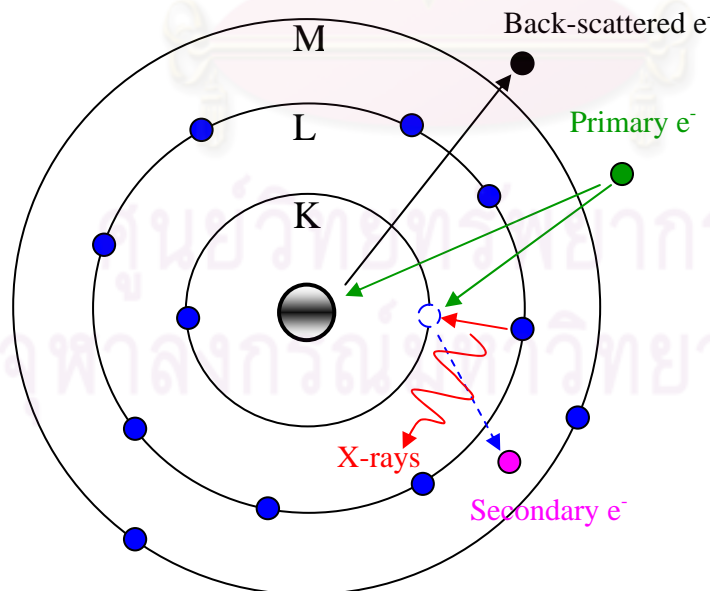
Figure 3.8: Schematic drawings of the x-ray radiation from an atom.

3.3 X-ray Diffraction Technique (XRD)

X-ray diffraction (XRD) is a technique used to characterize the crystallographic structure, grain size, preferred orientation in polycrystalline or powdered solid samples, chemical composition, and physical properties of materials and thin films. The diffraction technique is commonly used to identify unknown substances, by comparing diffraction data against a database maintained by the International Centre for Diffraction Data. The x-ray diffraction techniques are based on the elastic scattering of X-rays from structures that have long range order. These techniques are based on observing the scattered intensity of an X-ray beam hitting a sample as a function of incident and scattered angle, polarization, and wavelength or energy.

As the crystal lattice is a regular three-dimensional distribution (cubic, rhombic, etc.) of atoms in space. These are arranged so that they form a series of parallel planes separated from one another by a distance *d*, which varies according to the nature of the material. For any crystal, planes exist in a number of different orientations - each with its own specific *d*-spacing. When a monochromatic X-ray beam with wavelength is projected onto a crystalline material at an angle *theta (θ)*, diffraction occurs only when the distance traveled by the rays reflected from successive planes differs by a complete number *n* of wavelengths. By varying the angle *theta (θ)*, the Bragg's Law conditions, are satisfied by different *d*-spacings in crystalline materials.

$$2d_{hkl}\sin\theta = n\lambda \tag{3.1}$$

where *n* is an integer determined by the order given, λ is the wavelength of the X-rays, d_{hkl} is the spacing between the planes in the atomic lattice, and θ is the angle between the incident ray and the scattering planes(see Fig. 3.9). Plotting the angular positions and intensities of the resultant diffracted peaks of radiation produces a pattern, which is characteristic of the sample. Where a mixture of different phases is present, the resultant diffractogram is formed by addition of the individual patterns [24].
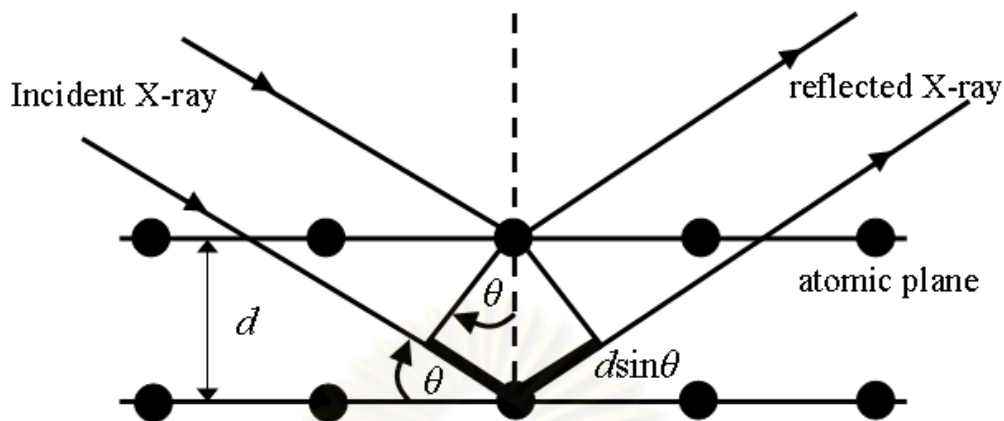
Figure 3.9: Schematic representation of x-ray scattering from a crystalline material.

3.4 Nanoindentation

Nanoindentation is a new method to characterize mechanical properties on a very small scale of materials, as well as thin films. The idea of nanoindentation arose from the realization that an indentation test is an excellent way to measure very small volumes of materials. In principle, if a very sharp tip is used, the contact area between the sample and the tip, and thus the volume of material that is tested, can be made arbitrarily small. The only problem is determining the indentation area. It is easy to make an indentation that is so small that it is difficult to see without a powerful microscope.

In this work, a Berkovich diamond tip, which is a three sided pyramid with a total included angle of 142.3° and a half angle of 65.35°, pressed into the sample with a known load. After some time, the load is removed, and then the area of the residual indentation in the sample is measured. A set of tools can be seen in the schematic of a nanoindentation (Fig. 3.10). As the load is increased, the indenter sinks into the material due to both elastic and plastic deformation. An analysis models can be done from an indentation load-displacement curves, see Fig. 3.11, and interpreted to obtain hardness, modulus, and other mechanical properties.[25]
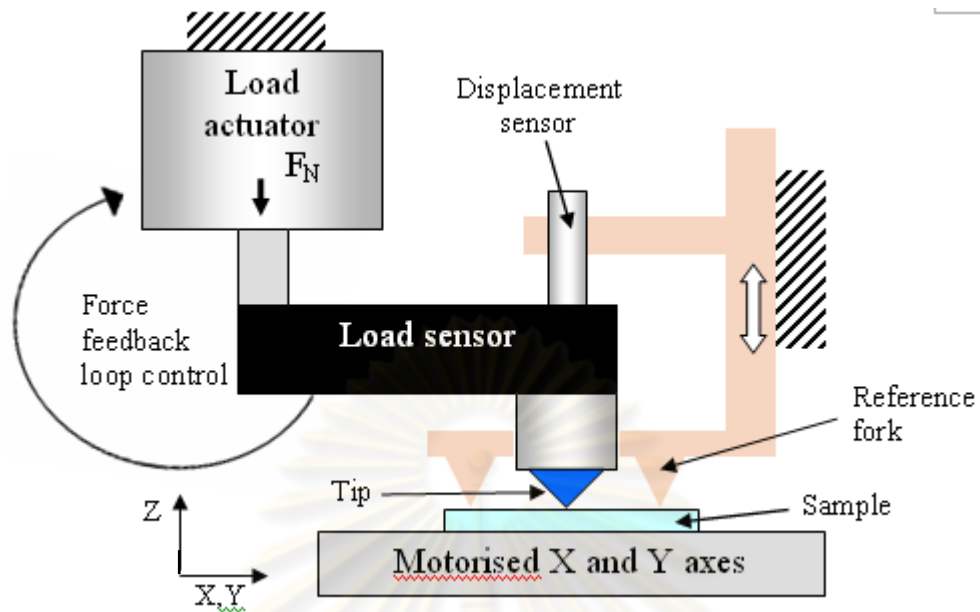
Figure 3.10: Schematic of a nanoindentation machine.
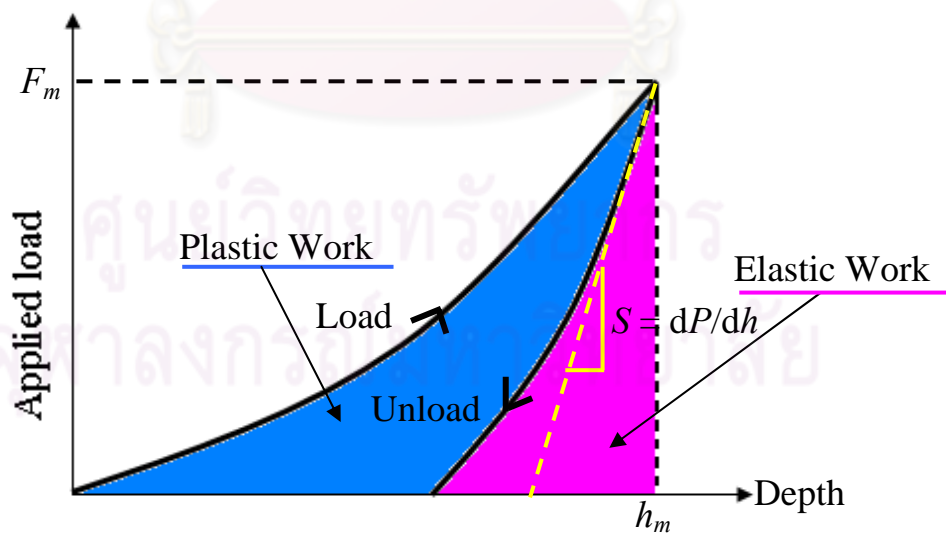
Figure 3.11: Load-displacement curve of indentation process.
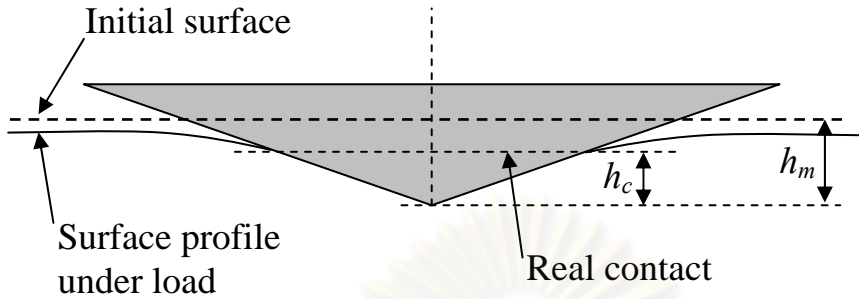
Figure 3.12: Schematic representation of the indentation processes showing the decreasing of the penetration depth during loading

The previous curve can be used to extract mechanical properties of the the material. The slope of the curve, dP/dh, upon unloading is stiffness(S) of the contact. The stiffness of the contact can be used to calculate the reduced modulus of elasticity (E_r) as [26]

$$E_r = \frac{\sqrt{\pi}}{2} \frac{S}{\sqrt{A_p}}$$
(3.2)

Where A_p is the area of the indentation at the contact depth, called *projected contact area*. A_p is calculated from

$$A_p = C_0 h_c^2 + C_1 h_c + C_2 h_c^{\frac{1}{2}} + C_3 h_c^{\frac{1}{4}} + ...$$
(3.3)

and

$$h_c = h_m - \varepsilon \frac{F_m}{S} \qquad \text{(see } h_c \text{ and } h_m \text{ in Fig. 3.12)}$$
(3.4)

The reduced modulus E_r is related to the modulus of elasticity E_s of the test specimen through the following relationship from contact mechanics [26]:

$$\frac{1}{E_r} = \frac{(1-\upsilon_s^2)}{E_s} + \frac{(1-\upsilon_i^2)}{E_i}$$
(3.5)

Here, the subscript i indicates a property of the indenter material and υ is Poisson's ratio. For a diamond indenter tip, E_i is 1140 GPa and υ_i is 0.07. Poisson's ratio of the specimen υ_s generally varies between 0 and 0.5 for most materials and is typically around 0.3.

The hardness (H) is given by the equation below, relating the maximum load(F_m) to the projected contact area(A_p).

$$H = \frac{F_m}{A_p} \tag{3.6}$$

The fracture toughness is a property which describes the ability of a material containing a crack to resist fracture. It is denoted K_I and has the units of $Pa\sqrt{m}$. It is another mechanical property that can be measured using nanoindentation technique. For the calculation of the fracture toughness, the relationship can be considered using the following equation.[27]

$$K_{IC} = \psi(\frac{E}{H})^{1/2}(\frac{F_m}{c^{3/2}}) \tag{3.7}$$

Where K_{IC} is the mode I critical stress intensity factor, ψ is a material-independent constant that is 0.016 for Berkovich-type indenters and c is the length of the radial cracks.

CHAPTER IV

EXPERIMENTAL PROCEDURE

In this work, we attempt to synthesize two forms of hydroxyapatite, one is hydroxyapatite powders and another is hydroxyapatite sol for the sol-gel process. The HAp powders are synthesized in order to use as a reference. To confirm the previous work [18], the HAp powders are characterized for their crystal structures by X-ray diffraction comparing with the standard HAp data. The HAp sol is prepared in order to produce the HAp films on substrates by the sol-gel method. Moreover, we synthesize HAp substituted with strontium in the form of powder and sol to improve the properties. The HAp/TiO_2 composite film has also been fabricated and characterized for mechanical properties modification.

4.1   Synthesis of Hydroxapatite

4.1.1 Introduction

The HAp powders can be synthesized by means of various techniques, either by the dry or the wet method. The dry chemical method makes use of the solid-state reactions between calcium and phosphorus compounds and has the advantage of providing stoichiometric HAp powders (at Ca/P = 1.67). For example, the HAp powders can be synthesized by the solid state reaction between calcium carbonate ($CaCO_3$) and calcium hydrogen phosphate ($CaHPO_4$) powders. The chemical of the reaction can be described as [28]

$$4CaCO_3 + 6CaHPO_4 \longrightarrow Ca_{10}(PO_4)_6(OH)_2 + 4CO_2 + 2H_2O.$$

Another method is the wet chemical synthesis, which utilizes either the precipitation from mixed aqueous solution or hydrolysis of calcium phosphate. In the precipitation reaction, the solution of $Ca(NO_3)_2$, which is a source of Ca, and $(NH_4)_3PO_4$, which is a source of P, are brought to pH 11-12 with concentrated NH_4OH. The phosphate solution is dropwise added to the stirred calcium solution. The HAp can be synthesized by the chemical reaction below [12],

$$10Ca(NO_3)_2 + 6(NH_4)_3PO_4 + 2NH_4OH \longrightarrow Ca_{10}(PO_4)_6(OH)_2 + 20NH_4NO_3.$$

.
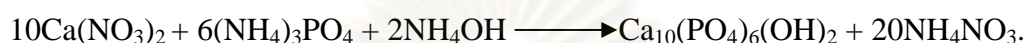
4.1.2 Synthesizing Procedure of Hydroxyapatite Powder

The precipitation reaction method is used to synthesize HAp powders. The Fig. 3.1 is the flow chart summarized the synthesizing procedure employed in this work and the details are shown in following steps below.

I. Seventy-eight and seven-tenth grams (0.33 mol) of $Ca(NO_3).4H_2O$ were dissolved in 300 ml of de-ionized water to get 1.00 M concentration. The solution was adjusted to pH 11 to 12 by the addition of ammonium hydroxide and then diluted to 600 ml.

II. Twenty-six and four-tenth grams (0.20 mol) of $(NH_4)_2HPO_4$ were dissolved in 300 ml of de-ionized water in flask to get 0.60 M concentration. The solution was adjusted to pH 11 to 12 by the addition of ammonium hydroxide and then diluted to 800 ml.

III. Calcium solution, vigorously stirred for 3.5 hours, was dropped slowly into a solution of di-amonium hydrogen phosphate at the speed of 40-50 drops per minute. The milky reaction mixture was set under the pH control (pH 11 to 12) at room temperature (25ºC) during synthesizing process (see Fig. 4.1).

IV. The reaction mixture was boiled for 30 minutes and left overnight at room temperature to allow the precipitate to settle in the supernatant solution.

V. The supernatant solution was filtered from the precipitate by using a suction filter, with the application of a weak vacuum from mechanical pump.

VI. The filtered cake was dried in an oven for 24 hours at 100ºC, and then broken down by grinding in a mortar. The powders were calcined within 60 minutes at 240ºC to remove the ammonium nitrate (NH_4NO_3).
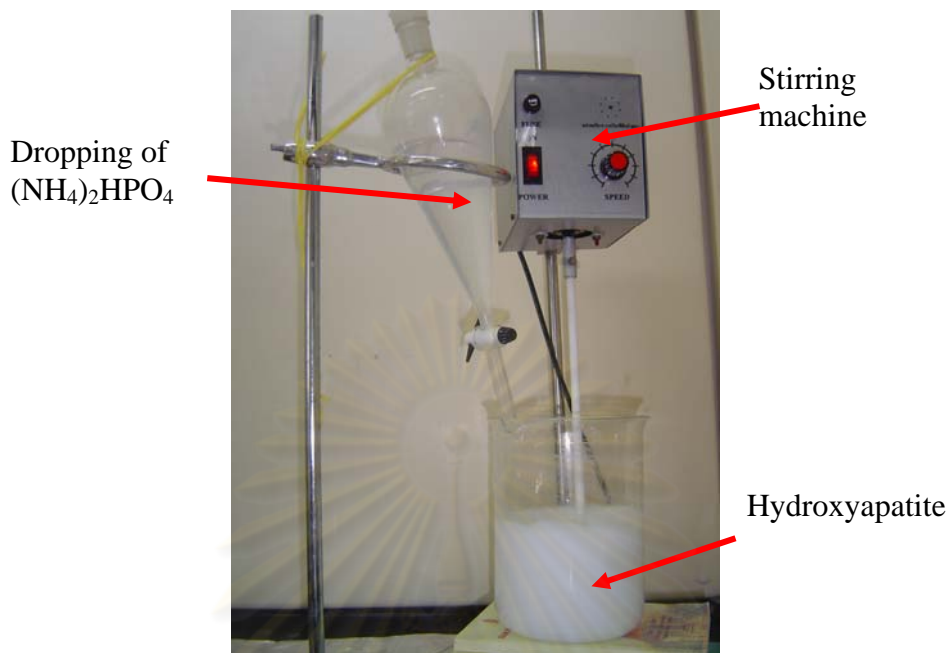
Figure 4.1: The experimental set up of HAp synthesis procedure

4.1.3 Preparation of Hydroxyapatite Sol

An inorganic route Ca-P sol-gel solution was made by the same procedure of Hydroxyapatite powder. According to the details in the previous part, calcium nitrate [Ca(NO$_3$).4H$_2$O] and ammonium dihydrogen phosphate [(NH$_4$)H$_2$PO$_4$] were used as calcium and phosphorus precursors, respectively, and the molar ratio of Ca/P was controlled at 1.67. Concentrated ammonium hydroxide was used to adjust the pH of solution to be about 11-12. The mixed HAp sol was ready for coating process after ageing and boiling. Fig. 4.2 shows the schematic representation of HAp synthesizing process.

4.2 Synthesis of Strontium-Substituted Hydroxyapatite

Strontium(Sr) is an alkaline earth metal with the atomic number 38. Strontium is also present in the mineral phase of bone like calcium, and it increases the number of osteoblasts and reduces the number and activity of osteoclasts [17]. The radius of strontium ion is 0.118 nm., which a bit larger than calcium ion (0.100 nm.). Both chemical and physical properties of strontium are closely related to calcium, it can be substituted in calcium site.

Therefore, in this study, we prepared Sr-substituted hydroxyapatite (SrHAp) using a precipitation method. To synthesize SrHAp, calcium nitrate 4-hydrate $[Ca(NO_3).4H_2O]$ and/or strontium nitrate $[Sr(NO_3)_2]$ were dissolved in 200 ml of distilled water. The pH of the solution was adjusted to 11 using ammonium hydroxide (NH_4OH) then 400 ml of distilled water was added to the solution. At the same time, ammonium dihydrogen phosphate $[(NH_4)H_2PO_4]$ was dissolved in 120 ml of distilled water and adjusted pH = 11 before distilled water (160 ml) was then added. The weights used for each composition are shown in Table 4.1 and the summary of thin film and powder forms are shown in Fig. 4.3, respectively. After that, $Ca(NO_3).4H_2O$ and/or $Sr(NO_3)_2$ and $(NH_4)H_2PO_4$-droped were mixed together and stirred. The mixed solution was boiled and then filtered. The filtered cake was dried in the oven for 24 hours at 100ºC, and then broken down by grinding in a mortar. The powders were calcined within an hour at 240ºC before characterization. The chemical formula of SrHAp is represented $(Sr_xCa_{1-x})_5(PO_4)_3OH$, where x is the atomic ratio. In this work, x was adjusted to be equal to 1.00 and 0.50.

4.3 Synthesis of Hydroxyapatite/TiO$_2$ Composite

The HAp sol was prepared by the same as previous method that explained in topic 4.1.3. The TiO$_2$ sol was prepared by dissolving 7.98 g of TiO$_2$ (Alfa Aesar 99.9%) in 100 ml of distilled water under stirring at room temperature for 1 h. After that the HAp sol was finally added to the TiO$_2$ sol with 20 vol.% concentration and continuously stirred for 2 h. The mixed sol was moved to the spin coater for the coating. The coating condition and the annealing temperatures were followed the same way as previous method.

4.4 Preparation of Coatings

Metallic implants are the main materials in orthopedic and dental applications due to their high mechanical properties. Among the standard surgical

implant materials, the most uses are stainless steel 316L, cobalt based alloys and titanium alloys. The stainless steel 316L is defined as a steel alloy with a minimum of 11% chromium content by mass (see Table 4.2). Stainless steel has sufficient amount of chromium present so that a passive film of chromium oxide forms which prevents further surface corrosion and blocks corrosion from spreading into metal's internal structure. The L-grade has 0.03% carbon maximum and resists to sensitization in short-term exposures or heat treatments. The 316L stainless steel is widely used in applications where the implant is temporary or permanent because of high mechanical properties (see Table 4.3), but it is also bioinert materials [29]. Therefore, the coating of HAp on stainless steel 316L substrate has been investigated in this work.

We use two types of substrate, silicon pieces from a wafer and stainless steel 316L. Flat sheets of stainless steel 316L with 1 mm thick were used as substrate. They were cut into area of 1 cm^2, and then were surface polished with 150, 320, 600 grit SiC, respectively, for enhancing the adhesion of coating material. Then, these substrates were cleaned with a soap solution, alcohol, acetone in ultrasonic bath and dip in hydrofluoric acid, respectively, to remove impurities before the coating process. At the same time, Si wafer were prepared by the same method as stainless steel 316L but they were surface polished only 150 grit. We selected to use silicon substrate because it can be used as reference peak position in X-rays diffraction technique and separated the film and substrate composition in EDS.

Sr (x)	Ca(NO$_3$).4H$_2$O	wt.%	mol. %	Sr(NO$_3$)$_2$	wt.%	mol. %	(NH$_4$)H$_2$PO$_4$	wt.%	mol. %
1.00	-	-	-	42.34	72.76	62.50	15.85	27.24	37.50
0.50	23.62	38.95	31.25	21.17	34.91	31.25	15.85	26.14	37.50

Table 4.1: Experimental weights (in gram) synthesis for $(Sr_xCa_{1-x})_5(PO_4)_3OH$

Grade		C	Mn	Si	P	S	Cr	Mo	Ni	N
316L	Min	-	-	-	-	-	16.00	2.00	10.00	-
	Max	0.03	2.00	0.75	0.045	0.03	18.00	3.00	14.00	0.10

Table 4.2: Composition ranges for 316L stainless steel

Grade	Tensile Strength (MPa) min	Yield Strength 0.2% Proof (MPa) min	Elongation (% in 50mm) min	Hardness	
				Rockwell B (HR B) max	Brinell (HB) max
316L	485	170	40	95	217

Table 4.3: Mechanical properties of 316L stainless steel
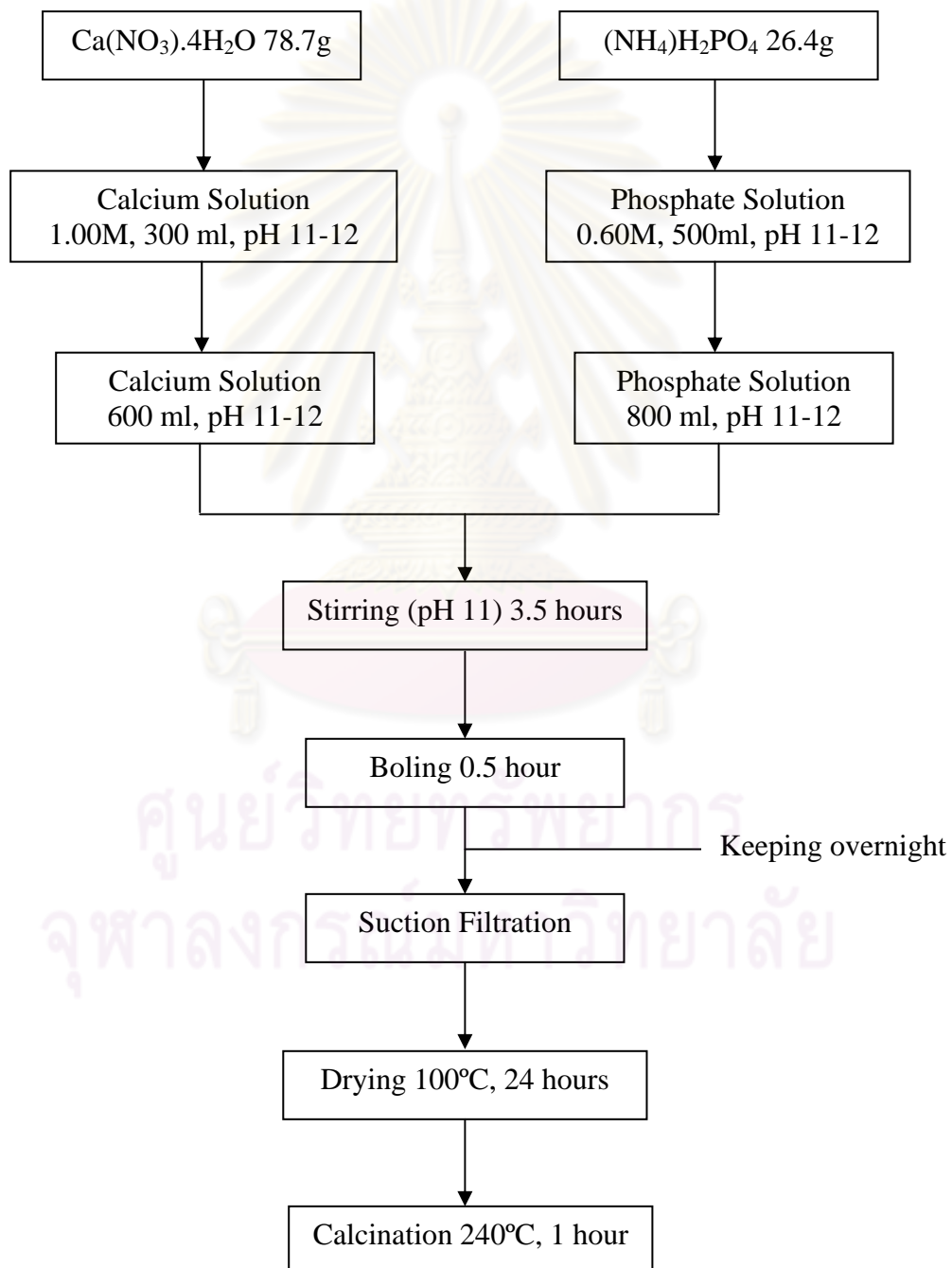
Figure 4.2: The flow chart for synthesis of hydroxyapatite powder employed in this work
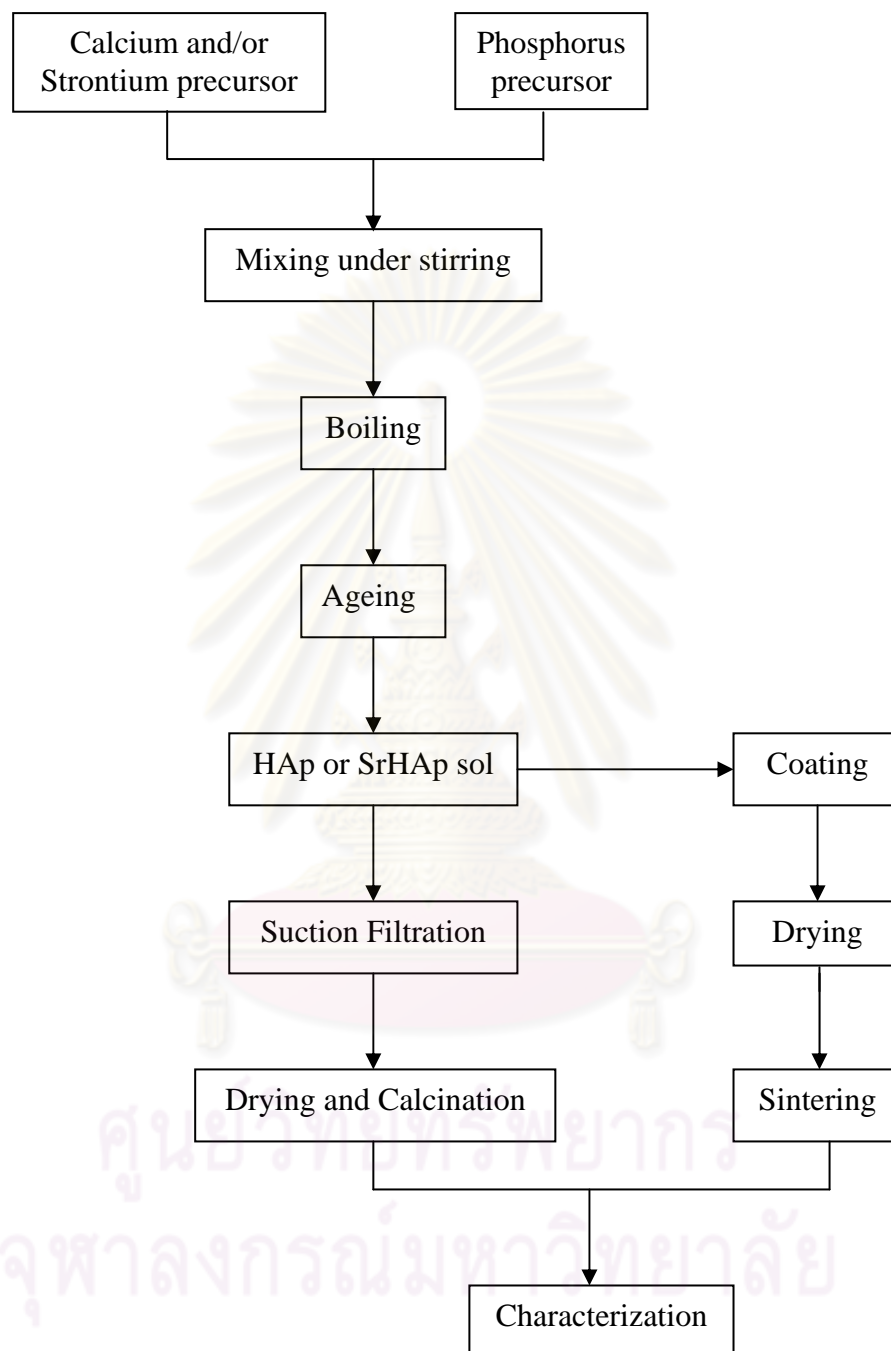
Figure 4.3: The flow chart of synthesis and preparation of thin film and powder forms of HAp and SrHAp

4.5   Spin Coating

In this work, HAp and SrHAp films were prepared by a sol-gel spin coater. The spin coater, model P6700 series, which is shown in Fig. 4.4, was used to cast the film. These films were deposited at a speed of 2,000 rpm at room temperature. After that, the prepared films were dried in an oven at 150ºC. Then, these were sintered in various temperatures of 300, 500, 700, 900 and 1,100ºC for 10 minutes, finally cooled to room temperature before characterizations.

4.6   Sample Characterizations

4.6.1 Scanning electron microscope (SEM) and energy dispersive x-ray spectroscopy (EDS)

Scanning electron microscope, SEM (JEOL JSM-6480 LV), see Fig. 4.5, was used to investigate the microstructure and the grain size of HAp and SrHAp films. Energy dispersive x-ray spectroscopy (EDS) was used to measure the elemental composition of the specimen, which are films and reference powders. The specimen for SEM was stuck on the stub by carbon tape and coated on the surface with very thin larger gold by sputtering, but non-coated specimens were used for EDS analysis.

4.6.2 X-ray diffractometer (XRD)

The structure of synthesized HAp and SrHAp powders were determined by a Rigaku D/MAX-2200 Ultima$^+$ X-ray diffractometer equipped with Cu target X-ray tube (40 kV, 30mA) at 2-theta between 0.5 to 3.00 degrees. The scattering slit, divergent slit and receiving slit were fixed at 0.5 degree, 0.5 degree, and 0.15 mm, respectively. X-ray instrument (Bruker-AXS D8 DISCOVER, see Fig. 4.6) was used to characterize the crystal structure of HAp and SrHAp films with conventional Cu target operated at 40 kV and 40 mA. The Cu$K\alpha$ radiation is monochromatized into $K\alpha_1$ with the incident X-ray wavelength of 1.5406 Å.

4.6.3 Nanoindentation

The mechanical property of the films was measured by nanoindentation system (CSM instrument), which illustrated in Fig. 4.7. A Berkovich three-sided pyramid indenter tip was used in this study. Before measurement, calibration was performed on the fused silica (FS) standard, which is normally used to calibrate due to its low modulus to hardness ratio [26]. The elastic modulus of FS, assuming a Poisson's ratio of 0.16, was measured to be $73.4 \pm 4\%$ GPa. Then, the experiment was carried out and calculated from load-unload curve by using the Oliver-Pharr calculation method [30]. In this study, the tests were performed at three different loads of 20, 30 and 40 mN, respectively.

Sample holder

Start/Stop
button

Speed & Time
Controller
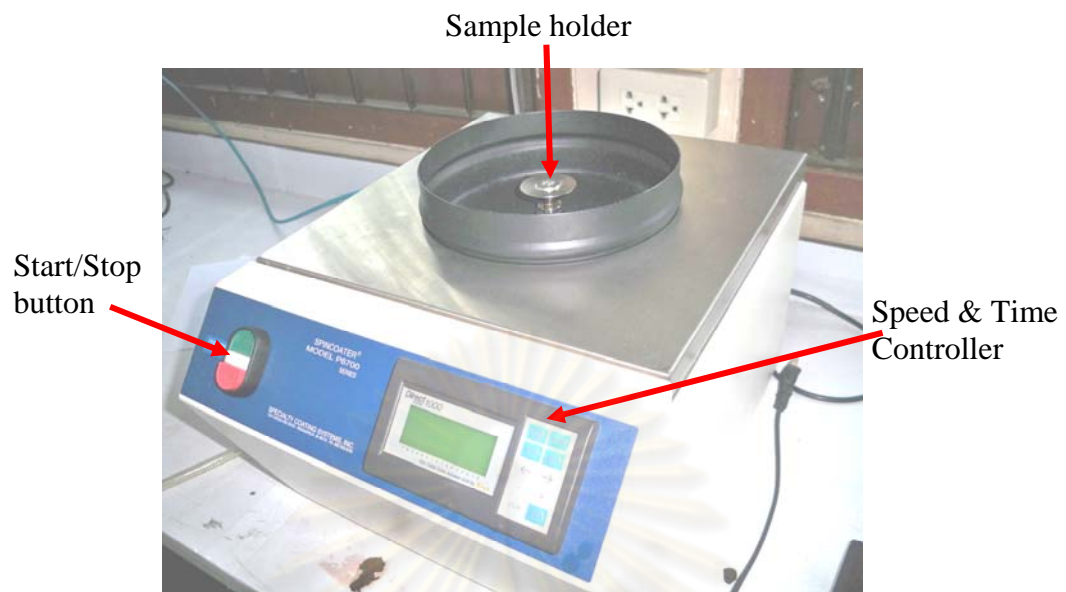
Figure 4.4: The spin coater machine (model P6700 series) at Department of
Physics, Faculty of Science, Chulalongkorn University

EDS
Detector

Electron gun

Monitor

Chamber

Focus, Magnify,
Position Controller
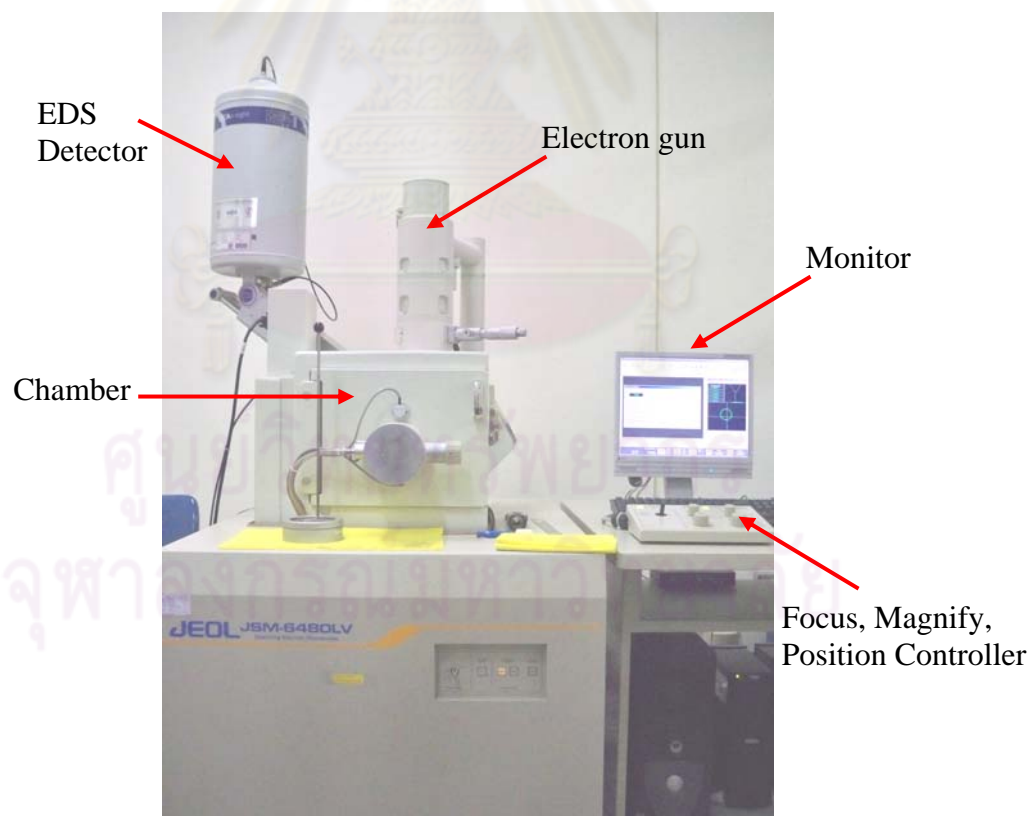
Figure 4.5: Scanning electron microscopy (JEOL, JSM-6480LV) at Faculty of
Science, Chulalongkorn University
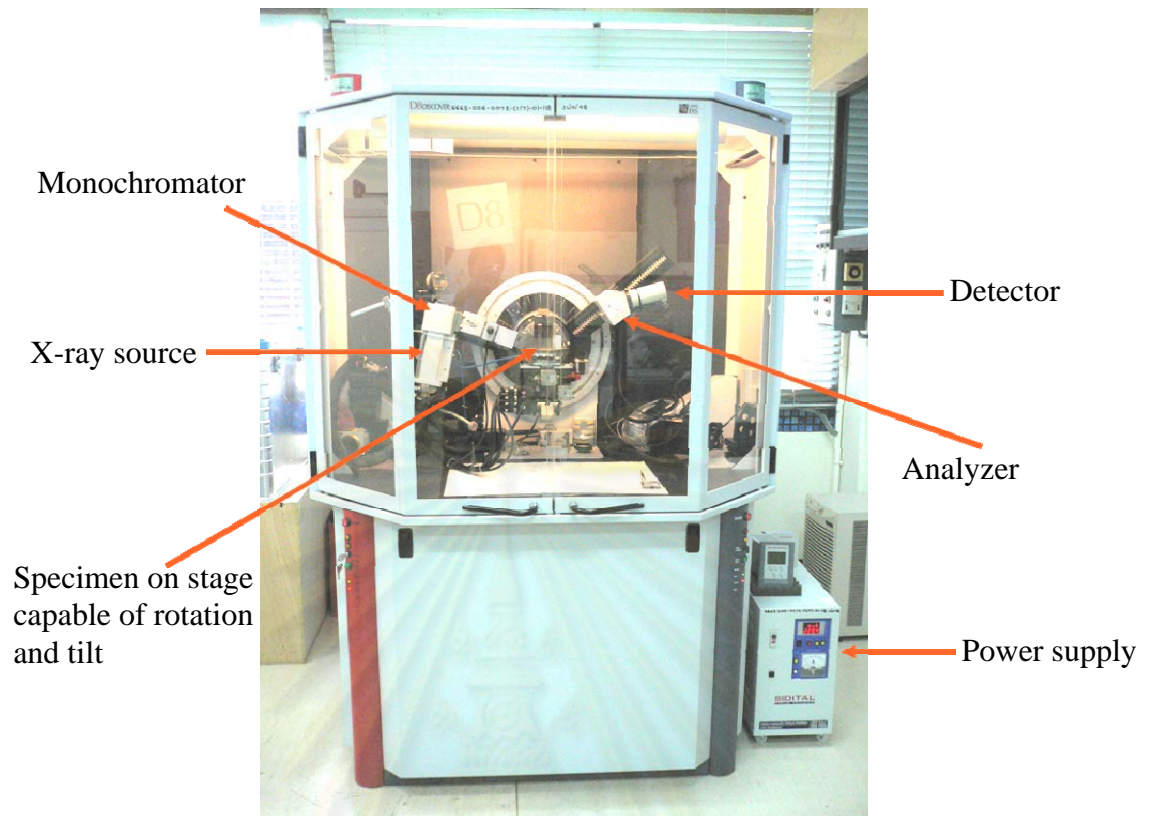
Figure 4.6: The X-ray diffractometer (Bruker-AXS D8 DISCOVER) at Scientific and Technology Research Equipment Center, Chulalongkorn University
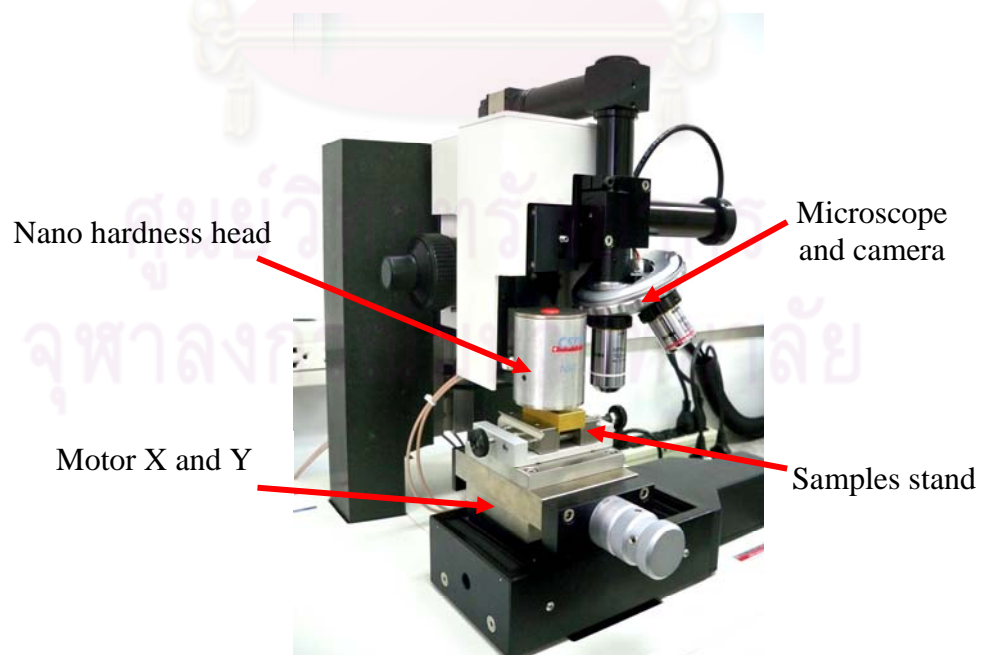
Figure 4.7: The nanoindentation tester (CSM instruments) at Metallurgy and Materials Science Research Institute, Chulalongkorn University

CHAPTER V
RESULTS AND DISCUSSIONS

In this chapter, the results and discussions of the whole will be divided into three parts, regarding the materials aspect; hydroxyapatite, strontium-substituted hydroxyapatite and hydroxyapatite/TiO_2 composite. Each part consists of XRD, SEM and EDS results, analyses and discussions. Furturemore, the characterization results on the mechanical property of HAp and HAp/TiO_2 composite films will be demonstrated.

5.1   Results and Discussions of Hydroxyapatite Powder

5.1.1 XRD Analysis of Hydroxyapatite Powder

The powder form of hydroxyapatite was synthesized to identify and use as the reference, so that the obtained materials consisted of hydroxyapatite phase. The powder specimen was dried and calcined at 240ºC before characterization. The phase structure of calcined powder was investigated by powder X-ray diffractometery, using CuKα with 2θ scanning from 15º to 60º. The X-ray diffraction pattern (Fig. 5.1) illustrates that the maximum diffraction peak was at 2θ = 31.8º referring to the reflection plane of (211). Most peaks are clearly observed for instance (002), (300), (310) planes, etc. Also, it shows the comparison of XRD patterns of the obtained powders (black line) with the standard reference HAp according to JCPDS #9-432 (gray dash line). This can be seen that both patterns are closely matched, thus confirming that the obtained powder are polycrystalline hexagonal structure without impurity phase.

5.1.2 EDS Analysis of Hydroxyapatite Powder

The elemental compositions of the HAp powder were measured by EDS. The EDS spectrum of the sol-gel HAp powder is given in Fig. 5.2. The atomic percentage of Ca and P are calculated as 22.36% and 13.8%, respectively. This

represent in Ca/P ratio 1.62, which is close to the theoretical value 1.67. This confirms that the sol mixture in our sol-gel technique is able to synthesize and reproduce HAp in the form of powder.
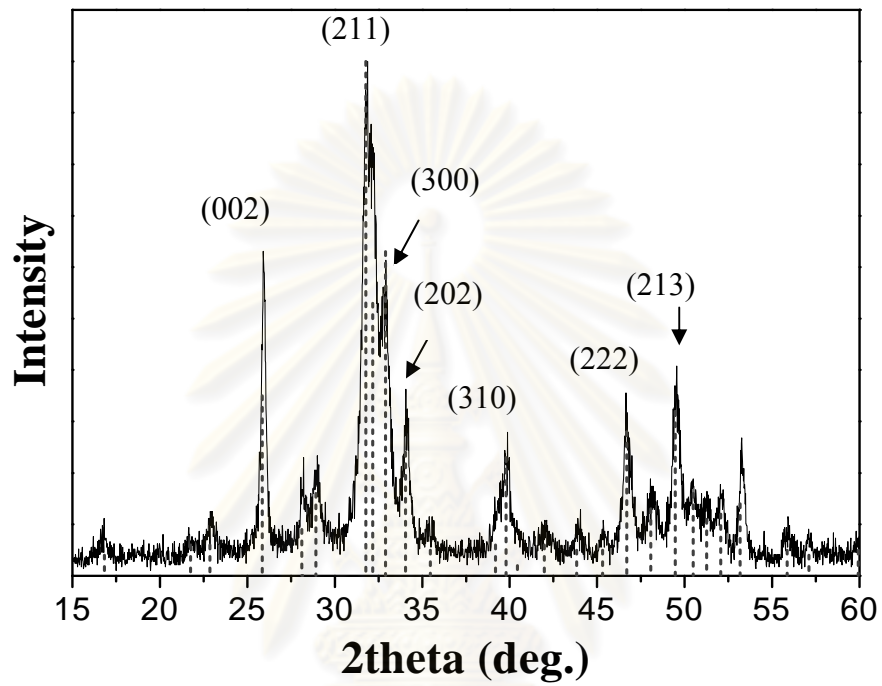
Figure 5.1: The XRD diffraction pattern of HAp powder comparing with the standard reference according to JCPDS #9-432
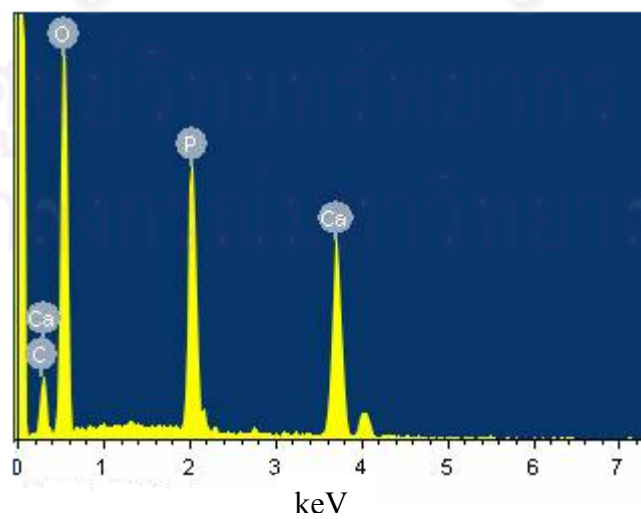
Figure 5.2: The EDS spectra of HAp powder calcined at 240ºC

5.2   Results and Discussions of Hydroxyapatite Film

5.2.1 XRD Analysis of Hydroxyapatite Film

As confirmed that the HAp powder form can be synthesized HAp without impurity phase. The HAp thin films were also structural characterized by XRD. We used two types of substrate, silicon and stainless steel 316L. The obtained films were annealed at various temperatures. The XRD diffractograms of the HAp thin films which annealed at various temperatures and different substrates show in Fig. 5.3 and Fig. 5.4. The XRD patterns in Fig. 5.3 showed the coatings on silicon annealed at 300°C, 500°C, 700°C, 900°C and 1,100°C, respectively. The broad peak of the main reflection that corresponding to the HAp (211) plane appears at 300°C, 500°C and 700°C. This indicates that the HAp sintered at these temperatures has a poor cystallinity. At higher temperatures (900 and 1,100°C), the HAp structure peaks become stronger, which corresponds to the (002), (211), (202), (310), and (222) reflections. This suggests that the HAp coatings structure develop to polycrystalline with preferred orientations. The β-tricalcium phosphate (β-TCP) peaks can be detected at $2\theta=30.7^\circ$ and 27.7°[10] only in the HAp film that is annealed at 1,100 °C. It can be explained that the HAp may be decomposed at temperature above 1050 ºC, as the following [18],

$$Ca_{10}(PO_4)_6(OH)_2 \longrightarrow 2\beta Ca_3(PO_4)_2 + Ca_4P_2O_9 + H_2O.$$
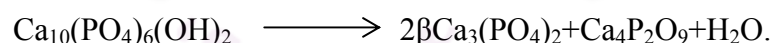
The XRD pattern of HAp on stainless steel 316L annealed at different temperatures also shows in Fig. 5.4. The results are quite similar to the previous pattern on the silicon substrate, but only the peaks in XRD pattern of substrate are not the same. The results show that the strongest peak of HAp still observed from all annealed films and the intensity is sharper as temperature increase. There is no impurity phase in the films that annealed reach 900ºC. From these XRD analysis results, it indicates that the structural evolution of HAp film develope as the annealing temperature increased and β-TCP can be found at the annealing temperature of 1,100ºC and above.
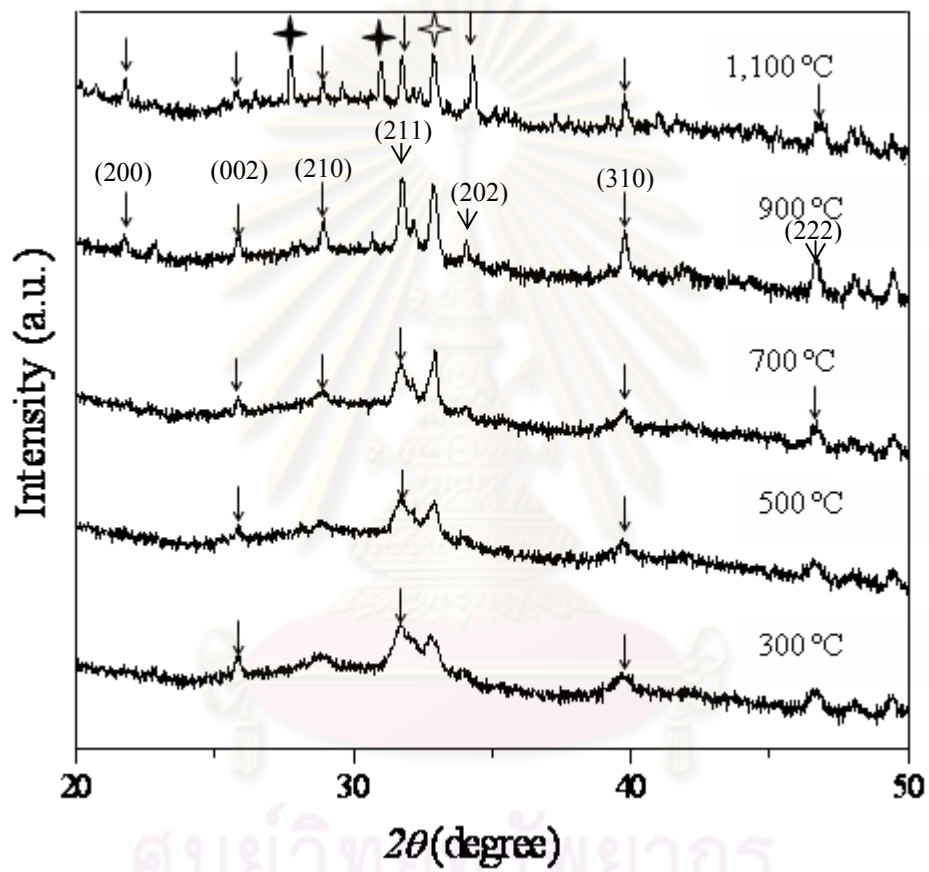
Figure 5.3: The XRD patterns of HAp films on silicon (Si) substrate annealed at various temperatures. ($\vee$): HAp, (✦): β-TCP, (✧): Si
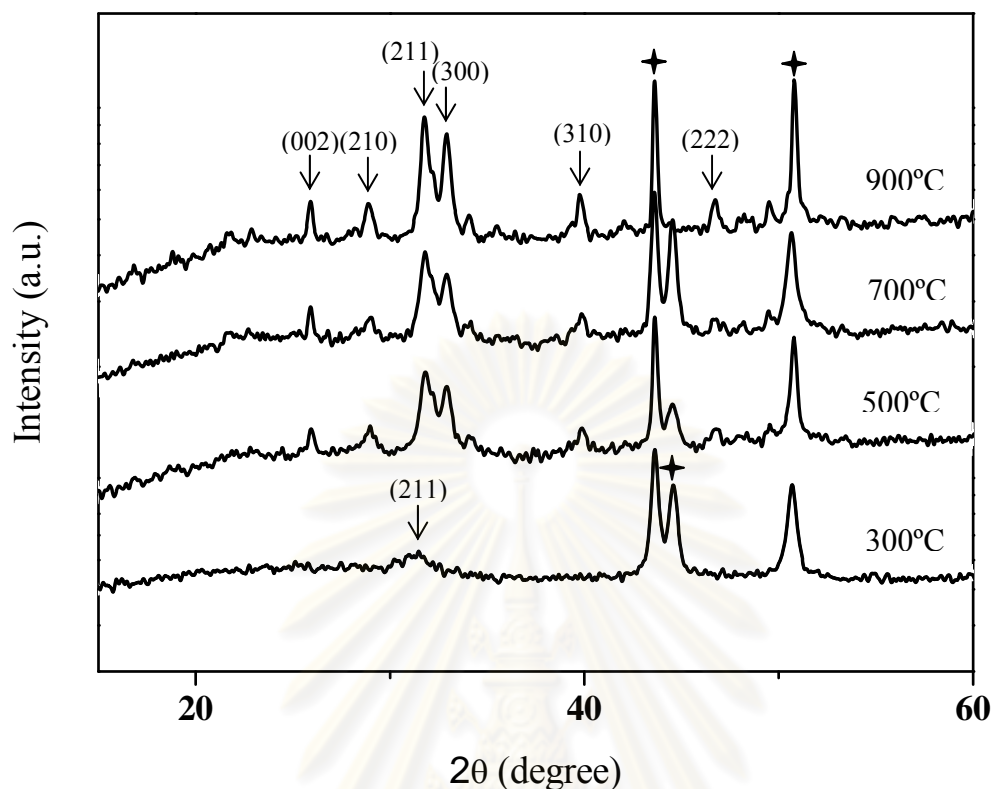
Figure 5.4: The XRD patterns of HAp films on stainless steel 316L substrate annealed at various temperatures. (∨): HAp, (✚): stainless steel 316L

5.2.2 EDS Analysis of Hydroxyapatite Film

The elemental composition of HAp films on silicon and 316L stainless steel substrates that annealed at various temperatures is shown in Table 5.1. The results indicate that the obtained films consist of calcium, phosphorus, oxygen and carbon, while silicon was also detected as substrate. The atomic percent of Ca, P and O are closely resemble values in both films on silicon and 316L stainless steel. The carbon content appears at every annealing temperature except 1,100°C, but it decrease as temperature increased. It can be explained that carbon may come from the atmosphere during synthesis process and sintering [12]. It completely occurs pyrolysis at higher temperatures [31]. The Ca/P ratios of the films are in the range of 1.61 to 1.65 in both substrates, which are nearly close to stoichiometric HAp (Ca/P = 1.67).

		Atomic %				
Annealing temperature (°C)		300	500	700	900	1,100
Si substrate	Carbon (C)	10.1	7.04	5.04	3.87	0
	Oxygen (O)	57.5	60.1	60.2	62.72	64.44
	Phosphorus (P)	12.2	11.9	12.8	12.17	12.81
	Calcium (Ca)	19.6	19.7	20.6	19.92	20.81
	Silicon (Si)	0.65	1.26	1.45	1.32	1.94
	Ca/P ratio	**1.61**	**1.65**	**1.61**	**1.64**	**1.62**
316L SS substrate	Carbon (C)	10.2	7.96	5.53	4.03	-
	Oxygen (O)	59.2	59.6	61.1	61.93	-
	Phosphorus (P)	11.6	12.4	12.8	12.88	-
	Calcium (Ca)	19	20	20.6	21.16	-
	Ca/P ratio	**1.64**	**1.62**	**1.61**	**1.64**	-

Table 5.1: The atomic percent of each element found in HAp films on Si and 316L SS substrate annealed at various temperatures

5.2.3 SEM Analysis of Hydroxyapatite Film

SEM technique was used to observe the microstructure of the HAp films. The SEM micrographs of the HAp films annealed at various temperatures are shown in Fig. 5.5. All images (using 15 keV in secondary electron mode) were captured at the same magnification of 30,000 times. Fig. 5.5 (a) and (b) show that the films are quite homogeneous, while the film annealed at 700 °C (Fig. 5.5(c)) exhibited small fine grain structure. At 900 °C (Fig. 5.5(d)), the grain size is increased and some pores can be observed. When the film was annealed at 1,100 °C, the grains size is still increase and had a cross-linking structure. The HAp grains size is found to be approximately 0.5 μm. at 1,100 ºC. Therefore, the evolution of grain size depends on the annealing temperatures and the structure of the film develops from amorphous to more crystalline. Moreover, the SEM micrographs represent that the HAp has porous structure, which can be observed from the pore in the microstructure.
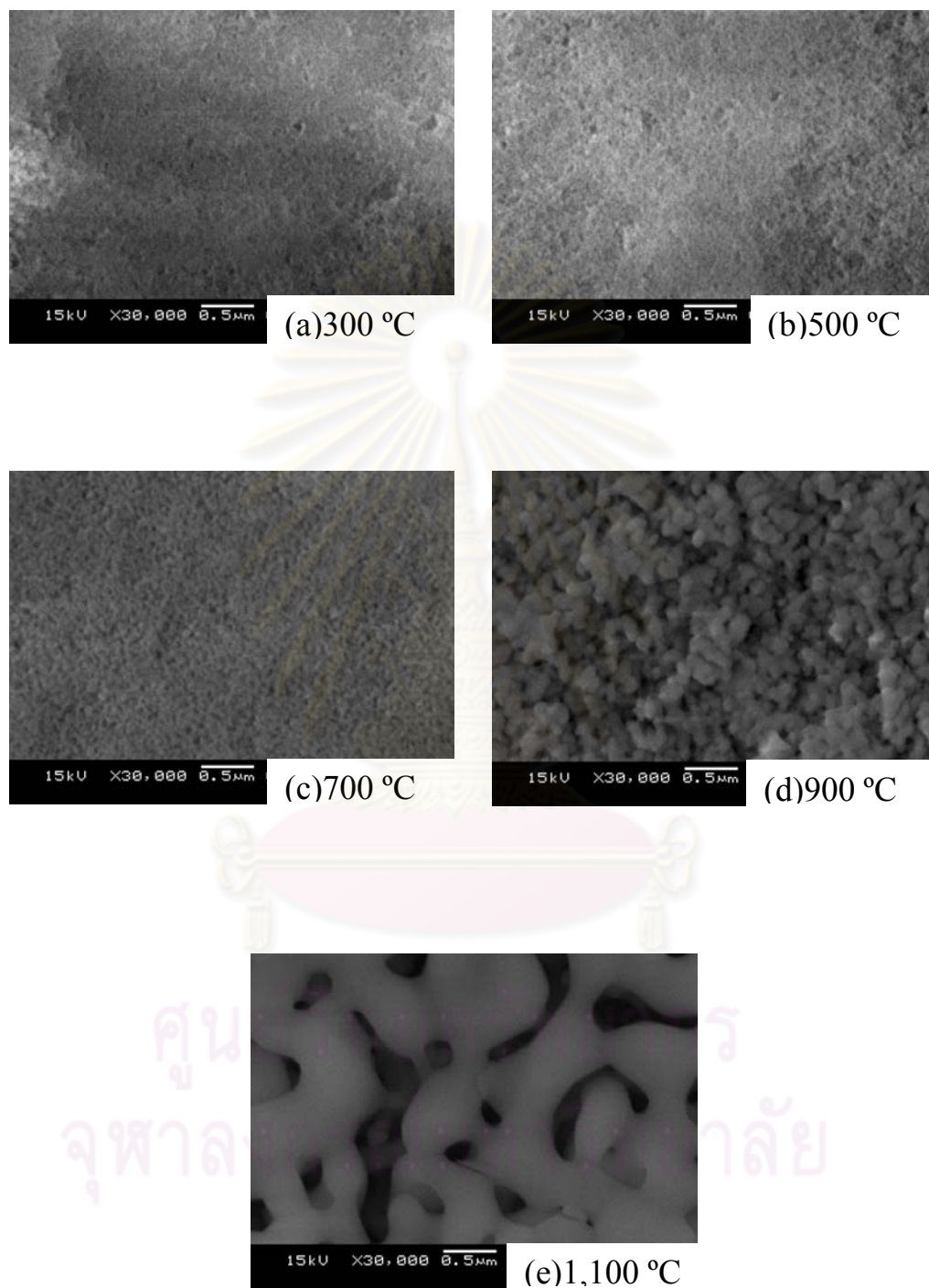
Figure 5.5: The SEM micrographs of HAp films annealed at (a) 300 ºC, (b) 500 ºC, (c) 700 ºC, (d) 900 ºC and (e) 1,100 ºC
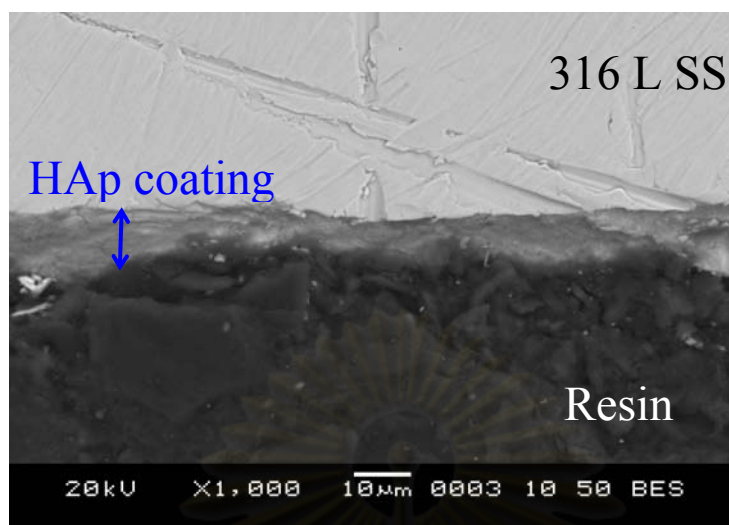
Figure 5.6: The SEM cross-section image of HAp coating on 316L SS substrate

The back scattered electrons mode (BSE) in SEM technique was used to view the cross-section image due to the contrast of image depending on atomic number of each material. Fig. 5.6 displays the cross-section SEM micrograph of annealed HAp film on stainless steel 316L substrate. As seen from the image, the HAp layer covers entire surface of the substrate. The thickness of the coating layer is approximately 10 μm. A close interfacial bond between the film and the substrate is observed without any cracks and voids.

5.3 Results and Discussions of Strontium-Substituted Hydroxyapatite

5.3.1 XRD Analysis of Strontium-Substituted Hydroxyapatite Powder

Both powder and thin film forms of strontium-substituted hydroxyapatite (SrHAp) have been synthesized and characterized the phase structure by the XRD technique. The XRD pattern of fully substituted Sr in HAp is illustrated in Fig. 5.7. It shows that the strongest diffraction peak is at $2\theta = 30.67º$ referring to the reflection plane (112). All the peaks are well-defined and sharp for example (211), (300), (210) planes, etc. As seen from the Fig. 5.7, the pattern agrees with the

standard reference SrHAp according to JCPDS #70-1511. It also can be seen that both patterns are closely correlated, thus confirming that the obtained powders has polycrystalline hexagonal structure without impurity phase.
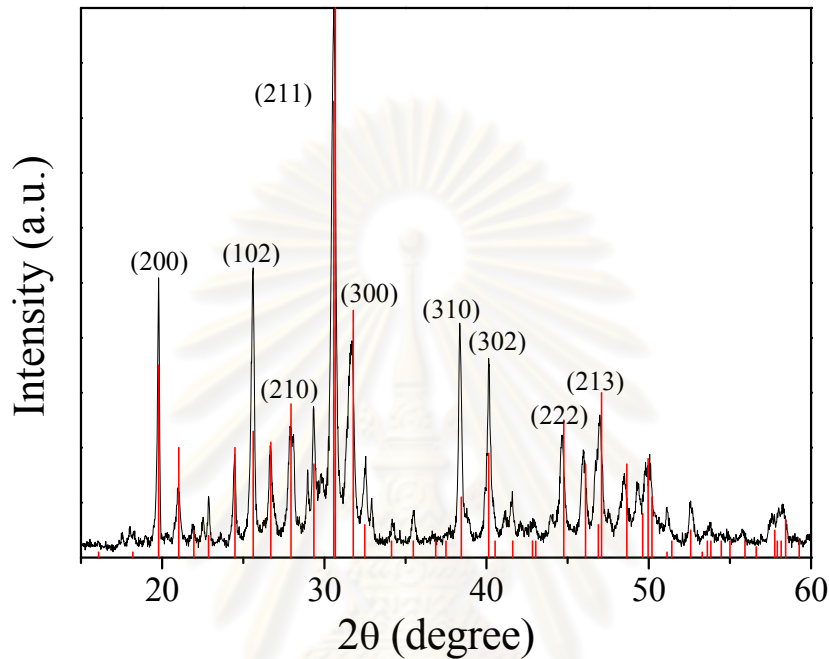
Figure 5.7: The XRD diffraction pattern of SrHAp powder comparing with the standard reference according to JCPDS #70-1511

5.3.2 XRD Analysis of Strontium-Substituted Hydroxyapatite Film

Fig.5.8 exhibits the XRD patterns of SrHAp film on stainless steel 316L annealed at 300°C, 500°C, 700°C and 900°C, respectively. The broad reflection of the dominated peak, other than substrate's peaks corresponding to the SrHAp, appeares at 300 and 500°C. It indicates that the annealed SrHAp has poor cystallinity at these temperatures. At higher temperatures (700°C and 900ºC), the SrHAp structure becomes strong and well-defined peaks. This suggests that the SrHAp coatings develop from nanocrystalline toward polycrystalline with preferrd orientations. The peak that corresponding to $Sr_3(PO_4)_2$ phase, which refer to the impurity, was found in the specimen annealed at the temperature of 900ºC at $2\theta =$

33.6º . The XRD analysis indicates that the evolution of SrHAp film structure develops as the post-annealing temperature increased.
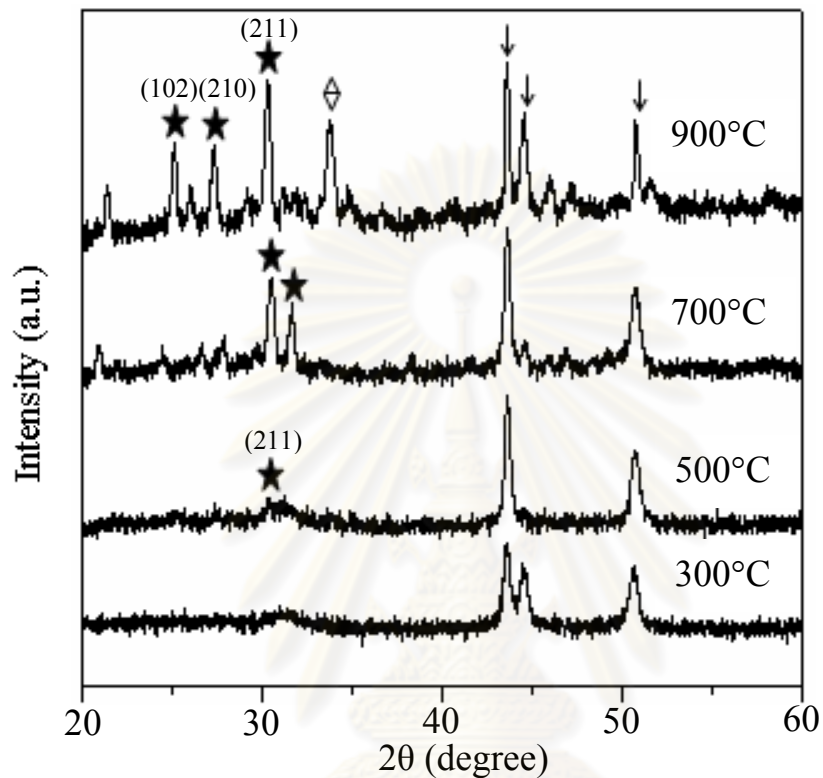
Figure 5.8: The XRD patterns of SrHAp films annealed at various temperatures (★): SrHAp, (⇓): stainless steel 316L, (◇): $Sr_3(PO_4)_2$

5.3.3 EDS and SEM Analysis of Strontium-Substituted Hydroxyapatite Powder and Film

Elemental analysis of powders by EDS is shown in Table 5.2. It clearly indicates that the atomic percent of Sr and Ca in SrCaHAp are quite at similar value. The amounts of calcium and strontium are detected in SrCaHAp and SrHAp, respectively. This confirms that the sol-gel technique is able to synthesize $(Sr_xCa_{1-x})_5(PO_4)_3OH$ in the form of powder.

Element	Atomic %							
	SrCaHAp				SrHAp			
	point 1	point 2	point 3	average	point 1	point 2	point 3	average
Calcium (Ca)	7.96	7.06	10.28	8.4333	0	0	0	0
Strontium (Sr)	7.81	7.65	11.77	9.0767	20.34	18.05	17.21	18.533
Phosphorus (P)	11.15	11.97	15.15	12.757	13.59	13.92	10.66	12.723
Oxygen (O)	59.79	65.35	51.51	58.883	45.92	46.92	46.8	46.547
Carbon (C)	13.3	7.96	11.28	10.847	20.15	21.11	25.33	22.197

Table 5.2: The atomic percent of the powder calculated from EDS

The cross-sectional SEM micrograph of annealed SrHAp film is shown in Fig. 5.9. The structure of the layer was not uniform comparing with HAp coating because SrHAp sol did not have good solubility as HAp. Moreover, the thickness was greater than HAp, it was around 15-20 μm. There are some voids that can be observed.

The SEM micrographs of the SrHAp film annealed at various temperatures shown in Fig. 5.10. The morphology and microstructure of SrHAp film annealed at 300ºC and 500ºC (Fig. 4a and b) exhibited almost a rod shape. On the other hand, at 700ºC it can be observed as fine grains. As the film was annealed at 900°C, the grains size had developed and formed as cross-linking network structure. Therefore, the evolutions of the grain size depend on the annealing temperatures. This can be due to the crystalline of SrHAp coexists with tricalcium phosphate and tetracalcium phosphate phases and starts recrystallization at the annealing temperature over 700ºC. Moreover, the SEM micrographs also indicated that SrHAp has porous structure the same as in HAp.
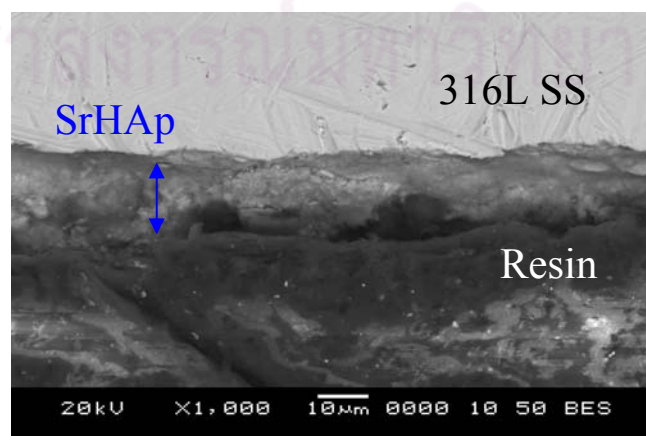
Figure 5.9: The SEM cross-section image of SrHAp coating on 316L SS substrate
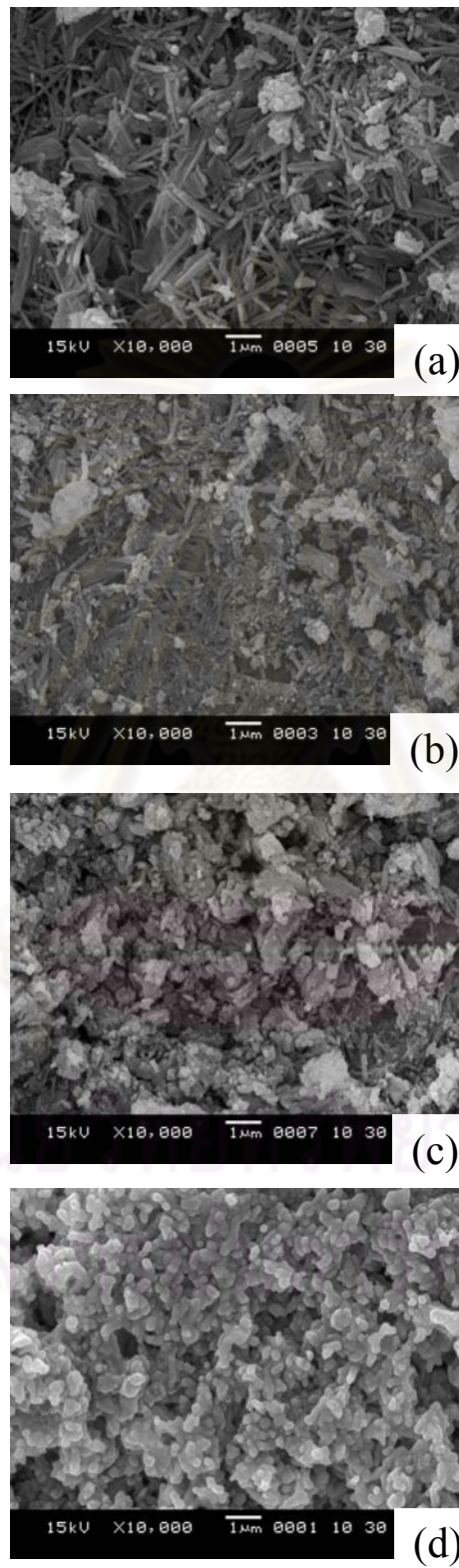
Figure 5.10: The SEM micrographs of SrHAp films annealed at (a) 300 ºC, (b) 500 ºC, (c) 700 ºC and (d) 900 ºC

5.4   Crystal Structure Analysis of Powder

The crystal structure of three types powder, HAp (0% Sr), SrCaHAp (50% Sr) and SrHAp (100% Sr) was investigated by XRD technique using CuKα with scanning from $2\theta = 15^\circ$ to 60°. The x-ray diffraction patterns of the powder, synthesized with different [Sr]/[Ca+Sr] atomic ratios, are shown in Fig. 5.11. Bragg's law and the geometric relationship for hexagonal lattice system, shown in equation below, were used to calculate the lattice parameters from the obtained powder diffractograms.

$$\frac{1}{d^2} = \frac{4}{3}\left(\frac{h^2 + hk + k^2}{a^2}\right) + \frac{l^2}{c^2} \tag{5.1}$$

The XRD patterns of the samples corresponding to HAp and to SrHAp display well-defined and sharp peaks. Their diffraction planes are clearly explained and discussed in previous topics. On the other hand, the pattern of the sample containing both Ca and Sr generally exhibits a broader diffraction peak. They indicate that the crystallinity is decreased after Ca^{2+} is half substituted by Sr^{2+} in the structure. The Sr substitution may affect the growth of HAp lattice and consequently decreases the crystalline quality because the lattice strains due to Sr-atoms substitution in HAp matrix. All patterns also demonstrate that the reference powders have no other unusual phases and impurity can be observed.

The diffraction peaks of the SrHAp shift to lower 2θ values due to an increasing in d-spacing and lattice parameters. The crystal structure of HAp and SrHAp are in hexagonal system. The plot of lattice parameters ($a = b$ and c) of the series powders, as seen from Fig. 5.12, were calculated from the equation 5.1. The results show that a and c increase linearly with the amount of Sr incorporate. It is known that the larger ionic radius of Sr compared to Ca (Ca^{2+} = 1.00 Å and Sr^{2+} = 1.18 Å) [32] can cause the apatite lattice to expand in both the a- and c-axis directions.
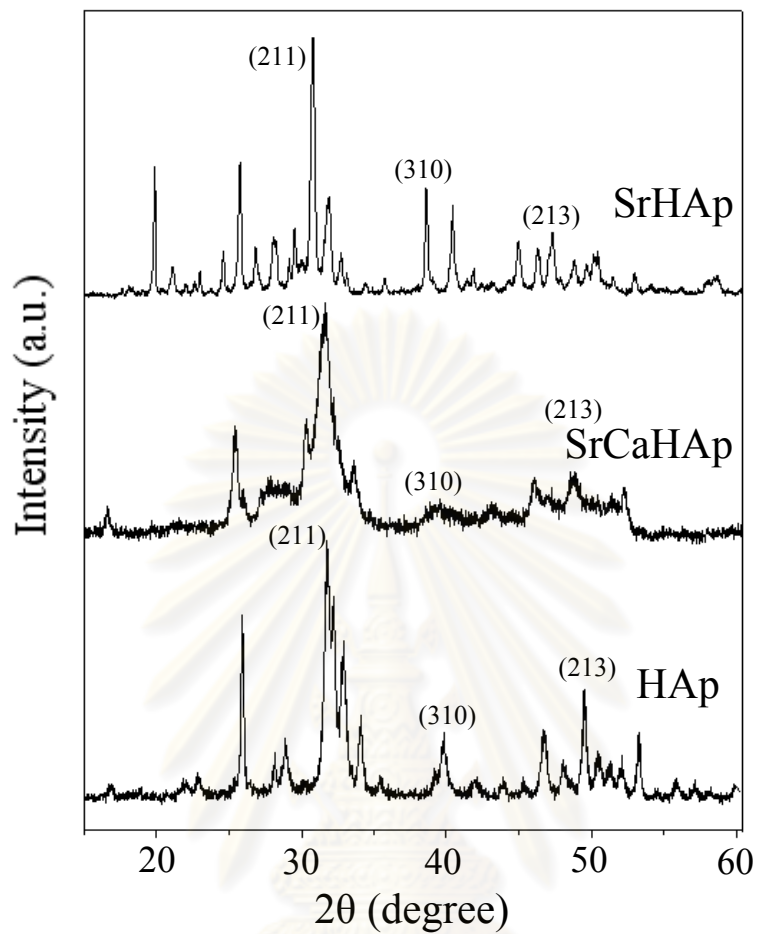
Figure 5.11: The XRD patterns of HAp, SrCaHAp and SrHAp powder
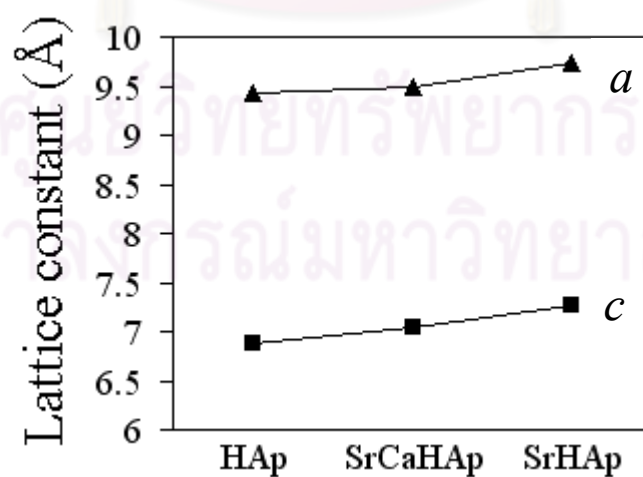
Figure 5.12: The plot of lattice parameters of the obtained powders

5.5 Results and Discussions of Hydroxyapatite/TiO$_2$ Composite

The typical XRD patterns of the HAp/TiO$_2$ composite films annealed at various temperatures are shown in Fig. 5.13. They exhibit a typical characteristic pattern of HAp with well-defined and more sharpen intensity when annealing temperature increased. Furthermore, the sharp peaks at 25.3°, 37.9° and 48.1° correspond to the TiO$_2$ anatase phase, respectively. This can be observed in all temperatures. In contrast, the (110) plane of TiO$_2$ rutile phase is found from the sample annealed at 700ºC; the board peak at 27.6º, and this peak became sharpen at 900ºC. Another peak of rutile at 36.1º can also be detected from 900ºC. This can be concluded that some of TiO$_2$ anatase phase transforms to rutile phase at annealing temperature above 500ºC.
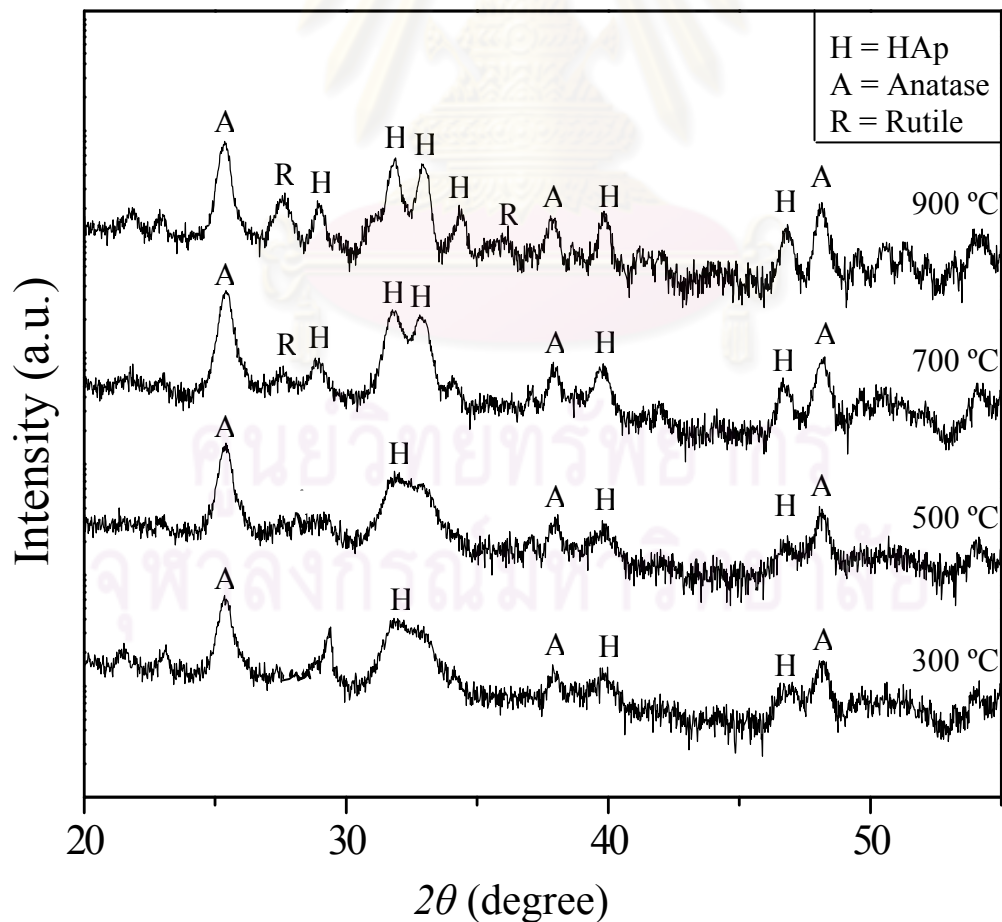
Figure 5.13: XRD patterns of HAp/TiO$_2$ composite films annealed at various temperatures (H): HAp, (A): Anatase, (R): Rutile

The SEM micrographs of HAp/TiO$_2$ composite films annealed at various temperatures are shown in Fig. 5.14. The grain size of films increases with an increasing temperature like in the case of HAp and SrHAp films. The TiO$_2$ particles can be seen in this composite film and it exhibits nano-size of particle linking with HAp structure.
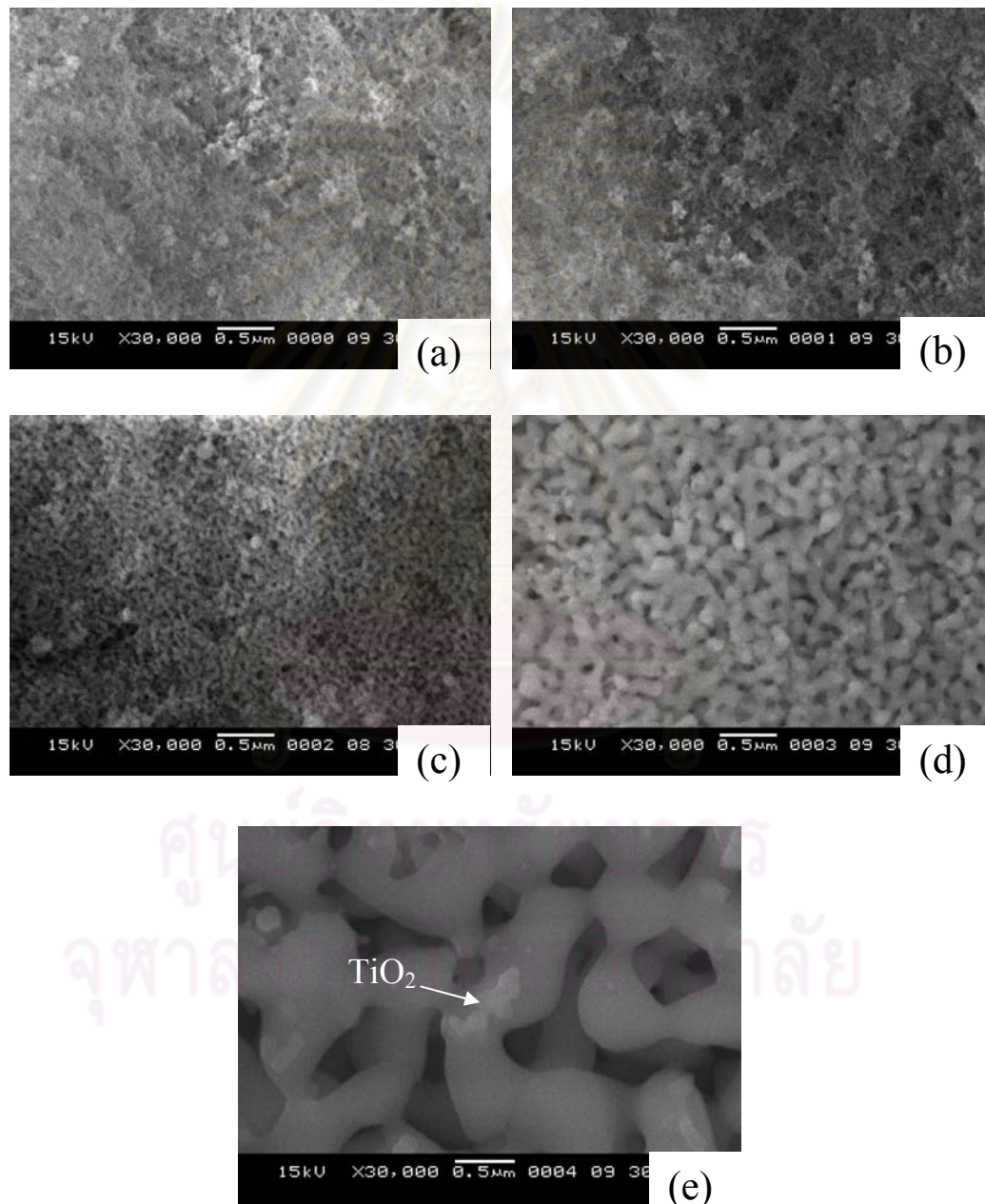
Figure 5.14: The SEM micrographs of HAp/TiO$_2$ composite films annealed at (a) 300 ºC, (b) 500 ºC, (c) 700 ºC, (d) 900 ºC and (e) 1,100 ºC

5.6 Mechanical Properties Investigated by Nanoindentation

Nanoindentation test were carried out using nanoindentation system (CSM instrument) with a Berkovich tip throughout this study. The measurement was done at 20, 30 and 40 mN loads. The hardness plot of the HAp and HAp/TiO$_2$ films annealed at various temperatures are exhibited in Fig. 5.15. Furthermore, the plots of elastic modulus are also shown in Fig. 5.16. It was found that hardness and elastic modulus of HAp films are around 1.2 and 35 GPa, respectively, while the values of HAp/TiO$_2$ composite film are 2.4 and 54 GPa, but these values are independent with the annealing temperatures. From this result, hardness of HAp/TiO$_2$ is two times comparing with HAp film. The HAp/TiO$_2$ film is harder than HAp film. The reasons of increasing in hardness and elastic modulus are caused by TiO$_2$ nanoparticle reinforced HAp matrix which gave higher mechanical property in the material.
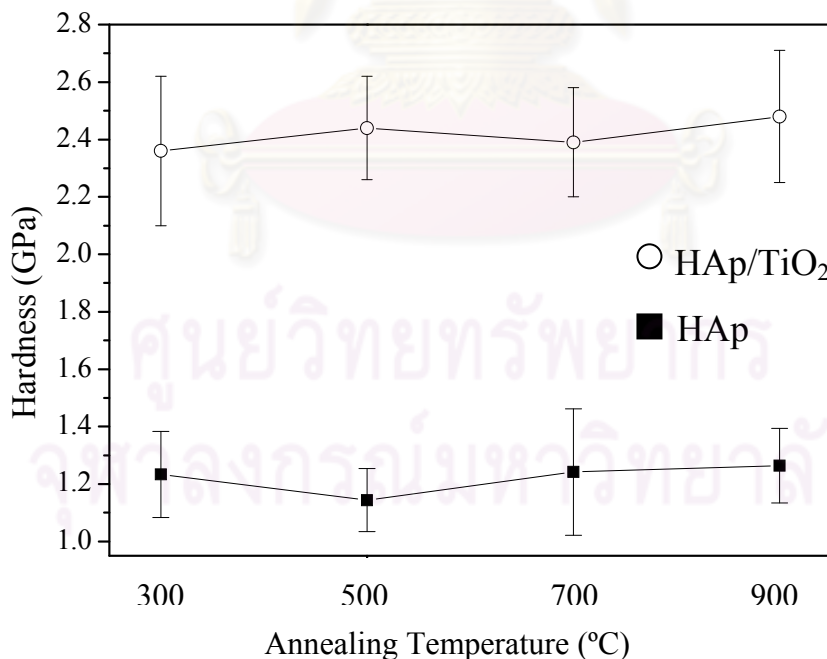
Figure 5.15: The plot of hardness of HAp and HAp/TiO$_2$ films annealed at 300, 500, 700 and 900°C
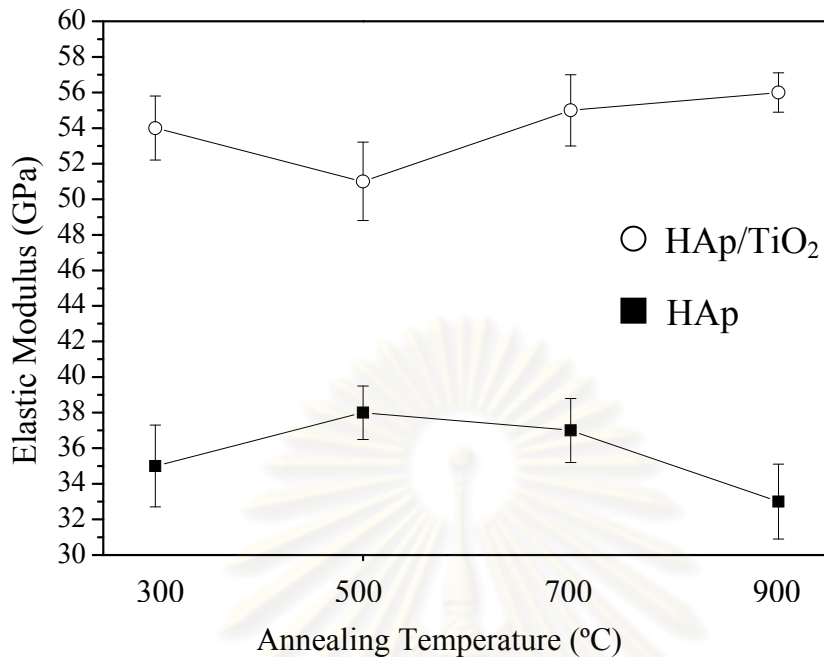
Figure 5.16: The plot of elastic modulus of HAp and HAp/TiO$_2$ films annealed at 300, 500, 700 and 900ºC
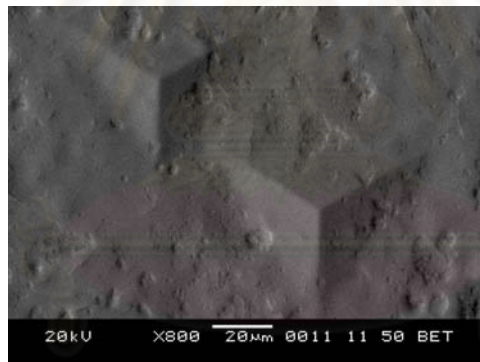
Figure 5.17: Example of an indent left by a Berkovich tip in HAp films

The examples of load-unloading curves from 3 indentations which made on the HAp film annealed at 700°C are shown in Fig. 5.18. For the HAp/TiO$_2$ films with the same temperature are also shown in Fig. 5.19. From observation these curves, the area under the curve is divided into two parts, one is elastic work and the other is plastic (or inelastic) work. The slope of unloading curve is performed the stiffness, which is directly related to elastic modulus. To compare HAp with HAp/TiO$_2$, we found that the stiffness of HAp is less than that of HAp/TiO$_2$ as a result in the elastic work is higher. This can be concluded that the HAp/TiO$_2$ film has more elastic modulus and harder than the ordinary HAp film.
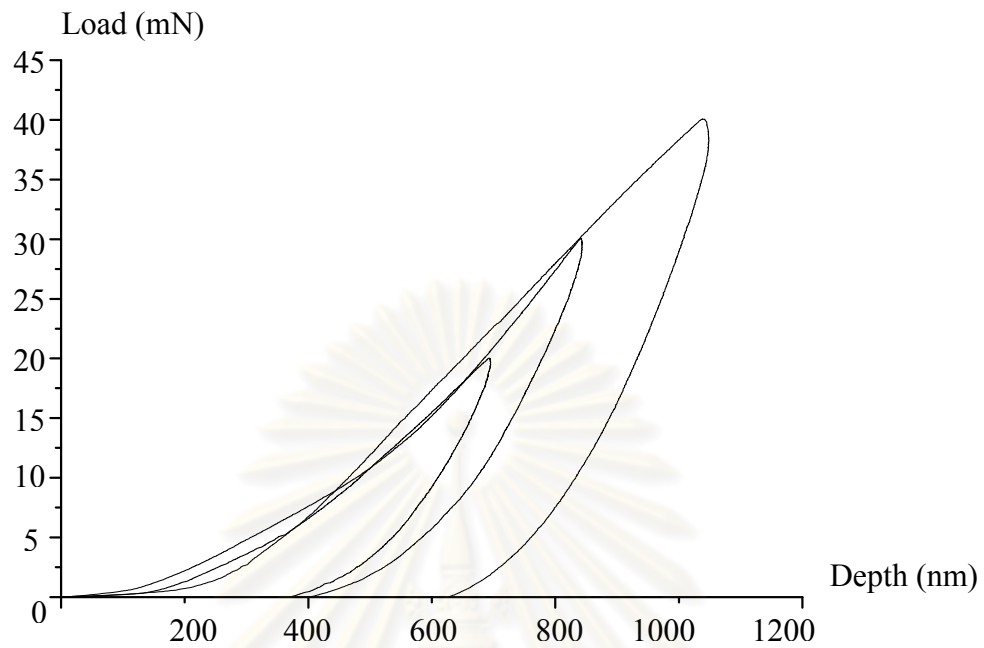
Figure 5.18: Example of load-unloading curves of 3 indentations made on the HAp film annealed at 700°C
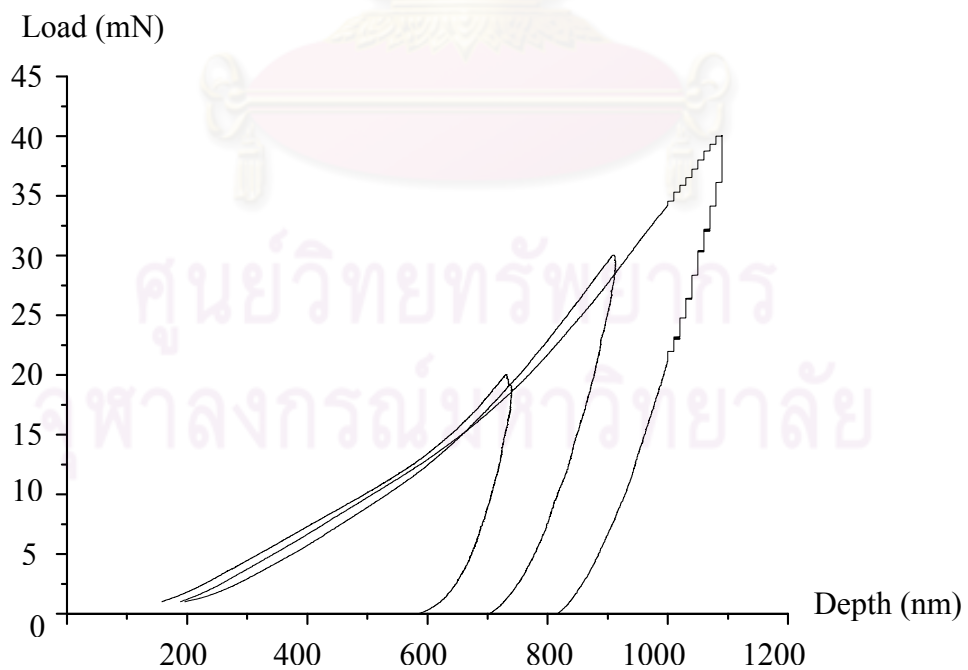
Figure 5.19: Example of load-unloading curves of 3 indentations made on the HAp/TiO$_2$ film annealed at 700°C

5.7 Antibacterial Test on SrHAp

In this study, the *in vitro* test bacteria was *Stqhylococcus aureus* and the test inhibitors was SrHAp sol. The SrHAp sol was diluted to difference concentrations. The positive control test was done by dropping only Luria–Bertani (LB) medium, which is food for bacteria, without bacteria. In contrast, the negative control was prepared by adding bacteria mixed with Luria–Bertani (LB) medium. The test was done in micro titer plate (see Fig. 5.20(a)) and kept for 24 hours. After that, the solution from each well was dropped into the plate. Zone A was dropped with negative control and SrHAp with concentration of 50, 25 and 12.5. Zone B and Zone C were 100 mM and 200 mM of SrHAp, respectively. The positive control with 400, 800 mM of SrHAp were exhibited in Zone D. The results from Fig. 5.20(b) show that there are many bacteria colonies in Zone A and Zone B, while in Zone C is displayed tiny colonies and Zone D shows without any bacteria. This can be concluded that SrHAp has an inhibition on the growth of *Stqhylococcus aureus* bacteria in concentration higher than 200 mM. This can be applied that the SrHAp can be used in the antimicrobacterial applications.
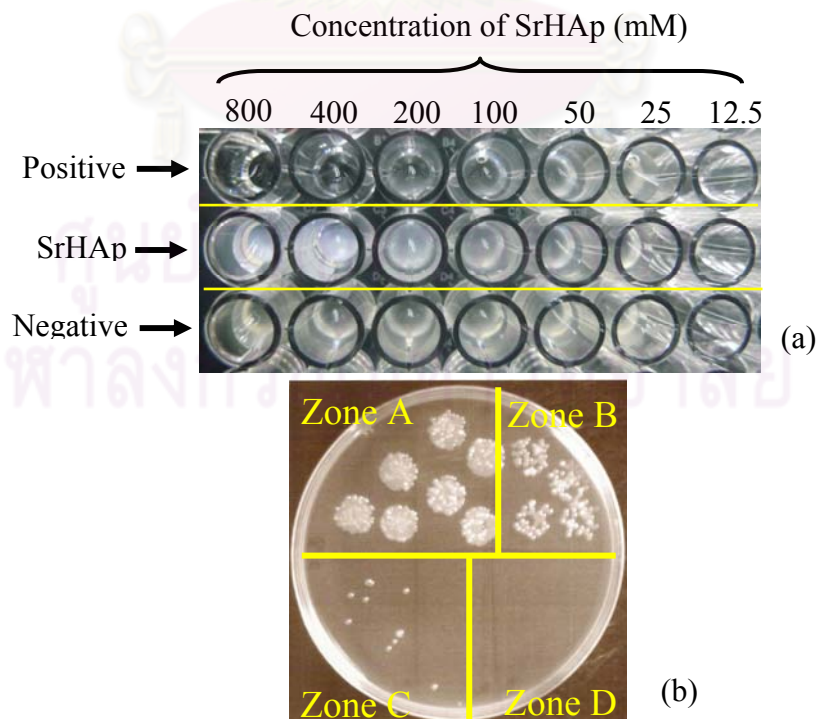
Figure 5.20: The experimental procedure of antibacterial test

CHAPTER VI
CONCLUSIONS

In this thesis, the author has described and illustrated the synthesis process of HAp, SrHAp and HAp/TiO$_2$ solution for thin film coating, and their characterizations. The main results and conclusions obtained in this study are summarized as follow:

I.) HAp powder can be prepared by following to the previous work [18] without any impurity phase, which observed from XRD and EDS results.

II.) HAp thin films coatings on both silicon and 316L stainless steel substrate can be successfully fabricated by sol-gel spin coating. The evolution of phase and structure can be observed by XRD. It shows that the structure develops toward more crystalline with an increasing temperature. The HAp phase has decomposed to β-TCP phase at 1,100 ºC of annealing temperature. The SEM micrographs show that the crystal size increased with an increasing annealing temperature to 1,100 ºC and the structure of HAp is porous. The thickness of the coating is approximately 10 μm. Moreover, hardness and elastic modulus of HAp films annealed at various temperatures are average values of 1.2 and 35 GPa, respectively, and there are no significant effects related to the annealing temperatures.

III.) The strontium-substituted hydroxyapatite in both powder and thin film can also be prepared by sol-gel technique. Sr^{2+} can half and totally replaced Ca^{2+}, and incorporate into the apatite structure with the atomic ratios of [Sr]/[Ca+Sr] as 0.5 and 1, respectively. Increasing Sr substitution for Ca exhibited the expansion of the crystal structure, explained by a linear increasing in lattice

parameters (*a* and *c*). The evolution of phase and structure of SrHAp films can be observed by XRD. It showed that the structure develop to more crystalline with an increasing temperature. The $Sr_3(PO_4)_2$ phase was detected at 900ºC of annealing temperature. The SEM micrographs showed that the crystal size increased with increasing annealing temperature and the same for the microstructure evolution of SrHAp materials. Moreover, SrHAp also has antibacterial property.

IV.) The HAp/TiO_2 composite films can be fabricated by sol-gel spin coating technique. The phase structure of TiO_2 particle is anatase at temperature below 500ºC. In contrast, some of TiO_2 anatase phase transformed to rutile phase at temperature above 500ºC and more crystallinity at higher temperature. From SEM micrographs, it shows that TiO_2 nanoparticles are distributed and linked with HAp microstructure. Hardness and elastic modulus of HAp/TiO_2 composite films are 2.4 and 54 GPa, which higher than HAp film. So, we can successfully prepare TiO_2 reinforced HAp film to improve mechanical properties.

REFERENCES

[1] J.B. Park. *Biomaterials Science and Engineering*. New York : Plenum Press, 1987.

[2] L.L. Hench. Bioceramics: from Concept to Clinic, *J.Am.Ceram.Soc.* **74** (1991): 1487-1510.

[3] L.L. Hench and E.C. Ethridge. *Biomaterials*. New York : Academic Press, 1982.

[4] A. Bigi, E. Boanini, C. Capuccini and M. Gazzano. Strontium-substited Hydroxyapatite Nanocrystals, *Inorganica Chimica Acta* **360** (2007): 1009-1016.

[5] E.A. Monroe, W. Votava, D.B. Bass and J. McMullen. New Calcium Phosphate Ceramic Material for Bone and Tooth Implant, *J.Dental.Res.* **50** (1971): 860-861.

[6] W. Suchanek and M. Yoshimura. Processing and Properties of Hydroxyapatite-based Biomaterials for Use as Hard Tissue Replacement Implants, *J.Mater.Res.* **13** (1998): 94-116.

[7] H. Aoki. *Science and Medical Applications of Hydroxyapatite*. Tokyo: JAAS, (1991).

[8] N. Thangamani, K. Chinnakali and F. D. Gnanam. The Effect of Powder Processing on Densification, Microstructure and Mechanical Properties of Hydroxyapatite, *Ceram.Inter.* **28** (2002): 355-362.

[9] W. Suchanek, M. Yashima, M. Kakihana and M. Yoshimura. Hydroxyapatite/Hydroxyapatite-Whisker Composites without Sintering Additives: Mechanical Properties and Microstructural Evolution, *J.Am.Ceram.Soc.* **80** (1997): 2805-13.

[10] A. Nakahira, K. Sakamoto, S. Yamaguchi, M. Kaneno, S.Takeda and M. Okazaki. Novel Synthesis Method of Hydroxyapatite Whiskers by Hydrolysis of α-Tricalcium Phosphate in Mixtures of Water and Organic Sovent, *J.Am.Ceram.Soc.* **82** (1999): 2029-32.

[11] H. Li, K. A. Khor and P. Cheang. Impact Formation and Microstructure Characterization of Thermal Sprayed Hydroxyapatite/titania Composite Coatings, *Biomaterials* **24** (2003): 949-957.

[12] KANAZAWA, Takafumi. *Inorganic Phosphate Materials*. Tokyo: Kodansha Ltd., (1989).

[13] A. Laghzizil, N. Elherch, A. Bouhaouss, G. Lorente, T. Coradin and J. Livage. Electrical Behavior of Hydroxyapatites $M_{10}(PO_4)_6(OH)_2$ (M = Ca, Pb, Ba), *Mater.Res.Bullet.* **36** (2001): 953-962.

[14] T.J. Webster, E.A. Massa-Schlueter, J.L. Smith and E.B. Slamovich. Osteoblast Response to Hydroxyapatite Doped with Divalent and Trivalent Cations, *Biomaterials* **25** (2004): 2111-2121.

[15] S. Pors Nielsen. The Biological Role of Strontium, *Bone*, **35** (2004): 583-588.

[16] K.L. Wong, C.T. Wong, W.C. Liu, H.B. Pan, M.K. Fong, W.M. Lam, W.L. Cheung, W.M. Tang, K.Y. Chiu, K.D.K. Luk and W.W. Lu. Mechanical Properties and *in vitro* Response of Strontium-containing Hydroxyapatite/polyetheretherketone Composites, *Biomaterials* **30** (2009): 3810-3817.

[17] C. Capuccini, P. Torricelli, F. Sima, E. Boanini, C. Ristoscu, B. Bracci, G. Socol, M. Fini, I.N. Mihailescu and A. Bigi**.** Strontium-substituted Hydroxyapatite Coatings Synthesized by Pulsed-laser Deposition: In vitro Osteoblast and Osteoclast Response**,** *Acta Biomaterialia* **4** (2008): 1885-1893.

[18] L. Pinyo. *Processing and Mechanical Propertied of Hydroxyapatite/tetragonal Zirconia Bilayer Structure*. Master's thesis, Department of Physics, Faculty of Science, Chulalongkorn University, 2002.

[19] Alain C. Pierre. *Introduction to Sol-Gel Processing*. Massachusetts: Kluwer Academic Publishers, 1998.

[20] John D. Wright and Nico A.J.M. Sommerdijk. *Sol-Gel Materials Chemistry and Applications*. Florida: CRC PRESS, 2000.

[21] Yet-Ming Chiang, Dunbar Birnie III and W. David Kingery. *Physical Ceramics*. New York: John Wiley & Sons, Inc., 1997.

[22] Stanley L. Flegler, John W. Heckman and Karen L. Klomparens. *Scanning and Transmission Electron Microscopy an Introduction*. New York: John Wiley & Sons, Inc., 2006.

[23] M.H. Loretto. *Electron Beam Analysis of Materials*. London: Chapman & Hall, 1994.

[24] Mario Birkholz. *Thin Film Analysis by X-Ray Scattering*. Weinheim: Wiley-Vch Verlag GmbH & Co., 2006.

[25] Anthony C. Fischer- Cripps. *Mechanical engineering series nanoindentation*. New York: Spring-Verlag New York, LLC, 2004.

[26] Saeed Saber-Samandari and Kārlis A. Gross. Nanoindentation Reveals Mechanical Properties within Thermally Sprayed Hydroxyapatite Coatings, *Surf.Coat.Technol.* **203** (2009), 1660-1664.

[27] Saeed Saber-Samandari and Kārlis A. Gross. Micromechanical Properties of Single Crystal Hydroxyapatite by Nanoindentation, *Acta Biomaterialia* **5** (2009): 2206-2212.

[28] Sang-Hoon Rhee. Synthesis of Hydroxyapatite via Mechanochemical Treatment, *Biomaterials*, **23** (2002): 1147-1152.

[29] Sindo Kou Hoboken. *Welding Metallurgy [electronic resource]*. Newjersy: Wiley-Interscience, 2003.

[30] W.C. Oliver and G.M. Pharr, Measurement of Hardness and Elastic Modulus by Instrumented Indentation: Advances in Understanding and Refinements to Methodology, *J. Mater. Res.* **19** (2004): 3–20.

[31] Ming-Fa Hsieh, Li-Hsiang Perng and Tsung-Shune Chin. Hydroxyapatite Coating on Ti6Al4V Alloy Using a Sol–Gel Derived Precursor, *Materials Chemistry and Physics* **74** (2002): 245-250.

[32] M.D. O'Donnell, Y. Fredholm, A. de Rouffignac and R.G. Hill. Structural Analysis of a Series of Strontium-substituted Apatites, *Acta Biomaterialia* **4**(2008): 1455-146

APPENDICES

APPENDIX A

CONFERENCE PRESENTATIONS

1.) **B. Hongthong**, S.K. Hodak and S. Tungasmita. Synthesis of Hydroxyapatite Thin Films by Sol-Gel Technique. *Siam Physics Congress (SPC)*, March 19-21, 2009 (Poster Presentation).

2.) **B. Hongthong**, S.K. Hodak and S. Tungasmita. Synthesis and Characterization of Strontium Doped Hydroxyapatite Thin Films. *35th Congress on Science and Technology of Thailand (STT.35)*. October 15-17, 2009 (Oral Presentation).

3.) **B. Hongthong**, S.K. Hodak and S. Tungasmita. Synthesis and Characterizations of Strontium Substituted Hydroxyapatite Thin Films. *International Conference on Functionalized and Sensing Materials (FuSeM 2009)*. December 7-9, 2009 (Oral Presentation).

APPENDIX B

INTERNATIONAL SCIENTIFIC PAPER

Synthesis and Characterizations of Strontium Substituted Hydroxyapatite Thin Films

B. Hongthong[a], S. K. Hodak[b], S. Tungasmita[c*]

Department of Physics, Faculty of Science, Chulalongkorn University, Bangkok, 10330 Thailand

[a] bingo_bhasit30@hotmail.com, [b] satreerat.h@chula.ac.th, [c] sukkaneste.t@chula.ac.th

Keywords: hydroxyapatite, strontium, sol-gel, thin film

Abstract. Strontium substituted hydroxyapatite(SrHAp) were fabricated both in the form of powder as reference and thin film by using inorganic precursor reaction. The sol-gel process has been used for the deposition of SrHAp layer on stainless steal 316L substrate by spin coating technique, after that the films were annealed in air at various temperatures. The chemical composition of SrHAp is represented $(Sr_xCa_{1-x})_5(PO_4)_3OH$, where x is equal to 0, 0.5 and 1.0. Investigations of the phase structure of SrHAp were carried out by using X-ray diffraction technique (XRD). The results showed that strontium is incorporated into hydroxyapatite where its substitution for calcium increases in the lattice parameters, and $Sr_3(PO_4)_2$ can be detected at 900ºC. The SEM micrographs showed that SrHAp films exhibited porous structure before develop to a cross-linking structure.

Introduction

Hydroxyapatite [HAp:$Ca_{10}(PO_4)_6(OH)_2$] is widely used as a biomaterial, especially in orthopedic and dental applications because its chemical composition is quite similar to the human bone and teeth[1]. Among the ionic groups consisting of HAp structure, Ca^{2+} can be replaced by various ions, such as Na^+, K^+ and Mg^{2+}[2-4]. Strontium is also one on the metal that can replace calcium in the HAp structure to form strontium substituted hydroxyapatite (SrHAp) because strontium is chemically and physically closely related to calcium. There are many *in-vitro* studies indicated that strontium can increases bone formation and reduces bone resorption[5,6].

There are some surgical treatment of bone defects, metallic implants, such as hip-joint replacements and artificial tooth sockets, are high mechanical stability, but do not form directly bonds to bone tissue. To improve implant fixation to hard tissues, it can be done by coating the metallic surface with a thin film of calcium phosphate-based materials. Many different coating techniques have been used for the preparation of HAp or SrHAp coatings, for examples, plasma spray[6,7], laser ablation[8,9], RF sputtering[10], and sol-gel technique[11,12]. The sol-gel processing represents an alternative approach for the coating preparation with potential advantages, such as higher purity and homogeneity, lower processing temperatures, simple and cheap method of preparation. For this work, we have studied and explored the synthesis of SrHAp both in powder form and fabricate as a thin film on stainless steal 316L substrate using sol-gel technique. The crystal structure and the microstructure of a series of SrHAp were investigated by XRD and SEM, respectively. The elemental composition of the materials was measured by EDS.

Experimental Procedure

Materials Preparation

HAp, as a reference and SrHAp materials were synthesized both in the form of powder and solution for thin film casting, by precipitation from mixed inorganic solution, regarding to previous report[13]. Briefly, calcium nitrate tetrahydrate [$Ca(NO_3).4H_2O$] and strontium nitrate [$Sr(NO_3)_2$] in different ratios were dissolved in distilled water to prepare the Ca+Sr containing solutions (the molar ratios of [Sr]/[Ca+Sr] were set as 0, 0.5 and 1). The pH of the solution was adjusted to 11 to avoid the precipitation of $CaHPO_4$ and/or $SrHPO_4$ as an impurity phase by adding ammonia solution. Another set of phosphorus precursor [$(NH_4)_2HPO_4$] was dissolved in distilled water to prepare the P-containing solutions by setting the molar ratio of (Ca+Sr)/P as 1.67, and then were

added dropwise to the Ca+Sr-containing solutions under vigorous stirring at constant pH 11. Table 1 shows the weights used for each composition. After additional stirring for 4 h. and ageing for overnight, the colloidal sol was filtered under vacuum, and then dried at 100°C for 24h. The dried product was crushed and sieved to obtain the powders. The dried powders were calcined at 240°C for 24 h.

Table 1. Experimental weights(in g) for synthesis of $(Sr_xCa_{1-x})_5(PO_4)_3OH$

Sr(x)	Ca(NO$_3$).4H$_2$O	wt.%	mol%	Sr(NO$_3$)$_2$	wt.%	mol%	(NH$_4$)$_2$HPO$_4$	wt.%	mol%
1.00	-	-	-	42.34	72.72	62.50	15.85	27.24	37.50
0.50	23.62	38.95	31.25	21.17	34.91	31.25	15.85	26.14	37.50
0.00	47.23	74.87	62.50	-	-	-	15.85	25.13	37.50

Thin Films Deposition

HAp and SrHAp thin films were prepared from the prepared colloidal solution by spin coating technique. These films were spin-deposited at a speed of 2000 rpm at room temperature. Stainless steel 316L plates (10x10x1mm) were used as substrates. Prior to coating, these substrates were polished using #180-600 SiC polishing papers to improve the interface adhesion, and then ultrasonically cleaned with acetone and methanol, finally rinsed with distilled water. The coated layers were dried at 150 °C for 10 min, and then annealed in air at various temperatures: 300°C, 500°C, 700°C and 900°C for 10 min, finally cooled down to room temperature.

Analytical Methods

The structure of synthesized powders and thin films were characterized by using X-ray diffractometer (Bruker-AX8 D8 DISCOVER and Rigaku D/MAX-2200 Ultima$^+$) with CuK$_d$ (λ= 1.5406 Å), from 2θ=15-60°. The microstructure, morphology and elemental composition were investigated by using SEM/EDS (JEOL, JSM-6480LV)

Results and Discussions
Crystal Structure Analysis of Powder

The x-ray diffraction patterns of the powder synthesized with different [Sr]/[Ca+Sr] molar ratios are shown in Fig.1. The XRD patterns of the samples corresponding to HAp(Sr0) and to SrHAp(Sr1) displayed well-defined and sharp peaks. On the other hand, the pattern of the sample containing both Ca and Sr generally exhibited a broader diffraction peaks indicating that the crystallinity is decreased after Ca^{2+} is half substituted by Sr^{2+} in the structure. The Sr substitution may effect the growth of HAp lattice and consequently decreased the crystalline quality because lattice strains due to Sr-atoms substitution. All of patterns also demonstrated that the reference powders show no another phases or no impurity can be observed.
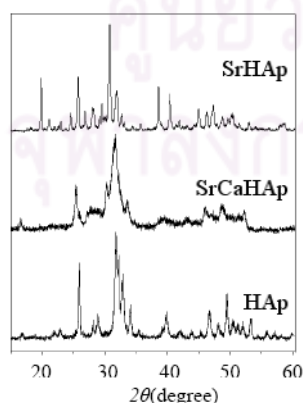
Fig. 1 Powder X-ray diffraction patterns of Hap, SrCaHAp and SrHAp.
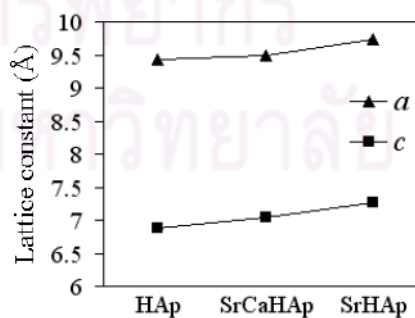
Fig. 2 Lattice parameters of the powders.

The diffraction peaks of the SrHAp shifted to lower 2θ values due to an increasing in d-spacing and lattice parameters. The crystal structure of HAp and SrHAp is hexagonal system. The lattice parameters ($a = b$ and c) of the series powders, as shown in Fig.2, were determined by using Bragg's law and the geometric relationship for a hexagonal crystal system. The results show that a and c increase linearly with Sr-addition. It is known that the larger ionic radius of Sr compared to Ca ($Ca^{2+} = 1.00$ Å and $Sr^{2+} = 1.18$ Å) causes the apatite lattice to expand in both the a- and c-axis directions.

XRD Analysis of SrHAp Films

Fig.3 shows the XRD patterns of SrHAp thin film on stainless steel 316L annealed at 300°C, 500°C, 700°C and 900°C, respectively. The broad reflection of the dominated peak, other than substrate's peaks, that corresponding to the SrHAp appeared at 300 and 500°C. It indicated that SrHAp sintered at these temperatures has poor cystallinity. At higher temperatures (700°C and 900ºC), the SrHAp structure became strong and well-defined peaks. This suggested that the SrHAp coatings develop from nanocrystalline toward polycrystalline with preformed orientations. The peak that corresponding to $Sr_3(PO_4)_2$ phase, as impurity, was found in annealing temperature of 900ºC at $2\theta=33.6°$. The XRD analysis indicated that the evolution of SrHAp film structure developed as the post-annealing temperature increased.

SEM Analysis of Annealed SrHAp Films

The SEM micrographs of the SrHAp film annealed at various temperatures shown in Fig.4. The morphology of SrHAp film annealed at 300ºC and 500ºC (Fig.4a and b) exhibited almost rod shape. On the other hand, at 700ºC it can be observed as fine grains and As the film was annealed at 900 °C, the grains size had developed and formed as cross-linking network structure. Therefore, the evolutions of the grain size depend on the annealing temperatures. This can be due to the crystalline of SrHAp coexists with tricalcium phosphate and tetracalcium phosphate phases and starts re-crystallization at the annealing temperature over $700°C$. Moreover, the SEM micrographs also indicated that SrHAp has porous structure.

EDX Analysis of Powder

Elemental analysis via EDX of powders were shown in Table 2, clearly indicated that the atomic percent of Sr and Ca in SrCaHAp were quite similar. The amounts of calcium and strontium also detected in HAp and SrHAp, respectively. This confirmed that sol-gel technique was able to synthesize $(Sr_xCa_{1-x})_5(PO_4)_3OH$ in the form of thin film and powder.
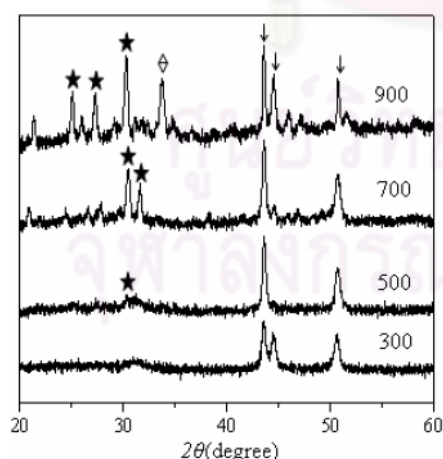
	Atomic percent		
	Calcium	Strontium	Phosphorus
HAp	21.62	-	13.83
SrCaHAp	7.06	7.65	11.97
SrHAp	-	20.34	13.59

Table 2. The atomic percent of the powder calculated from EDX.

Fig.3 The XRD patterns of SrHAp films annealed at various temperatures.(★): SrHAp, (↓): stainless steel 316L, (⬦): $Sr_3(PO_4)_2$
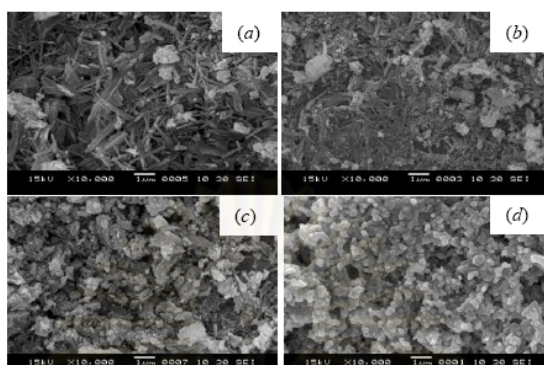
Fig. 4 SEM micrographs of SrHAp films annealed at (a) 300ºC, (b) 500ºC, (c) 700ºC and (d) 900ºC

The strontium substituted hydroxyapatite in both powder and thin film can be prepared by sol-gel technique. Sr^{2+} can half and totally replace Ca^{2+} and enter the apatite structure with the atomic ratios of [Sr]/[Ca+Sr] as 0.5 and 1, respectively. Increasing Sr substitution for Ca exhibited the expansion of the crystal structure, explained by a linear increasing in lattice parameters (*a* and *c*). The evolution of phase structure of SrHAp film can be observed by XRD. It showed that the structure develop to more crystalline with an increasing temperature. The $Sr_3(PO_4)_2$ phase was detected at 900ºC of annealing temperature. The SEM micrographs showed that the crystal size increased with increasing annealing temperature and the microstructure of SrHAp is porosity.

Reference
[1] E. A. Monroe, W. Votava, D. B. Bass and J. McMullen: J.Dental.Res. Vol. 50 (1971), p. 860
[2] T. Naddari, B. Hamdi, J.M. Savariault, H.E. Feki and A.B. Salah: Mater Res Bull Vol. 38 (2003), p. 221
[3] T.J. Wabster, E.A. Massa-Schlueter, J.L. Smith and E.B. Slamovich: Biomaterials Vol. 25 (2004), p. 2111
[4] S. Kannan, J.M.G. Ventura, J.M.F. Ferreira: Ceram. Inter. Vol. 33 (2007), p. 1489
[5] S. G. Dahl, P. Allain, P. J. Marie, Y. Mauras, G. Boivin, P. Ammann,Y. Tsouderos, P. D. Delmas and C. Christiansen: Bone Vol.28 (2001), p. 446
[6] W. Xue, H.L. Hosick, A. Bandyopadhyay, S. Bose, C. Ding, K.D.C. Cheung and W.W. Lu: Surf. Coat. Tech. Vol. 201 (2007), p. 4685
[7] C. Renghini, E. Girardin, A.S. Fomin, A. Manescu, A. Sabbioni, S.M. Barinov, V.S. Komlev, G. Albertini and F. Fiori: Mater. Sci. Eng. B Vol. 152 (2008), p. 86
[8] C. Capuccini, P. Torricelli, F. Sima, E. Boanini, C. Ristoscu, B. Bracci, G. Socol, M. Fini, I.N. Mihailescu and A. Bigi: Acta Biomater. Vol. 4 (2008), p. 1885
[9] C.F. Koch , S. Johnson , D. Kumar , M. Jelinek ,D.B. Chrisey , A. Doraiswamy ,C. Jin , R.J. Narayan and I.N. Mihailescu: Mater. Sci. Eng. C Vol. 27 (2007), p. 484
[10] B. Feddes, J.G.C. Wolke, A.M. Vredenberg and J.A. Jansen: Biomaterials Vol. 25 (2004), p. 633
[11] A. Balamuruga, G. Balossier, P. Torres, J. Michel and J.M.F. Ferreira: Mater. Sci. Eng. C Vol. 29 (2009), p. 1006
[12] L. Gan and R. Pilliar: Biomaterials Vol. 25 (2004), p. 5303
[13] H.W. Kim, Y.H. Koh, YM Kong, J.G. Kang and H.E. Kim: J. Mater. Sci. Vol. 15 (2004), p. 1129
[13] H.W. Kim, Y.H. Koh, YM Kong, J.G. Kang and H.E. Kim: J. Mater. Sci. Vol. 15 (2004), p. 1129

Functionalized and Sensing Materials
doi:10.4028/www.scientific.net/AMR.93-94

Synthesis and Characterizations of Strontium Substituted Hydroxyapatite Thin Films
doi:10.4028/www.scientific.net/AMR.93-94.231

References
[1] E. A. Monroe, W. Votava, D. B. Bass and J. McMullen: J.Dental.Res. Vol. 50 (1971), p. 860

[2] T. Naddari, B. Hamdi, J.M. Savariault, H.E. Feki and A.B. Salah: Mater Res Bull Vol. 38 (2003), p. 221
doi:10.1016/S0025-5408(02)01033-4

[3] T.J. Wabster, E.A. Massa-Schlueter, J.L. Smith and E.B. Slamovich: Biomaterials Vol. 25 (2004), p. 2111
doi:10.1016/j.biomaterials.2003.09.001
PMid:14741626

[4] S. Kannan, J.M.G. Ventura, J.M.F. Ferreira: Ceram. Inter. Vol. 33 (2007), p. 1489
doi:10.1016/j.ceramint.2006.05.016

[5] S. G. Dahl, P. Allain, P. J. Marie, Y. Mauras, G. Boivin, P. Ammann,Y. Tsouderos, P. D. Delmas and C. Christiansen: Bone Vol.28 (2001), p. 446
doi:10.1016/S8756-3282(01)00419-7
PMid:11336927

[6] W. Xue, H.L. Hosick, A. Bandyopadhyay, S. Bose, C. Ding, K.D.C. Cheung and W.W. Lu: Surf. Coat. Tech. Vol. 201 (2007), p. 4685
doi:10.1016/j.surfcoat.2006.10.012

[7] C. Renghini, E. Girardin, A.S. Fomin, A. Manescu, A. Sabbioni, S.M. Barinov, V.S. Komlev, G. Albertini and F. Fiori: Mater. Sci. Eng. B Vol. 152 (2008), p. 86
doi:10.1016/j.mseb.2008.06.016

[8] C. Capuccini, P. Torricelli, F. Sima, E. Boanini, C. Ristoscu, B. Bracci, G. Socol, M. Fini, I.N. Mihailescu and A. Bigi: Acta Biomater. Vol. 4 (2008), p. 1885
doi:10.1016/j.actbio.2008.05.005
PMid:18554996

[9] C.F. Koch, S. Johnson, D. Kumar, M. Jelinek, D.B. Chrisey, A. Doraiswamy, C. Jin, R.J. Narayan and I.N. Mihailescu: Mater. Sci. Eng. C Vol. 27 (2007), p. 484
doi:10.1016/j.msec.2006.05.025

[10] B. Feddes, J.G.C. Wolke, A.M. Vredenberg and J.A. Jansen: Biomaterials Vol. 25 (2004), p. 633

doi:10.1016/S0142-9612(03)00574-X
PMid:14607501

[11] A. Balamuruga, G. Balossier, P. Torres, J. Michel and J.M.F. Ferreira: Mater. Sci. Eng.
C Vol. 29 (2009), p. 1006
doi:10.1016/j.msec.2008.09.005

[12] L. Gan and R. Pilliar: Biomaterials Vol. 25 (2004), p. 5303
doi:10.1016/j.biomaterials.2003.12.038
PMid:15110481

[13] H.W. Kim, Y.H. Koh, YM Kong, J.G. Kang and H.E. Kim: J. Mater. Sci. Vol. 15 (2004),
p. 1129

[13]H.W. Kim, Y.H. Koh, YM Kong, J.G. Kang and H.E. Kim: J. Mater. Sci. Vol. 15 (2004),
p. 1129

APPENDIX C

PROCEEDING

SYNTHESIS OF HYDROXYAPATITE THIN FILMS BY SOL-GEL TECHNIQUE

B. Hongthong[*], S. Kampangkeaw Hodak and S. Tungasmita

Department of Physics, Faculty of Science, Chulalongkorn University, Bangkok, Thailand

Abstract

Hydroxyapatite [HAp: $Ca_{10}(PO_4)_6(OH)_2$], HAp, was synthesized both in the form of powder as reference and thin film. The materials were prepared using inorganic precursor solutions: calcium nitrate tetrahydrate [$Ca(NO_3).4H_2O$] and diammonium hydrogen phosphate [$(NH_4)_2HPO_4$]. The sol-gel process has been used for the deposition of HA layer on Si substrate by spin coating technique. The HAp thin films were annealed in air at 300°C, 500°C, 700°C, 900°C and 1,100°C. The evolution of structure and morphology as a function of the sintering temperature was investigated by XRD and SEM. HAp films were also characterized by EDX in order to measure their elemental compositions. The results show that the HAp structure developed within annealing at temperature of 700°C, 900°C and 1,100°C. The SEM micrograph showed that HA films have porous structure before develop to a cross-linking structure with an indication of β-TCP.

1 INTRODUCTION

Hydroxyapatite [HAp:$Ca_{10}(PO_4)_6(OH)_2$] is frequently used in orthopedic and dental surgery because its chemical composition is similar to the human bone and teeth[1]. HAp is also osteoconductive which accelerates bone growth. It has been well known that HAp is bioactive and biocompatible with human tissues, while the others phases such as tricalciumphosphate [TCP:$Ca_3(PO_4)_2$] and tetracalciumphosphate [TTCP:$Ca_4(PO_4)_2O$] are highly bioresorbable[2]. However, due to the brittleness of HAp, low fracture toughness ($K_{IC} < 1$ MPa m$^{1/2}$)[3], the scope of its application is limited. It is known that the application of HAp coatings on metallic implant devices offers the possibility of combining the strength of the metals and the bioactivity of the ceramics.

Many different techniques have been used for the preparation of HAp coatings such as plasma spray[4], laser ablation[5], RF sputtering[6], and sol-gel technique[7,8]. Plasma spray operates under extremely high temperatures, so HAp can be decomposed into the others phases. Furthermore, the main problem associated with RF sputtering technique is lack of an exact stoichiometry. Therefore, sol-gel processing represents an alternative approach for the coating preparation with potential advantages, such as higher purity and homogeneity, lower processing temperatures, simple and cheap method of preparation.

The present paper describes the synthesis of HAp either in the form of powder or thin film by using inorganic precipitation method[9]. We used Si wafer as substrates for studying sol-gel HAp coatings. In this study, the evolution of structure and morphology was investigated by XRD and SEM techniques as a function of the sintering temperature. HAp films were characterized by EDX in order to measure their elemental compositions.

2 EXPERIMENTAL

2.1 Materials Preparation

HAp was synthesized both in the form of powder and sol by using precipitation from mixed aqueous inorganic solution[10]. Briefly, calcium nitrate tetrahydrate [$Ca(NO_3).4H_2O$] and diammonium hydrogen phosphate [$(NH_4)_2HPO_4$] were used as calcium and phosphorous precursors, and the molar ratio of Ca/P in these starting reactants was set equal to 1.67. The reaction occurred at room temperature and the pH was adjusted to 11-12 by adding ammonia solution. The colloidal sol was mixed during 3 hours under vigorous stirring, then ageing for 24 hours. In figure 1 shows a schematic representation of synthesized HAp process. Prior to coating, silicon wafer, which is used as substrate, was ultrasonically cleaned with acetone and methanol in order to remove dust or impurities and finally washed with deionized water.

2.2 HAp Films Deposition

In this study, HAp thin films were prepared by spin coating technique from prepared sol. These films were deposited at a speed of 2000 rpm at room temperature. The coatings were dried at 150 °C for 10 minutes, and then annealed in air at 300°C, 500°C,

[*]Tel: 02-2187689; E-mail: bingo_bhasit30@hotmail.com

700°C, 900°C and 1,100°C for 10 minutes, finally cooled to room temperature.

2.3 Analytical Methods

The characterization of the coatings has been carried out using X-ray diffraction (XRD), energy dispersive analysis (EDX) and scanning electron microscopy (SEM). The phase identification of HAp powders and films was characterized by using X-ray diffractometer (XRD, Bruker-AX8 D8 DISCOVER) with $CuK_{\alpha 1}$ (λ= 1.5406 Å), from 2θ=15-60°. The structure, morphology and elemental composition of the film were observed by SEM and EDX (JEOL, JSM-6480LV).
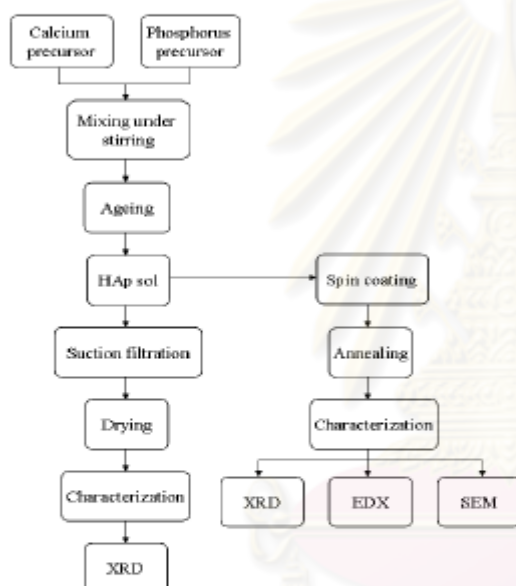
Figure 1 Schematic representation of synthesized HAp process.

3 RESULTS AND DISCUSSION

3.1 Crystal Structure Analysis

The XRD analysis of the synthesized reference powder as shown in Figure 2. exhibited peaks that corresponded to standard reference HAp[11]. It can be seen that both patterns are closely correlated, thus confirming that the obtained powders are monophase HAp.

Figure 3. shows the XRD patterns of the coatings annealed at 300°C, 500°C, 700°C, 900°C and 1,100°C, respectively. The broad reflection of the main peak that corresponding to the HAp (211) appears at 300°C, 500°C and 700°C. It indicates that HAp sintered at these temperatures has poor

cystallinity. At higher temperatures (900 and 1,100°C), the HA structure become stronger peaks corresponding to the (002), (211), (202), (310), and (222) reflections. This suggests that the HAp coatings develop from nanocrystalline toward polycrystalline with preformed orientations. The β-tricalcium phosphate (β-TCP) peaks can be detected at 2θ=30.7° and 27.7°[10] only in the HAp film, which is annealed at 1,100 °C. It can be explained that the HAp may be decomposed at temperature above 1050 °C[12], as the follow,

$$Ca_{10}(PO_4)_6(OH)_2 \longrightarrow 2\beta Ca_3(PO_4)_2 + Ca_4P_2O_9 + H_2O[10]$$

XRD analysis indicates that the evolution of HAp film structure developed as the temperature increased.
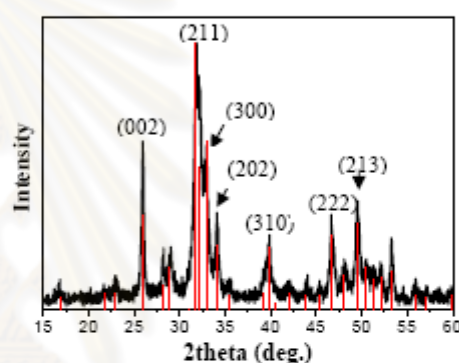
Figure 2 XRD pattern of HAp powder synthesized by inorganic precipitation compared with reference HAp.
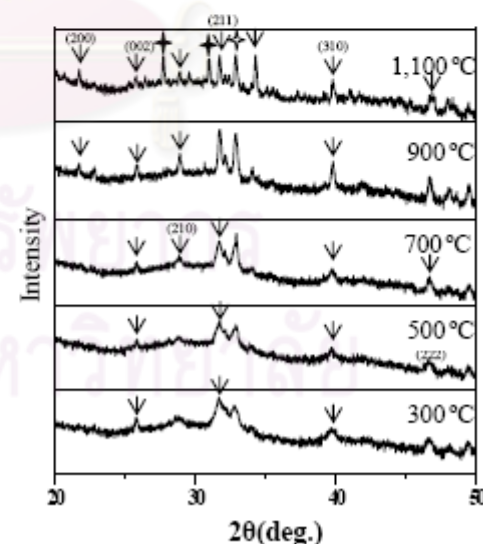
Figure 3 XRD patterns of HAp films on Si substrate annealed at various temperatures. (∀): HAp, (✛): β-TCP, (⟠): Si

3.2 EDX Analysis

The EDX spectrum of the sol-gel HAp coated on Si substrate is given in Figure 4. It indicates the elemental composition of the coated substrate. Intense peaks for calcium, phosphorus and oxygen were obtained. The Si peak, which is the substrate, was detected. It was calculated from EDX analysis that the atomic percent of Ca and P are 18.57 and 14.18 %, respectively.
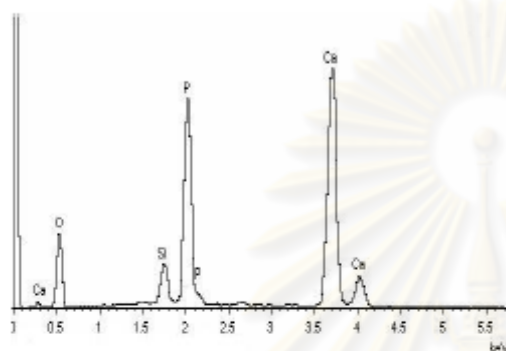
Figure 4 EDX analysis of HAp film on Si substrate

3.3 SEM Analysis

The SEM micrographs of the HAp film annealed at various temperatures show in Figure 5 (a), (b), (c), (d) and (e). Figure 5 (a) and (b) show that the films were quite homogeneous, while the film annealed at 700 °C(Figure 5.(c)) exhibited small fine grains. At 900 °C(Figure 5.(d)), the grain size was more expand and can be observed some pores. When the film was heated at 1,100 °C, the grains size increased and had a good connection with cross-linking. The HAp grains size was found to be approximately 0.5 μm. at 1,100 °C. Therefore, the evolutions of grain size depend on the annealing temperatures. Moreover, from the SEM micrographs represent that HAp has porous structure.
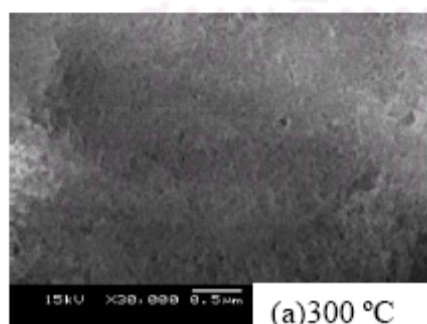
(a)300 °C
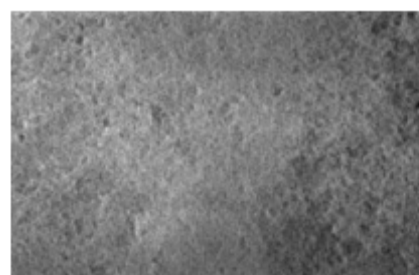
(b)500 °C
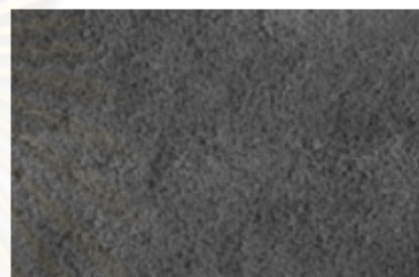
(c)700 °C
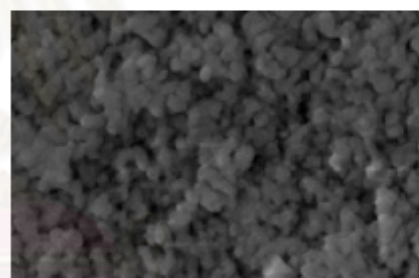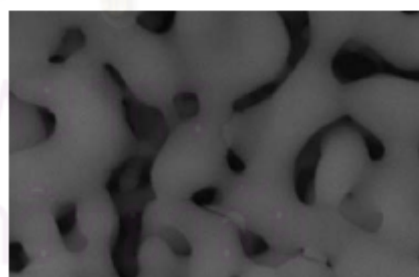
(d)900 °C

(e)1,100 °C

Figure 5: SEM micrographs of HAp films annealed at (a) 300 °C, (b) 500 °C, (c) 700 °C, (d) 900 °C and (e) 1,100 °C

4 CONCLUSION

HAp thin films coatings on Si substrate can be successfully formed by sol-gel process. The evolution of phase structure can be observed by XRD. It shows that the structure develop to more crystalline with an increasing temperature. The HAp phase decomposes to β-TCP phase at 1,100 °C of annealing temperature. The SEM micrographs showed that the crystal size increased with increasing annealing temperature to 1,100 °C and the structure of HAp is porosity.

ACKNOWLEDGEMENT

REFERENCE

[1] E. A. Monroe, W. Votava, D. B. Bass and J. McMullen, J.Dental.Res. 50 (1971) 860-861.

[2] S.K. Nandi, S.K. Ghosh, B. Kundu , D.K. De and D. Basu, Small Rumin. Res. 75 (2008) 144-153

[3] S. Wuttipan, Strength and Microstructure of Hydroxyapatite Ceramics (M.Sc. Thesis. Physics Science Chulalongkorn University, 1993).

[4] C. Renghini, E. Girardin, A.S. Fomin, A. Manescu, A. Sabbioni, S.M. Barinov, V.S. Komlev, G. Albertini and F. Fiori, Mater. Sci. Eng. B 152 (2008) 86-90.

[5] C.F. Koch , S. Johnson , D. Kumar , M. Jelinek ,D.B. Chrisey , A. Doraiswamy ,C. Jin , R.J. Narayan and I.N. Mihailescu, Mater. Sci. Eng. C 27 (2007) 484-494.

[6] B. Feddes, J.G.C. Wolke, A.M. Vredenberg and J.A. Jansen, Biomaterials, 25 (2004) 633-639

[7] L. Gan and R. Pilliar, Biomaterials 25 (2004) 5303-5312.

[8] K. Hwang and Y. Lim, Surf. Coat. Tech. 115 (1999) 172-175.

[9] T. Kanazawa, Inorganic Phosphate Materials (Kodansha, Tokyo, 1989), p.16.

[10] L. Pinyo, Processing and Mechanical Properties of Hydroxyapatite/tetragonal zirconia Bilayer Structure (M.Sc. Thesis. Physics Science Chulalongkorn University, 2002).

[11] Certificate of analysis, Standard Reference Material 2910 (National Institute of Standards & Technology).

[12] H.S. Ryu, H.J. Youn, K. S. Hong, B.S. Chang, C.K. Lee and S.S. Chung, Biomaterials 23 (2002) 909-914.

APPENDIX D

STANDARD REFERENCE

09-0432 Quality: I

CAS Number: 1306-06-5

Molecular Weight: 502.32
Volume[CD]: 528.80
Dx: 3.155 Dm: 3.080

S.G.: P63/m (176)
Cell Parameters:
a 9.418 b c 6.884
α β γ

SS/FOM: F30=54(.0158, 35)
I/Icor:
Rad: CuKa1
Lambda: 1.54056
Filter:
d-sp: Debye-Scherrer

Mineral Name:
Hydroxylapatite, syn

Ca5 (P O4)3 (O H)
Calcium Phosphate Hydroxide
Ref: de Wolff, P., Technisch Physische Dienst, Delft, The Netherlands, ICDD Grant-in-Aid

d(A)	Int-f	h	k	l	d(A)	Int-f	h	k	l	d(A)	Int-f	h	k	l
8.1700	12	1	0	0	2.0650	8	1	1	3	1.4650	4	5	1	0
5.2600	6	1	0	1	2.0400	2	4	0	0	1.4520	13	3	0	4
4.7200	4	1	1	0	2.0000	6	2	0	3	1.4520	13	3	2	3
4.0700	10	2	0	0	1.9430	30	2	2	2	1.4330	9	5	1	1
3.8800	10	1	1	1	1.8900	16	3	1	2	1.4070	4	4	2	2
3.5100	2	2	0	1	1.8710	6	3	2	0	1.4070	4	4	1	3
3.4400	40	0	0	2	1.8410	40	2	1	3	1.3480	3	5	1	2
3.1700	12	1	0	2	1.8060	20	3	2	1	1.3160	5	4	3	1
3.0800	18	2	1	0	1.7800	12	4	1	0	1.3160	5	4	0	4
2.8140	100	2	1	1	1.7540	16	4	0	2	1.3060	4	5	2	0
2.7780	60	1	1	2	1.7220	20	0	0	4	1.3060	4	2	0	5
2.7200	60	3	0	0	1.6840	4	1	0	4	1.2800	7	4	2	3
2.6310	25	2	0	2	1.6440	10	3	2	2	1.2650	3	3	2	4
2.5280	6	3	0	1	1.6110	8	3	1	3	1.2650	3	6	0	2
2.2960	8	2	1	2	1.5870	4	5	0	1	1.2570	9	2	1	5
2.2620	20	3	1	0	1.5420	6	4	2	0	1.2490	1	4	3	2
2.2280	2	2	2	1	1.5300	6	3	3	1	1.2350	11	5	1	3
2.1480	10	3	1	1	1.5030	10	2	1	4	1.2210	9	5	2	2
2.1340	4	3	0	2	1.4740	12	5	0	2					

70-1511 Quality: C

CAS Number:

Molecular Weight: 740.02
Volume[CD]: 597.49
Dx: 4.113 Dm:

S.G.: P63/m (176)
Cell Parameters:
a 9.745 b c 7.265
α β γ

I/Icor: 2.23
Rad: CuKa1
Lambda: 1.54060
Filter:
d-sp: calculated

ICSD # : 002855

Sr5 (P O4)3 (O H)
Strontium Hydroxide Phosphate
Ref: Calculated from ICSD using POWD-12++, (1997)
Ref: Sudarsanan, K., Young, R.A., Acta Crystallogr., Sec. B, 28, 3668 (1972)

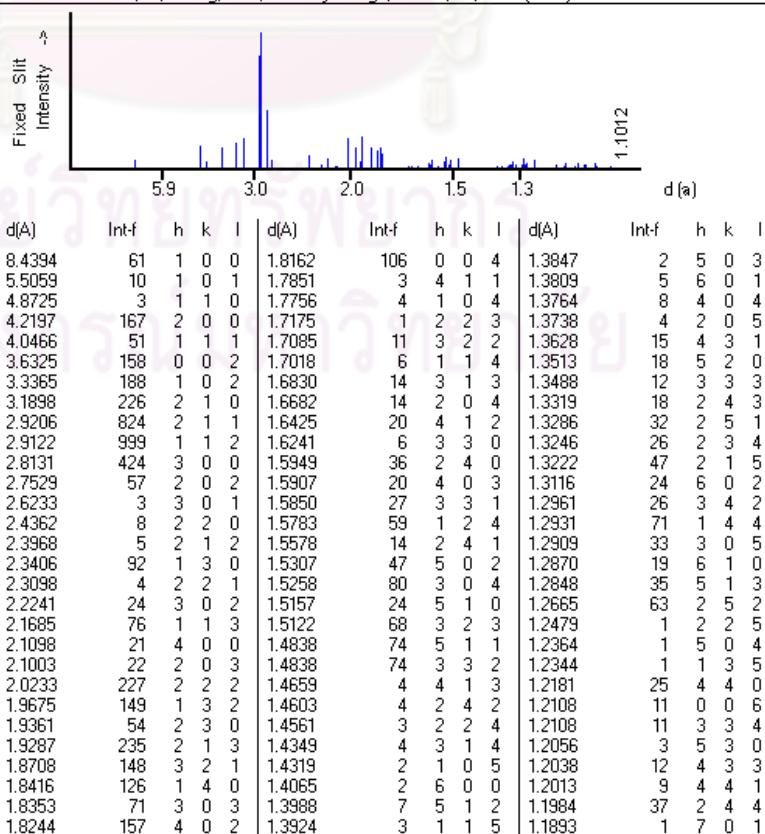| d(A)	Int-f	h	k	l	d(A)	Int-f	h	k	l	d(A)	Int-f	h	k	l
8.4394	61	1	0	0	1.8162	106	0	0	4	1.3847	2	5	0	3
5.5059	10	1	0	1	1.7851	3	4	1	1	1.3809	5	6	0	1
4.8725	3	1	1	0	1.7756	4	1	0	4	1.3764	8	4	0	4
4.2197	167	2	0	0	1.7175	1	2	2	3	1.3738	4	2	0	5
4.0466	51	1	1	1	1.7085	11	3	2	2	1.3628	15	4	3	1
3.6325	158	0	0	2	1.7018	6	1	1	4	1.3513	18	5	2	0
3.3365	188	1	0	2	1.6830	14	3	1	3	1.3488	12	3	3	3
3.1898	226	2	1	0	1.6682	14	2	0	4	1.3319	18	2	4	3
2.9206	824	2	1	1	1.6425	20	4	1	2	1.3286	32	2	5	1
2.9122	999	1	1	2	1.6241	6	3	3	0	1.3246	26	2	3	4
2.8131	424	3	0	0	1.5949	36	2	4	0	1.3222	47	2	1	5
2.7529	57	2	0	2	1.5907	20	4	0	3	1.3116	24	6	0	2
2.6233	3	3	0	1	1.5850	27	3	3	1	1.2961	26	3	4	2
2.4362	8	2	2	0	1.5783	59	1	2	4	1.2931	71	4	4	4
2.3968	5	2	1	2	1.5578	14	2	4	1	1.2909	33	3	0	5
2.3406	92	1	3	0	1.5307	47	5	0	2	1.2870	19	6	1	0
2.3098	4	2	2	1	1.5258	80	3	0	4	1.2848	35	5	1	3
2.2241	24	3	0	2	1.5157	24	5	1	0	1.2665	63	2	5	2
2.1685	76	1	1	3	1.5122	68	3	2	3	1.2479	1	2	2	5
2.1098	21	4	0	0	1.4838	74	5	1	1	1.2364	1	5	0	4
2.1003	22	2	0	3	1.4838	74	3	3	2	1.2344	1	1	3	5
2.0233	227	2	2	2	1.4659	4	4	1	3	1.2181	25	4	4	0
1.9675	149	1	3	2	1.4603	4	2	4	2	1.2108	11	0	0	6
1.9361	54	2	3	0	1.4561	3	2	4	2	1.2108	11	3	3	4
1.9287	235	2	1	3	1.4349	4	3	1	4	1.2056	3	5	3	0
1.8708	148	3	2	1	1.4319	2	1	0	5	1.2038	12	4	3	3
1.8416	126	1	4	0	1.4065	2	6	0	0	1.2013	9	4	4	1
1.8353	71	3	0	3	1.3988	7	5	1	2	1.1984	37	2	4	4
1.8244	157	4	0	2	1.3924	3	1	1	5	1.1893	1	7	0	1

VITAE

   Mr. Bhasit Hongthog was born on January 2, 1985 in Bangkok, Thailand. He finished high school from Sarasit Phitayalai, Bangpong, Ratchaburi, then received his bachelor degree of Science in Physics from Silpakorn University, Nakornphathom in 2006, and continued his master's study at Chulalongkorn University. During studying undergraduate and two years in graduate level, he was a student in the Development and Promotion for Science and Technology Talents Project (DPST).